Studies on zoonotic viruses isolated from wild animals with an optimal isolation method for protease-dependent viruses

（プロテアーゼ依存性ウイルスの高効率分離法により分離された
野生動物由来ウイルスに関する研究）

Mai Kishimoto

Contents

Abbreviations

293T-ACE2 cells	HEK293T cells stably expressing human ACE2
ACE2	Angiotensin-converting enzyme 2
ANOVA	Analysis of variance
AUC	Area under the curve
BLASTn	Basic local alignment search tool for nucleotide sequences
bp	Base pairs
COVID-19	Coronavirus disease 2019
CPE	Cytopathic effect
DMEM	Dulbecco's modified eagle medium
dpi	Days post-infection
EMCV	Encephalomyocarditis virus
FBS	Fetal bovine serum
FFU	Focus forming units
FRNT	Focus reduction neutralization test
$FRNT_{50}$	50% focus reduction neutralizing titer
GC	Genotype constellation
H&E	Hematoxylin and eosin
HEPES	4-(2-hydroxyethyl)-1-piperazineethanesulfonic acid
hpi	Hours post-infection
HRP	Horseradish peroxidase
ICTV	International Committee on Taxonomy of Viruses
IFA	Indirect immunofluorescence assay
IUCN	International Union for Conservation of Nature and Natural Resources
MEM	Maintained in Eagle's minimum essential medium
ML	Maximum-likelihood
MOI	Multiplicity of infections
NA	Neuraminidase
NeuAc	N-acetylneuraminic acid
NeuGc	N-glycolylneuraminic acid

NGS	Next-generation sequencing
ORF	Open reading frame
P1-3	Precursor 1-3
PBS	Phosphate-buffered saline
PS	100 U/ml penicillin and 100 μg/ml streptomycin
RACE	Rapid amplification of the cDNA end
RCWG	the Rotavirus Classification Working Group
RVA	Rotavirus A
S	Spike
SA	Sialic acid
SARS-CoV-1	Severe acute respiratory syndrome coronavirus-1
SARS-CoV-2	Severe acute respiratory syndrome coronavirus-2
SD	standard deviation
SMI-100	Human EpiIntestinal Small Intestine Tissue Models
$TCID_{50}$	50% tissue culture infective dose
TMPRSS1-15	Transmembrane protease, serine 1-15
TPB	Tryptose phosphate broth
TTSP	Type II transmembrane serine protease
UTR	Untranslated region
Vero-T2 cells	Vero E6 cells stably expressing human TMPRSS2
Vero-T11D cells	Vero E6 cells stably expressing human TMPRSS11D
Vero-T11E cells	Vero E6 cells stably expressing human TMPRS11E
Vero-T13 cells	Vero E6 cells stably expressing human TMPRSS13
VPs	Structural viral proteins
NSPs	Nonstructural proteins

Notes

Chapter I:

Kishimoto, M., Uemura, K., Sanaki, T., Sato, A., Hall, W.W., Kariwa, H., Orba, Y., Sawa, H., Sasaki, M. TMPRSS11D and TMPRSS13 activate the SARS-CoV-2 spike protein. *Viruses*. **13(3)**, 384 (2021).

Chapter II:

Kishimoto, M., Hang'ombe, B.M., Hall, W.W., Orba, Y., Sawa, H., Sasaki, M. *Mastomys natalensis* is a possible natural rodent reservoir for encephalomyocarditis virus. *J. Gen. Virol*. **102(3)**, 001564 (2021).

Chapter III:

Kishimoto, M., Kajihara, M., Tabata, K., Itakura, Y., Toba, S., Ozono, S., Sato, Y., Suzuki, T., Ito, N., Changula, K., Qiu, Y., Mori-Kajihara, A., Eto, Y., Harima, H., Mwizabi, D., Hang'ombe, B.M., Hall, W.W., Takada, A., Orba, Y., Sawa, H., Sasaki, M. Isolation and characterization of distinct rotavirus A in bat and rodent hosts. *J. Virol.* (in press).

General introduction

In the past two decades, emerging and re-emerging zoonotic infectious diseases have threaten global and animal health and posed a great impact on human society [1]. About two-thirds of human pathogens and about three-quarters of emerging and re-emerging human pathogens are zoonotic [2]. Novel zoonotic diseases have emerged *via* increase contact between humans, livestock, and wild animals because of a complex set of multifactorial circumstance, including population growth, industrial globalization, and land development accompanied by urbanization and deforestation [3,4]. Wild animals are important natural hosts and reservoirs of zoonotic viruses. For examples, severe acute respiratory syndrome coronavirus-1 and -2 (SARS-CoV-1 and SARS-CoV-2), Marburg viruses, rabies and rabies-related lyssaviruses, and Nipah and Hendra viruses were spilled over from bats, whereas hantavirus and Lassa fever virus, and monkey pox virus were spilled over from rodents [5–11]. Thus, it is necessary to investigate the viruses harbored by wild animals and monitor the risks of novel zoonotic diseases from "One Health" point of view.

Recent advances in genome analysis technology have enabled the discovery of a huge number of previously-unidentified (novel) viruses from various specimens including wild animals; however, only a limited number of the viruses have been isolated. The number of uncultivated virus genomes are increasing rapidly and now accounts for more than 95% diversity of viral genome databases [12]. The virus isolation is essential for basic virological and ecological characterizations of isolated viruses by the following analysis: i) whole-genome phylogenetic analysis, ii) evaluation of host and cell tropism, iii) assessment of pathogenicity using animal models, iv) sero-epidemiological studies in wild animals [13,14]. Thus, the virus isolation is a bottleneck for assessment of zoonotic potential of novel viruses from the perspective of proactive strategies for zoonotic diseases. Compared with the development of genome detection methods, virus isolation methods remain to be improved, and there are few attempts for the virus isolation from a large number of wild animal specimens.

Some viruses in the family *coronaviridae*, *orthomyxoviridae*, *paramyxoviridae*, and *reoviridae* cause respiratory and gastrointestinal infections and show protease

dependency [15–17]. These protease−dependent viruses require cleavage of their outer structural proteins by host protease for cell entry and are proliferated in cell culture under the serum-free medium supplemented with trypsin. However, virus isolation in serum-free medium is sometimes difficult since cells are easily damaged by sample inoculation. Previous studies demonstrated that host type II transmembrane serine proteases (TTSPs) cleave viral outer structural proteins and facilitate the protease-dependent viral infection in the absence of trypsin [18–26]. In this study, virus isolation from wild animal specimens using TTSP-expressing cells and characterization of isolated viruses were performed.

To investigate optimal TTSPs for isolation of a broad range of viruses, TTSPs facilitating the infection of SARS-CoV-2, which suddenly emerged in 2019 and has caused a global pandemic, were examined (Chapter I). The infection and growth efficiency of SARS-CoV-2 in 12 types of TTSP-expressing cells, including a well−characterized TTSP to facilitate infection of various protease-dependent viruses, a plasma membrane-associated transmembrane protease, serine 2 (TMPRSS2) were determined. As a result, it was demonstrated that TMPRSS2, TMPRSS11D, and TMPRSS13 enhance cell entry of SARS-CoV-2. In addition, Sasaki *et al.* have demonstrated that TMPRSS2 and TMPRSS11D co-expressing cells enhance rotavirus A (RVA) infection and proliferation [27]. Based on these findings, virus isolation was performed from Zambian wild bat and rodent specimens using TMPRSS2 and TMPRSS11D co-expressing cells. Subsequently, virological characterization and epidemiological studies were performed on the isolated viruses; rodent encephalomyocarditis virus (EMCV) (Chapter II) and bat and rodent RVA (Chapter III). RVA is a protease-dependent virus and a zoonotic agent that causes diarrhea in humans and animals. EMCV is not a protease-dependent virus and causes encephalitis, myocarditis, and reproductive disorders in various animal species. These results improve protease-dependent virus isolation and facilitate subsequent virological and epidemiological characterizations of various wild animal-derived viruses.

Chapter I:
Investigation of host type II transmembrane serine protease (TTSP) to activate SARS-CoV-2 spike protein

Summary

SARS-CoV-2 utilizes host proteases, including TMPRSS2 to cleave and activate the virus spike protein to facilitate cellular entry. Although TMPRSS2 is a well-characterized TTSP, the role of other TTSPs on the replication of SARS-CoV-2 remains to be elucidated. Here, I have screened 12 TTSPs using human angiotensin-converting enzyme 2-expressing HEK293T (293T-ACE2) cells and Vero E6 cells and demonstrated that exogenous expression of TMPRSS11D and TMPRSS13 enhanced cellular uptake and subsequent replication of SARS-CoV-2. In addition, SARS-CoV-1 and SARS-CoV-2 share the same TTSPs in the viral entry process. This study demonstrates the impact of host TTSPs on infection of SARS-CoV-2, which may have implications for cell and tissue tropism, for pathogenicity, and potentially for vaccine development.

Introduction

Coronavirus disease 2019 (COVID-19) has emerged as a pandemic and poses a significant public health threat despite its often low morbidity and mortality rate in certain geographic locations. To date, > 640,000,000 people have been infected, resulting in > 6,600,000 deaths globally (https://coronavirus.jhu.edu/map.html, accessed on 28th November 2022). Infection is caused by a novel SARS-CoV-2, which is closely related to SARS-CoV-1 [28,29]. As with SARS-CoV-1, SARS-CoV-2 mainly infects the respiratory tract and is primarily transmitted *via* the respiratory route, causing respiratory illness that can partially progress to severe pneumonia [30]. In addition, gastrointestinal illness—possibly *via* a fecal-oral transmission route—was also observed in SARS-CoV-2 patients [31–33]. Moreover, it has been pointed out that the central nervous system can be involved in SARS-CoV-2 infection, and this may also contribute to respiratory failure [34,35]. However, the specific cellular and tissue tropisms and pathology of SARS-CoV-2 remains to be further clarified.

Host cell factors involved in the viral entry steps are major determinants of coronavirus tropism and efficiency of cellular entry. SARS-CoV-2 enters into cells in the following steps: i) Virion of SARS-CoV-2 attaches to the target cell by interaction between the S1 subunit of the spike (S) protein and its cognate receptor, angiotensin-converting enzyme 2 (ACE2), ii) the binding of the S protein to ACE2 provokes conformational change of the S protein to a pre-fusion state, iii) the S2 subunit of the S protein is cleaved by host proteases at the S2′ site to trigger irreversible refolding of the S2 subunit into a post-fusion conformation, and iv) fusion of the cell/viral membranes occurs to introduce the viral genome into the cytosol of the host cell [36–39]. While SARS-CoV-1 requires cleavage of the S protein at the S1/S2 site by host proteases in the entry steps, the S1/S2 site of the S protein of SARS-CoV-2 is cleaved by intracellular protease furin in the viral assembly step, which may affect the cell tropism and the entry efficiency of SARS-CoV-2 [40]. In addition, it is suggested that the stability and glycosylation state of the S protein regulates its conformations to maintain the contact with ACE2, which is also related to vital entry efficiency [41–43].

As with SARS-CoV-1, SARS-CoV-2 utilizes two different entry pathways which involve different host proteases for S2 subunit cleavage: a TTSP-dependent pathway, and a cathepsin B/L-dependent pathway [44,45]. In the former route, the S2 subunit is cleaved by TTSPs, including TMPRSS2 on the cell surface, and mediates direct fusion of the viral envelope with the cellular membrane [36,44,45]. In the latter route, the virions of SARS-CoV-2 are taken into an endosome, and then the S2 subunit is cleaved by lysosomal protease cathepsin B/L [44,45]. While SARS-CoV-2 exclusively depends on cathepsin B/L for its S2 subunit activation in some TTSP-deficient cell lines, TTSP-dependent activation enhances the spread of SARS-CoV-2 in TTSP-expressing cells [21].

Human TTSPs consist of four subtypes and 18 members: the hepsin/TMPRSS subfamily (including TMPRSS1–5, 12, 13 and 15), matriptase subfamily (including TMPRSS6, 7, 9 and 14), corin subfamily (including TMPRSS10), and human airway trypsin-like protease/differentially expressed in squamous cell carcinoma (HAT/DESC) subfamily (including TMPRSS11A, 11B, 11D, 11E, and 11F) [46]. TMPRSS2 is a well-characterized TTSP which serves as a host factor involved in the replication of certain viruses. In addition to TMPRSS2, the relationship between other TTSP families and viral life cycles, particularly for influenza viruses and coronaviruses, have been extensively investigated [24–26,47–50]. For SARS-CoV-1, TMPRSS2, 11A, 11D, 11E, and 13 were shown to activate the S protein [25,26,50]. For SARS-CoV-2, TMPRSS2, 4, 11A, 11D, and 11E all activate the S protein and enhance S-mediated cell fusion in HEK293 cells expressing human ACE2 [51,52]. It has also been demonstrated that TMPRSS4 promotes SARS-CoV-2 infection in cooperation with TMPRSS2 in human small intestinal enterocytes [53]. However, previous reports have essentially been limited to the detection of SARS-CoV-2 S protein activation, and only a small number has involved functional analysis using infectious SARS-CoV-2. In the present study, I have screened the activity of 12 TTSPs using infectious SARS-CoV-2 and SARS-CoV-1 and characterized the role of TMPRSS11D and 13 on viral entry. These findings demonstrate the potential ability of these TTSPs to enhance the SARS-CoV-2 life cycle, and this may have important implications for the cell and tissue tropisms and pathogenicity of the virus.

Materials and Methods

Cells and viruses

HEK293T cells were grown in Dulbecco's modified eagle medium (DMEM) with high glucose (Sigma-Aldrich, St. Louis, MO) with 10% fetal bovine serum (FBS). Vero E6 cells were grown in DMEM with 10% FBS and 100 U/ml penicillin and 100 μg/ml streptomycin (PS). Vero E6 cells stably expressing human TMPRSS2 (Vero-T2 cells) and HEK293T cells stably expressing human ACE2 (293T-ACE2 cells) were prepared as described previously [54]. Cells were cultured at 37°C with 5% CO_2. The SARS-CoV-2 isolated strain WK-521 and SARS-CoV-1 strain Hanoi were kindly provided by Dr. Saijyo, Dr. Shimojima (National Institute of Infectious Diseases, Tokyo, Japan) and Dr. Morita (Institute of Tropical Medicine Nagasaki University, Nagasaki, Japan), respectively, and propagated in Vero-T2 cells [55].

Plasmids and transfection

The cDNAs of TMPRSS1 and 11A were synthesized as gBlocks Gene Fragments (Integrated DNA Technologies, Coralville, IA). The cDNA clones of TMPRSS2, 11D, 11E, and 13 were obtained from DNAFORM (Yokohama, Japan). The cDNAs of TMPRSS3, 4, 5, 6, 10, and 14 were obtained by RT-PCR using total RNA from cell lines (Table 1). A total of 12 human TTSP genes were individually cloned into plasmid vector pCXSN—the pCMV derivative having the CMV promoter and a HA tag sequence at the C-terminus of the encoding sequences, prepared *via* XhoI/NotI or SalI/NotI restriction enzyme sites. The sequences of each cDNA clone were verified by sanger sequence (Table 1). For analysis of transient protease expression, 293T-ACE2 cells were seeded on 24-well plates at a density of 2.0×10^5 cells/well, which were transiently transfected with plasmids encoding 12 TTSPs with the C-terminal HA tag or an empty plasmid as a control using Polyethylenimine Max (Polysciences, Inc., Warrington, PA). Media were changed with fresh medium after 6 h post-transfection. At 48 h post-transfection, cells were used for immunoblotting assay and virus entry assays.

Generation of Vero E6 cells stably expressing TTSPs

Human TMPRSS11D, 11E, and 13 genes were individually cloned into the self-inactivating lentiviral vector plasmid CSII-CMV-MCS-IRES2-Bsd, which was kindly provided by Dr. Miyoshi (RIKEN, Ibaraki, Japan). Lentivirus particles were prepared by co-transfection with the lentiviral vector plasmid and Lentiviral High Titer Packaging Mix (Takara Bio, Shiga, Japan), and then inoculated to Vero E6 cells with 10 μg/ml of polybrene. Transduced cells were selected in the presence of 10 μg/ml of blasticidin-S (Wako, Osaka, Japan).

Immunoblotting

Cells were lysed in lysis buffer [1% NP-40, 20 mM Tris-HCl (pH 7.5), 150 mM NaCl, 5 mM EDTA] supplemented with a cOmplete ULTRA protease inhibitor cocktail (Roche Diagnostics, Mannheim, Germany). Cell lysates were separated by SDS-PAGE and transferred onto Immobilon-P PVDF membranes (Merck, Burlington, MA). For detection of HA-tagged TTSPs which were transiently expressed in 293T-ACE2 cells, blotted membranes were incubated in horseradish peroxidase (HRP)-conjugated anti-HA tag antibody (H6533, Sigma-Aldrich) diluted with 5% skim milk in TBS-T buffer [25 mM Tris-HCl (pH 7.5), 137 mM NaCl, 2.7 mM KCl]. For detection of TTSP-expression in Vero E6 cells, blots were incubated with primary antibodies: anti-TMPRSS2 (ab92323, Abcam, Cambridge, UK) antibody diluted with 5% skim milk in TBS-T buffer and anti-TMPRSS11D (GTX117370, GeneTex, Irvine, CA), anti-TMPRSS11E (PA5-48775, Invitrogen, Waltham, MA) and anti-TMPRSS13 (GTX117425, GeneTex) antibodies in Signal Booster (Beacle, Kyoto, Japan). The blots were then incubated with HRP-conjugated secondary antibodies. The HRP-conjugated anti-β-actin antibody (PM053-7, MBL, Nagoya, Japan) was used as a loading control. Signals were developed using Immobilon Western Chemiluminescent HRP Substrate (Merck).

Virus entry assay

Cells were incubated with SARS-CoV-1 or SARS-CoV-2 at a multiplicity of infections (MOI) of 1 in the presence of the cathepsin inhibitor, 25 μM E-64d (Abcam)

or DMSO as control. After 1 h absorption, cells were washed with phosphate-buffered saline (PBS) and cultured in maintenance medium. At 4 h post-infection (hpi), total RNAs were extracted from inoculated cells using ISOGEN (Nippon Gene, Tokyo, Japan) and a Direct-zol RNA MiniPrep Kit (Zymo Research, Irvine, CA). Extracted RNAs were subjected to qRT-PCR analysis with the THUNDERBIRD Probe One-step qRT-PCR Kit (TOYOBO, Osaka, Japan). The sequences of primers and probes targeting the N gene of SARS-CoV-1 and SARS-CoV-2 have been described previously [56,57]. Human ACTB (Beta Actin) Endogenous Control (Applied Biosystems, Foster City, CZ) and nonhuman primate ACTB were employed as endogenous controls [58].

Multi-cycle replication assay

Vero-T11D, Vero-T11E, and Vero-T13 cells were seeded on 12-well plates at a density of 2.0×10^5 cells/well and infected with SARS-CoV-1 and SARS-CoV-2 at MOI of 0.01. After 1 h incubation, cells were washed with PBS and cultured in fresh medium. At 24, 48, and 72 hpi, culture supernatants were collected and subjected to virus titration by plaque assay. For virus titration, Vero-T2 cells were inoculated with 10-fold serially diluted culture supernatants and then layered with DMEM containing 2% FBS and 0.5% agar. After 48 h incubation, cells were fixed with 3.7% buffered formaldehyde and stained with 1% crystal violet in absolute ethanol, and plaques were then manually counted.

Indirect immunofluorescence assay (IFA)

Vero E6, Vero-T2, Vero-T11D, Vero-T11E, and Vero-T13 cells were infected with SARS-CoV-2 at an MOI of 8. At 24 hpi, cells were fixed with 3.7% buffered formaldehyde. After treatment with ice-cold methanol, cells were stained with the primary antibody, anti-SARS-CoV-2 S antibody (GTX632604, GeneTex), and diluted with PBS buffer containing 1% Block Ace (KAC, Kyoto, Japan). Cells were then incubated with Alexa 488-conjugated anti-mouse IgG antibody (Invitrogen) in PBS buffer containing 1% Block Ace and 1% Hoechst 33342 (Invitrogen).

Statistical analysis

One-way analysis of variance (ANOVA) with Dunnett's test was used to determine statistical significance.

Results

Evaluation of the effects of TTSPs on the entry of SARS-CoV-1 and SARS-CoV-2 using 293T-ACE2 cells

To investigate the role of TTSPs in addition to TMPRSS2 in the entry steps of both SARS-CoV-1 and SARS-CoV-2, 293T-ACE2 cells were transiently transfected with each of the 12 different TTSP-encoding plasmids and subjected to virus entry assays. The expressions of HA-tagged TTSPs were confirmed by immunoblotting (Fig. 1A). Exogenous expressions of TTSPs were confirmed as bands of the expected molecular weight. In addition to bands of the predicted molecular weight, bands with smaller molecular weights were also observed, indicating autocatalytic activation of the TTSPs. Signals of full-length TMPRSS2 at 53 kDa and its cleaved form at 37 kDa were weaker than those of other TTSPs. SARS-CoV-2 employs two entry pathways—the direct fusion mode mediated by TTSP, and the endocytosis route mediated by cathepsin B/L [44,45]. To investigate the role of TTSPs on viral entry, the TTSP-expressing 293T-ACE2 cells were inoculated with either SARS-CoV-1 or SARS-CoV-2, and viral RNA levels at the early phase of infection were quantified using qRT-PCR (Fig. 1B and 1C). The assay was conducted in the presence of E-64d, an inhibitor of cathepsin B/L, in order to block TTSP-independent viral entry. Expression of TMPRSS2, 11D, 11E, and 13 significantly increased viral RNAs isolated from viral inoculated cells at 4 hpi, indicating that these TTSPs enhanced entry of both SARS-CoV-1 and SARS-CoV-2 in the presence of E-64d. Among the tested TTSPs, TMPRSS2 exhibited the highest enhancement of activity for entry of SARS-CoV-1 and SARS-CoV-2. Based on these results, TMPRSS11D, 11E, and 13 were further examined in subsequent experiments.

TMPRSS11D and 13 facilitate SARS-CoV-2 replication

I next established four different Vero E6 cells stably expressing TTSPs, including TMPRSS2 (Vero-T2 cells), 11D (Vero-T11D cells), 11E (Vero-T11E cells), and 13 (Vero-T13 cells). Vero-T2 cells were shown to be highly susceptible to both SARS-CoV-1 and SARS-CoV-2 [20,21,36,40]. Immunoblotting analysis using each specific antibody to four TTSPs revealed the expression of each TTSP gene in the transduced

cells, but not in parental Vero E6 cells (Fig. 2A). Subsequently, Vero E6, Vero-T2, T11D, T11E, and T13 cells were subjected to virus entry assay using SARS-CoV-1 or SARS-CoV-2 in the presence of E-64d (Fig. 2B and 2C). Cellular uptake of the viruses in Vero-T2, T11D, and T13 cells was significantly higher than in parental Vero E6 cells at 4 hpi, which was consistent with the results of transiently TTSPs-expressing 293T-ACE2 cells. However, no significant enhancement of viral entry was observed in Vero-T11E cells. These results suggest that not only TMPRSS2, but also TMPRSS11D and 13 enhance the entry of SARS-CoV-2, and that TMPRSS11D and 13 play roles in the entry steps of both SARS-CoV-1 and SARS-CoV-2.

To assess the impact of TTSPs on virus replication, Vero E6, Vero-T2, T11D, T11E, and T13 cells were infected with SARS-CoV-2, and the progeny virus in culture supernatants at 24, 48, and 72 hpi were titrated by plaque assay (Fig. 2D). Infectious virus titers of supernatants in Vero-T2, T11D, and T13 were approximately 100-fold higher than that of Vero E6 cells at 24 hpi. The viral titers of supernatants from all cells, including parental Vero E6 cells, were saturated at 48 hpi, and most of the cells were detached from the culture dishes at 72 hpi. Furthermore, large syncytia formations in Vero-T2, T11D, T11E, and T13 but not in Vero E6 cells were observed, and these phenomena suggested that the S protein induced cell-to-cell fusion through the activation of these TTSPs (Fig. 2E). These results support that TMPRSS11D and 13 enhance cellular entry and subsequent replication of SARS-CoV-2. Although TMPRSS11E did not enhance virus entry at 4 hpi and multicycle replication at 24 hpi in Vero E6 cells, cell fusion activity at 24 hpi was clearly observed. This contradiction may be due to the different efficiencies of fusion caused by TTSPs cleaving the S protein at cell-to-cell and cell-to-virion levels [25,40,59].

Discussion

In this study, 12 TTSPs were screened and TMPRSS11D and 13 were identified as potential proteases which could enhance SARS-CoV-2 entry into cells. Other studies have reported that the SARS-CoV-2 S protein gained cell-to-cell fusion ability in the presence of TMPRSS4, 11A, 11D, and 11E [51,52]. However, these reports were based on findings using cells co-expressing the S protein and TTSPs, and the relationships on the role of TTSPs and native SARS-CoV-2 remained to be elucidated. This study has demonstrated that the exogenous expressions of both TMPRSS11D and 13 facilitated viral entry into cells and the subsequent replication of SARS-CoV-2.

Consistent with a previous study, TMPRSS4 alone had little effect on SARS-CoV-2 entry into cells [53]. TTSP screen by transient transfection identified TMPRSS11E activity to facilitate viral entry in addition to TMPRSS11D and 13 (Fig. 1). However, TMPRSS11E did not affect SARS-CoV-2 entry and replication in Vero E6 cells. It has been reported that TMPRSS2 is involved in the entry of coronaviruses not only through the cleavage of the S protein at the S2′ site, but also by other different mechanisms, including S protein cleavage at multiple sites and association with ACE2 [60]. TMPRSS11E may fail to exert viral-entry enhancement in Vero E6 cells due to partial dysfunction of these interactions with the S protein or ACE2. Meanwhile, cell-to-cell fusion was observed in Vero-T11E cells infected with SARS-CoV-2 (Fig. 2C–2E). The mode of fusion mediated by S protein may be different in cell-to-cell fusion and cell-to-virion fusion [25,40,59]. Collectively, this suggests that the interpretation of cell-to-cell fusion assay, and the role of TMPRSS11E on SARS-CoV-2 infection remains to be clearly established.

Among TTSPs examined in this study, exogenous expression of TMPRSS2 conferred the highest susceptibility among others tested for the entry of SARS-CoV-2 into cells. TMPRSS11D is expressed in the vagina, esophagus, and submucosal serous glands of bronchi and trachea in the human body [61]. TMPRSS13 is predominantly expressed in human skin, lungs, peripheral blood lymphocytes, and certain other glandular epithelium cells [62]. These tissues and cells are not the main target for SARS-CoV-2. It is therefore still unclear whether TMPRSS11D and 13 are involved in the *in vivo* infection

and pathogenicity of SARS-CoV-2. Further studies using *in vivo* animal models are required to address this question. In conclusion, TMPRSS11D and 13 were identified as potential host serine proteases which can enhance SARS-CoV-2 propagation, and this expands our knowledge on TTSP function and the entry mode of SARS-CoV-2.

Table 1. Overview of TTSP family gene cloning

Subfamily	Protease name	Synonyms	Accession no.	cDNA origin		Sequence of cloning primer* (5'-3')
HAT/DESC	TMPRSS11A	HATL1	NM_182606.4	DNA synthesis	-	-
					-	-
	TMPRSS11D	HAT	NM_004262.3	cDNA clone	F	AAGTCGACGCCACCATGTATAGGCCAGCACGTGTAAC
					R	TAAGCGGCCGCGATCCCAGTTTGTTGCCTAATC
	TMPRSS11E	DESC1	NM_014058.4	cDNA clone	F	AACTCGAGGCCACCATGATGTATCGGCCAGATGTG
					R	TAAGCGGCCGCGATACCAGTTTTTGAAGTAATCCAG
Hepsin/TMPRSS2	TMPRSS1	hepsin, HPN	NM_182983.2	DNA synthesis	-	-
					-	-
	TMPRSS2	Epitheliasin	NM_005656.4	cDNA clone	F	TATCTCGAGACCATGGCTTTGAACTCAGGGTCAC
					R	TATGCGGCCGCGCCGTCTGCCCTCATTTG
	TMPRSS3	TADG-12	NM_024022.3	HepG2 cell	F	ATTCTCGAGCCACCATGGGGGAAAATGATCCGCC
					R	TAAGCGGCCGCGGTTTTTAGGTCTCTCTCCATCTGCTC
	TMPRSS4	CAPH2	NM_019894.4	Caco-2 cell	F	ATTCTCGAGCCACCATGTTACAGGATCCTGACAGTGATCAA
					R	TAAGCGGCCGCCAGCTCAGCCTTCCAGACATTGTAG
	TMPRSS5	Spinesin	NM_030770.4	Calu-3 cell	F	ATTCTCGAGCCACCATGAGCCTGATGCTGGATGACC
					R	TAAGCGGCCGCGAGGAGGGAGTCCTGAGCAGTGTC
	TMPRSS13	MSPL	NM_001077263.3	cDNA clone	F	TAACTCGAGACCATGGAGAGGGACAGCCACGGGA
					R	TATGCGGCCGCGGATTTTCTGAATCGCACCTCG
Matriptase	TMPRSS6	Matriptase-2	NM_153609.4	Hela cell	F	ATTCTCGAGCCACCATGCCCGTGGCCGAGGCCC
					R	TAAGCGGCCGCGGTCACCACTTGCTGGATCCAGCTG
	TMPRSS14	ST14, Matriptase	NM_021978.4	Caco-2 cell	F	ATTCTCGAGCCACCATGGGGAGCGATCGGGCCCG
					R	TAAGCGGCCGCTACCCCAGTGTTCTCTTTGATCCAGTC
Corin	TMPRSS10	Corin	NM_006587.4	MRC5 cell	F	ATTCTCGAGCCACCATGAAACAGTCTCCTGCCCTCGC
					R	TAAGCGGCCGCGTTTAGGAGAAAGGTCTGGATGTAAATC

* Underbars indicate the restriction enzyme site.

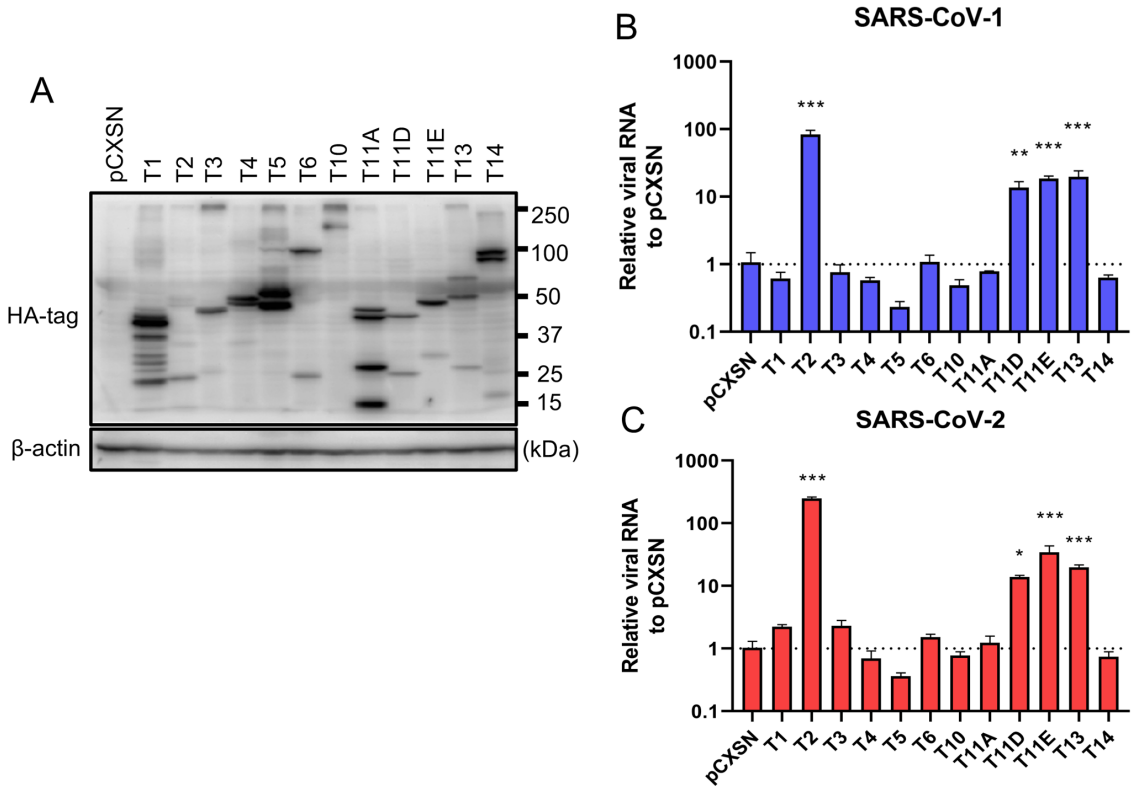

Fig. 1. Entry of SARS-CoV-1 and SARS-CoV-2 in TTSP-expressing 293T-ACE2 cells

(A) Expression of TTSPs in 293T-ACE2 cells. Plasmids encoding TMPRSS1 (T1, 45 kDa), TMPRSS2 (T2, 53 kDa), TMPRSS3 (T3, 49 kDa), TMPRSS4 (T4, 48 kDa), TMPRSS5 (T5, 50 kDa), TMPRSS6 (T6, 89 kDa), TMPRSS10 (T10, 116 kDa), TMPRSS11A (T11A, 48 kDa), TMPRSS11D (T11D, 46 kDa), TMPRSS11E (T11E, 48 kDa), TMPRSS13 (T13, 61 kDa), TMPRSS14 (T14, 95 kDa), and empty plasmid pCXSN (as a control) with a C-terminal HA tag were transiently transfected into 293T-ACE2 cells. Protease expressions in cell lysates were detected by immunoblotting with an anti-HA antibody. Detection of β-actin was employed as a loading control. Similar results were obtained in three independent experiments. (B,C) Twelve types of TTSP-transfected 293T-ACE2 cells were infected with SARS-CoV-1 (B) and SARS-CoV-2 (C). Total RNAs were extracted from cells at 4 hpi and analyzed by qRT-PCR. Levels of N gene of SARS-CoV-1 and SARS-CoV-2 were normalized with that of β-actin mRNA. The values in the graphs are shown as means ± standard deviation (SD) of triplicates. One-way ANOVA with Dunnett' s test was used to determine the statistical significance compared to no-TTSPs controls; *, $p < 0.05$, **, $p < 0.01$, ***, $p < 0.001$. Data are representative of two independent experiments.

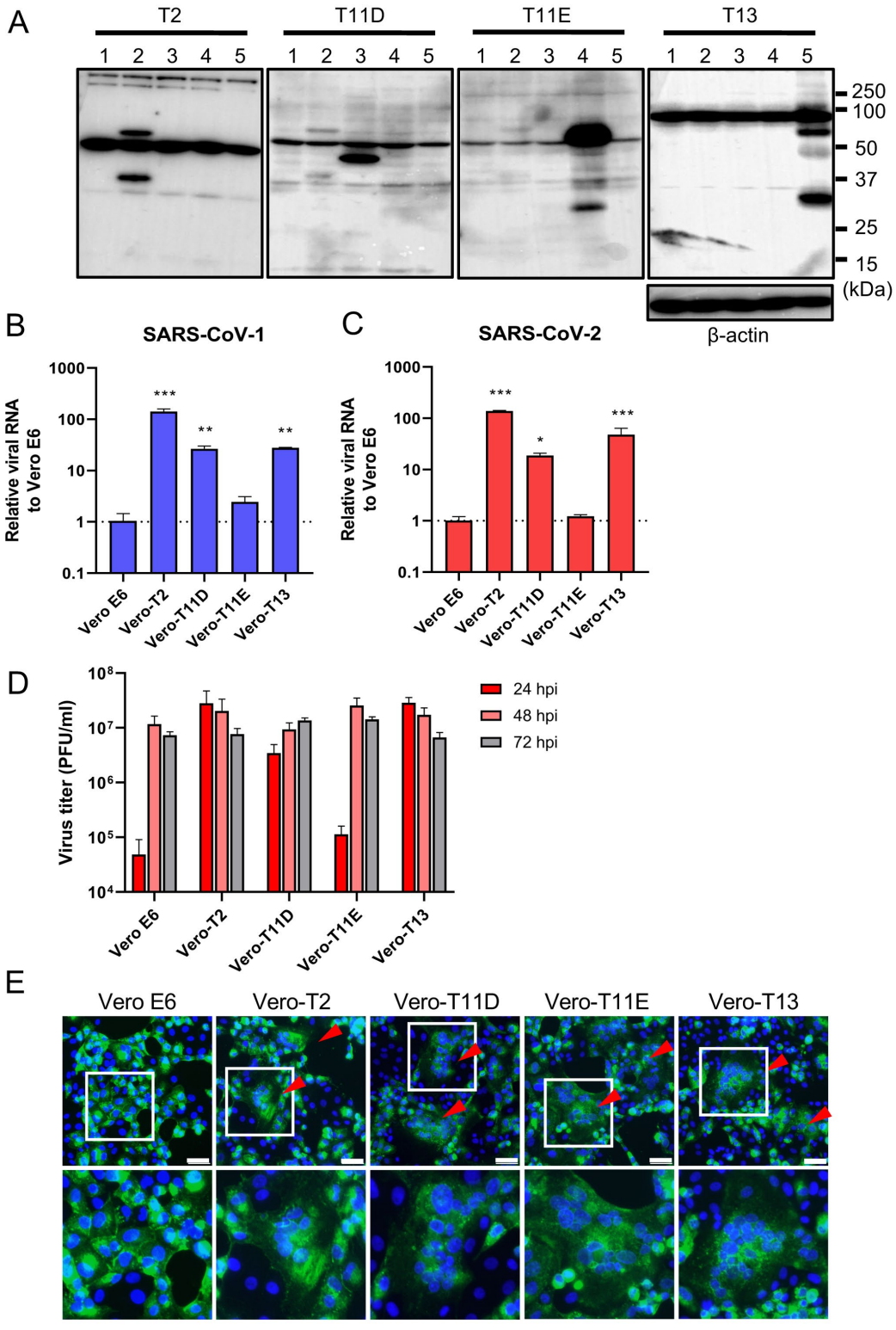

Fig. 2. Effect of TTSPs on viral entry and replication in TTSP-expressing Vero cells

(A) Expression of TTSP in Vero E6 cells which were transduced with a lentiviral vector expressing TMPRSS2, 11D, 11E, and 13 was confirmed by immunoblotting; lane 1: Vero E6, lane 2: Vero-T2, lane 3: Vero-T11D, lane 4: Vero-T11E, lane 5: Vero-T13. (B,C) TTSP-transduced Vero E6 cells were infected with SARS-CoV-1 (B) and SARS-CoV-2 (C). Total RNAs were extracted from cells at 4 hpi and analyzed by qRT-PCR. Levels of N genes of SARS-CoV-1 and SARS-CoV-2 were normalized to that of β-actin mRNA. The values in the graphs are shown as means ± SD of triplicates. One-way ANOVA with Dunnett's test was used to determine the statistical significance compared to no-TTSPs controls; *, $p < 0.05$, **, $p < 0.01$, ***, $p < 0.001$. Data are representative of two independent experiments. (D) Vero E6, Vero-T2, T11D, T11E, and T13 cells were infected with SARS-CoV-2 (MOI = 0.01). Culture supernatants were harvested at 24, 48, and 72 hpi and subjected to virus titration using plaque assays. The values in the graphs are shown as means ± SD of triplicates. (E) Fusion activity of SARS-CoV-2-infected cells. Vero E6, Vero-T2, T11D, T11E, and T13 cells were infected with SARS-CoV-2 (MOI = 8). At 24 hpi, cells were fixed and stained with anti-SARS-CoV-2 spike antibody (green) and Hoechst 33342 (blue). Scale bars indicate 50 μm. Red arrowheads demonstrate cell syncytia. Data are representative of two independent experiments. Areas in white squares are magnified in lower panels.

Chapter II:

Isolation and characterization of encephalomyocarditis virus (EMCV) in *Mastomys natalensis*, a possible natural rodent reservoir

Summary

EMCV infects a wide range of hosts and can cause encephalitis, myocarditis, reproductive disorders and diabetes mellitus in selected mammalian species. As for humans, EMCV infection seems to occur by the contact with animals and can cause febrile illnesses in some infected patients. Here EMCV strain ZM12/14 were isolated from a natal multimammate mouse (*Mastomys natalensis*) in Zambia. Pairwise sequence similarity of the ZM12/14 P1 region consisting of antigenic capsid proteins showed the highest similarity of nucleotide (80.7%) and amino acid (96.2%) sequence with EMCV serotype 1 (EMCV-1). Phylogenetic analysis revealed that ZM12/14 clustered into EMCV-1 at the P1 and P3 regions but segregated from known EMCV strains at the P2 region, suggesting a unique evolutionary history. RT-PCR screening and neutralizing antibody assays for EMCV were performed using collected tissues and serum from various rodents (n = 179) captured in different areas in Zambia. The EMCV genome were detected in 19 *M. natalensis* (19/179 = 10.6%) and neutralizing antibody for EMCV in 33 *M. natalensis* (33/179 = 18.4%). However, neither the genome nor neutralizing antibody were detected in other rodent species. High neutralizing antibody titers (≧ 320) were observed in both RT-PCR-negative and -positive animals. Inoculation of ZM12/14 caused asymptomatic persistent infection in BALB/c mice with high antibody titers and high viral loads in some organs, consistent with the above epidemiological results. This study is the first report of the isolation of EMCV in Zambia, suggesting that *M. natalensis* may play a role as a natural reservoir of infection.

Introduction

EMCV infects a wide range of animal species and causes various conditions ranging from subclinical to lethal disease with myocarditis, encephalitis, neurological disorders, reproductive failure, and diabetes mellitus in humans or animals [63]. EMCV infection results in different outcomes depending on the host animal species and the virus strains. For example, sudden death caused by EMCV infection has been reported in primates, elephants, and various captive animals in zoos [64–73]. Dogs show systemic symptoms with encephalitis and myocarditis [74]. Importantly, pigs are the most susceptible animal for EMCV, and EMCV infection causes a serious threat to the pig industry with sudden death often associated with myocarditis and reproductive failures including abortion [75–77]. As for humans, serological surveys for EMCV have shown seropositivity rates of up to 30%. In addition, higher seropositive rates were observed in populations that have more frequent contact with wild animals such as hunters, indicating that EMCV may be a zoonotic pathogen, which could be transmitted from animals to humans [78,79]. Subclinical or mild infections are thought to be predominant in humans, but there are some reports showing an association with febrile illness [80,81]. While EMCV infection provokes some symptoms in most animal species, rodents such as *Ruttus ruttus* and *Mus musculus* exhibit mainly asymptomatic persistence and disperse viruses for a relatively long period [82–84]. A reservoir has been defined as populations or environments in which the pathogen can be permanently maintained and from which infection is transmitted to susceptible animals [85]. Although there have been no reports of direct transmission from rodents to other animals or humans, these rodent species have been considered to be a potential EMCV reservoir for susceptible animals, such as pigs, wild animals or potentially humans.

EMCV is a member of the species of *Cardiovirus* A in the genus *Cardiovirus* in the family *Picornaviridae*, which is the largest group of small non-enveloped positive sense RNA viruses with an icosahedral capsid of 30 nm in diameter. The EMCV genome is approximately 7,800 base pairs (bp) in length and encodes a single open reading frame (ORF), which is translated as a single polyprotein precursor and cleaved by a viral protease to produce mature proteins. The genome organization is as follows:

VPg + 5′ untranslated region (UTR)$^{IRES\text{-}II}$ [L/1A-1B-1C-1D-2A^{npgp}/2B-2C/3A-3B^{VPg}-3C^{pro}-3D^{pol}] 3′UTR-poly(A). Precursor 1 (P1) composed of four proteins (1A-1D) is the capsid protein. P2 composed of 2A–2C and P3 composed of 3A–3D are nonstructural proteins [63,86]. Serologically, EMCV is classified as EMCV-1 and EMCV-2, both of which are assigned to the species Cardiovirus A by the International Committee on Taxonomy of Viruses (ICTV) [87]. Recently, Vyshemirskii *et al*. have proposed a detailed genetic classification of EMCV based on the nucleotide sequence identity, which contains four members of Cardiovirus A (EMCV-1 to 4) and EMCV-1 is subdivided into seven lineages (A to G) [67].

EMCV was firstly discovered in a gibbon ape in 1945 in Florida, USA [88]. Thereafter, EMCV was identified in a wide range of domestic and wild animals, including pigs, dogs, rodents, primates, elephants, antelopes, lions, and birds in all continents except for Antarctica [64,69,70,74,89]. In Africa, there were outbreaks in domestic pigs and wild elephants in South Africa [70,72] and primates in the Democratic Republic of the Congo [73]. In addition, Grobler *et al*. reported that seropositivity in *M. natalensis* captured in 1994 in the Kruger National Park, South Africa for EMCV was 37.9% (100/264) [72]. However, studies on the serosurveillance of EMCV has not been reported in the subsequent 26 years. Furthermore, there have been no reports on EMCV in either domestic or wild animals in Zambia. In this study, I have isolated infectious EMCV from *M. natalensis* and screened for EMCV infection in Zambian wild rodents using RT-PCR and neutralizing antibody tests. This study revealed a unique molecular evolution of Zambian EMCV and suggests *M. natalensis* is a natural reservoir of EMCV in Zambia. This is the first study of surveillance of EMCV in wildlife in Zambia.

Materials and Methods

Sample collection

A total of 179 wild rodents, including *M. natalensis* and shrews collected in three areas in Zambia from 2012 to 2013 were investigated: 67 rodents and shrews were captured in Mpulungu, 41 in Solwezi, and 71 in Mazabuka (Fig. 3). Rodents and shrews were captured using Sherman traps and cage traps and euthanized with diethyl ether, then sera, kidneys, spleens, and lungs were collected and kept at −80°C until use. In collected kidneys, spleens, and lungs, no macroscopical changes were observed. Captured rodents and shrews were classified into 13 species of rodents and two species of shrews by nucleotide sequence analysis of the mitochondrial cytochrome *b* gene, as described previously [90,91]. Ethical approval to undertake the present study was provided by the then Zambia Wildlife Authority, which is now the Department of National Parks and Wildlife, Ministry of Tourism and Arts, Zambia.

Cells and viruses

BHK-21 cells (C-13, JCRB Cell Bank, Osaka, Japan) were maintained in DMEM with 10% FBS and PS. Cells were constantly cultured at 37°C with 5% CO_2. For EMCV propagation, BHK-21 cells were infected with EMCV ZM12/14 at a MOI of 0.1 and maintained for 2 days in static culture with maintenance medium: DMEM with 2% FBS and PS. For virus titration, BHK-21 cells in 96-well plates were infected with EMCV with tenfold serial dilutions. Appearance of cytopathic effect (CPE) was monitored at 4 days post-infection (dpi) and the 50% tissue culture infective dose ($TCID_{50}$)/ml was calculated according to the Reed and Muench method.

Virus isolation

Mixed tissue homogenates of kidney, spleen, and lung of each rodent and shrew were prepared using BioMasher II (Nippi, Tokyo, Japan). After centrifugation at 3,000 × *g* for 5 min, supernatants were inoculated to BHK-21 cells with 2 ml isolation medium [DMEM supplemented with 10% FBS, PS, 25 μg/ml gentamycin, 1% antibiotic-antimycotic solution (Wako), and 25 mM 4-(2-hydroxyethyl)-1-

piperazineethanesulfonic acid (HEPES)] in 15 ml tissue culture tubes. Cells were cultured for 7 days in rolling condition of 0.3 rpm/min and inoculated cells were subsequently blind passaged twice in BHK-21 cells.

Viral genome sequencing

Viral RNA was extracted from the supernatant of the infected BHK-21 cells using TRIzol LS reagent (Invitrogen). Double-strand cDNA was constructed by PrimeScript Double Strand cDNA Synthesis Kit (Takara Bio) and subjected to sequence library construction using Nextera XT DNA Library Preparation Kit (Illumina, San Diego, CA). The 300 bp paired-end sequencing was performed on an illumina MiSeq sequencer (Illumina). Sequence reads were trimmed and assembled into contigs by *de novo* assembly using CLC Genomics Workbench 20.1 (Qiagen, Hilden, Germany). The obtained contigs were analyzed by Basic Local Alignment Search Tool for nucleotide sequences (BLASTn) program (National Center for Biotechnology Information, Bethesda, MD, USA).

qRT-PCR

Total RNA was extracted from culture supernatants or 10% tissue homogenates using TRIzol LS reagent and subjected to qRT-PCR using THUNDERBIRD Probe One-step qRT-PCR Kit (TOYOBO). The primer and probe sequences for EMCV ZM12/14 were as follows: forward primer 5′-TCTTCTTGTGGCGACGAATTA-3′; reverse primer 5′-GTCTTGTTAGCGGGTGTTATCT-3′; probe 5′-/FAM/TCCTGTCTT/ZEN/TGCCAGATTTGTTCTCACC/BHQ/−3′ (Integrated DNA Technologies). Serially diluted RNA from the culture supernatants containing EMCV were used to generate a standard curve for the conversion of Ct values to $TCID_{50}$.

RT-PCR and sequencing

Total RNA was extracted from kidneys of rodents and shrews from Mpulungu and spleens from Solwezi and Mazabuka using TRIzol (Invitrogen). To detect multiple EMCV strains with a high degree of nucleotide sequence diversity, a universal degenerate primer set was designed based on the consensus amino acid sequence of

EMCV 3D gene from 50 strains previously registered to GenBank: forward primer 5′-RARYCTVGCAAAGACAGG-3′; reverse primer 5′-CKGTACTCCACASTYTC-3′. RT-PCR assay was performed using SuperScript IV One-Step RT-PCR System (Invitrogen) with the following thermal cycling conditions: 50°C for 10 min, 98°C for 2 min, 40 cycles of 98°C for 10 sec, 50°C for 10 sec, and 72°C 30 sec, followed by 72°C for 5 min. PCR amplicons (312 bp in length) were sequenced by direct sequencing methods.

Virus neutralization tests

Sera from rodents and shrews were heat-inactivated at 56°C for 30 min and twofold serially diluted from 1 : 10 to 1 : 640 at the reaction steps with maintenance medium. Then the diluted serum (12.5 μl) was mixed with an equal volume of maintenance medium, containing 100 $TCID_{50}$ of EMCV. The mixture was incubated at 37°C for 2 h. After incubation, the serum-EMCV mixture was added to the suspension of BHK-21 cells (2×10^4 cells/175 μl) and cultured for 4 days in 96-well plates. Virus back-titration was included in each test to validate input amounts of the virus. The highest serum dilution, which completely inhibited CPE development was adopted to the neutralizing antibody titer, and a neutralizing antibody titer greater than 1 : 30 was considered seropositive according to a previous report [92].

Phylogenetic analysis

The genome sequence of EMCV ZM12/14 was aligned with reference EMCV sequences from GenBank using ClustalW algorithm with default parameters and applied to pairwise sequence identity comparison in CLC Genomics Workbench 20.1. Phylogenetic trees were constructed by the maximum-likelihood (ML) method using models of GTR + G + I for full-length of P1, P2, and P3 and K2 + G for PCR amplicons, as the best fit models, with bootstrap values of 1,000 replicates in the MEGA 10 software [93]. Possible recombination events were searched using the RDP4 software with default settings [94].

Experimental infection of isolated EMCV in laboratory mice

Five-week-old male BALB/c mice were inoculated intraperitoneally with 10^6 $TCID_{50}$ of EMCV. After the inoculation, clinical signs and body weight changes were monitored for 14 dpi. At 14 dpi, heart, brain, spleen, testis, serum, and feces were collected from the mice. The neutralizing antibody titers of the serum were determined, and the viral load of the organs and feces were estimated by qRT-PCR as described above. All animal experiments were performed at the Animal BSL-2 facility of the Research Center for Zoonosis Control of Hokkaido University, which has been certified by The Association for Assessment and Accreditation of Laboratory Animal Care International and followed the basic guidelines for animal experiments of the Ministry of Education, Culture, Sports, Science, and Technology of Japan. All animal experiments were approved by the President of Hokkaido University after review by the Animal Care and Use Committee of Hokkaido University (No. 19-0019).

Results

Virus isolation and genome sequencing

Obvious CPE with cell rounding and detachment was observed in BHK-21 cells inoculated with tissue homogenates from one *M. natalensis* captured in Mpulungu, which showed no macroscopic signs of serious infection. The isolated virus was tentatively named as ZM12/14. Titration assays revealed the infectious titer of ZM12/14 in the culture supernatant reached up to 2×10^9 $TCID_{50}$/ml. High-throughput sequencing and *de novo* assembly with an average contig coverage of 14172.4 allowed the determination of nearly the complete genome sequence of ZM12/14 consisting of a single ORF (6879 bp) encoding a polyprotein, incomplete 5′-UTR (576 bp), and a complete 3′-UTR (120 bp) with poly A tail. The determined sequence of ZM12/14 was deposited in GenBank (accession no. LC585221). BLASTn search revealed the genome sequence of ZM12/14 is the closest to that of EMCV strain M (accession no. M37588). Overall, the EMCV strain ZM12/14 was successfully isolated from a *M. natalensis* in Mpulungu, Zambia.

Sequence comparison and phylogenetic analysis

To investigate the degree of sequence similarity between ZM12/14 virus and EMCV reference strains, pairwise sequence identity was determined based on nucleotide and amino acid sequences of P1, P2, P3, and ORF, as well as 1D, 2C, and 3D (Table 2). The results revealed that the ZM12/14 isolate shared the highest sequence similarity with EMCV-1 strains in any examined regions and specifically P1 and 1D region, which contain the main antigenic determinants located on the capsid protein, ZM12/14 shared 80.7–77.5% nucleotide and 96.2–85.1% amino acid sequence identity in P1, and 82.4–75.5% nucleotide and 92.8–89.8% amino acid sequence identity in 1D with EMCV-1 strains.

ML phylogenetic analysis were also performed based on nucleotide sequences of P1, P2, and P3 region separately (Fig. 4). Virus names and lineages were annotated to the trees according to the previous study [67]. EMCV-4 was not included in the phylogenetic tree, because only a small part of P1 sequence was available. In the ML

trees of P1 and P3, ZM12/14 fell into a cluster of EMCV-1. Meanwhile, topology of P2 indicated that ZM12/14 were segregated from all EMCVs, including EMCV-1, EMCV-2, and EMCV-3. The phylogenetic incongruence led us to conduct an exploratory recombination analysis using RDP4 program based on the alignment of nucleotide sequence of ZM12/14 and other EMCV strains; however, this analysis detected no evidence of recombination in the genome of ZM12/14.

Prevalence of EMCV among wild rodents and shrews in Zambia

RT-PCR and virus neutralization test were performed to investigate EMCV prevalence among wild rodents and shrews in Mpulungu, Solwezi, and Mazabuka. Of the 179 serum samples of wild rodents and shrews, 33 samples (18.4%) were seropositive for EMCV, and 19 of these were positive in both RT-PCR and neutralization tests (3). EMCV genome was detected in samples from Mpulungu and Solwezi, whereas EMCV-seropositive individuals were confirmed in all three areas. Notably, all of the animals that were positive for EMCV genome and/or neutralizing antibodies for EMCV are *M. natalensis*. Most of serum samples that were positive in EMCV neutralization test had high neutralizing antibody titers (≧ 320 in Fig. 5). In addition, these high neutralizing antibody titers were observed in not only RT-PCR-negative samples (n = 14) but also RT-PCR-positive samples (n = 19) (Table 3). All amplicons were subsequently sequenced (accession no. LC585222–LC585240) and the partial 3D sequences were subjected to pairwise sequence comparison and construction of phylogenetic tree (Fig. 6). EMCV strains from Mpulungu and Solwezi shared 86.6–86.3% nucleotide sequence identity and independently formed clusters in EMCV-1, inferring geographic range evolution of EMCV in Zambian *M. natalensis* (Fig. 3).

Experimental infection of isolated EMCV in laboratory mice

It has been reported that EMCV strains isolated from symptomatic pigs and dogs cause various symptoms in laboratory rodents [74,89,95,96]. To investigate the pathogenicity of EMCV isolated from *M. natalensis*, three laboratory mice were experimentally inoculated with ZM12/14. All the inoculated mice did not develop clinical symptoms or significant weight loss during the observation period of 14 days.

After euthanizing at 14 dpi, serum samples were subjected to a neutralization test, and a neutralizing antibody titer of ≥ 260 was observed in all mice. The ZM12/14 genome was detected by qRT-PCR in hearts, brains, spleens, and feces with the wide titer range from 1.1×10^2 to 6.9×10^4 $TCID_{50}$/whole organ (Fig. 7). These results suggested that ZM12/14 causes asymptomatic persistent infection in rodents, which is consistent with the screening results in Zambian *M. natalensis*.

Discussion

Wild rodents are considered to be the natural reservoirs of EMCV. In previous studies, EMCV were isolated from a wide range of wild rodents; including rats *(Rattus spp.*) [97–100], mice (*Mus spp.*) [101,102], squirrels (*Sciurus spp.*) [103], dormice (*Myoxus glis*) [104], water-rats (*Hydromys chrysogaster*) [105], cotton rats (*Sigmodon hispidus*) [106], and spiny rats (*Proechimys guyannensis*) [107]. In South Africa, serological survey of wild rodents in the Kruger National Park revealed that *M. natalensis* showed high seropositivity rates (37.9%); however, further integrated studies of genetic and serological analysis are necessary to understand the distribution and evolution of EMCV [72]. In this study, an EMCV strain named as ZM12/14 was isolated from a wild *M. natalensis*. Thereafter Zambian wild rodents and shrews were screened for EMCV infection by RT-PCR and virus neutralization tests. Because available samples of the wild rodents kept at −80°C were limited, RNAs were extracted from kidneys of Mpulungu rodents and spleens of rodents in Solwezi and Mazabuka for RT-PCR screening, which were examined in a survey of poxviruses, paramyxoviruses, and parvoviruses [91,108,109]. As a result, a high prevalence of EMCV in *M. natalensis* was observed, consistent with the previous report from South Africa [72]. Interestingly, there were a certain number of *M. natalensis*, which had both high neutralizing antibody titer and detectable viral RNA. Wild rodents are considered to be a natural reservoir of EMCV [72–74] and these results provide evidence that *M. natalensis* is a possible reservoir of EMCV in the African continent, including Zambia.

EMCV can infect a wide range of animal species and impact especially on pig production. EMCV causes an acute myocarditis (usually causing sudden death) in young pigs and/or reproductive failure in sows, resulting in economic loss to pig farmers [75–77]. It has been reported that rodents contribute to outbreaks of EMCV in pig farms as transmitters [97,110–112]. Although EMCV infection has not been reported in any other animals in Zambia, this study demonstrated the high EMCV prevalence in Zambian *M. natalensis*, highlighting the possible risk of EMCV infection in other animals, such as pigs. In addition to pigs, EMCV infection can also cause fatal diseases in a wide range of non-livestock species [64–66], including many kinds of non-human

primates [67–69], African elephants (*Loxodonta africana*) [70,71], considered endangered species listed in the International Union for Conservation of Nature and Natural Resources (IUCN) red list. Africa is the only continent in which outbreaks of EMCV have been reported from a population of free-ranging wild animals [72,73], whereas most of the EMCV outbreaks among exotic animals in other areas occurred in zoos. From the perspective of species diversity conservation, EMCV transmission in wild rodents would be considered. Further studies of prevalence of EMCV in pig farms and wild animals should be directed to estimate the risk of EMCV outbreak and the need for rodent control programs in Zambia.

EMCV was initially assumed to consist of a single genotype; however, increasing numbers of EMCV sequence data have revealed high genetic diversity. Recently, EMCV was serologically divided into two groups, (EMCV-1 and 2) [87], that is also accepted by ICTV. It has been proposed that classification of EMCV based on nucleotide sequence should be divided into EMCV-1, 2, 3, and 4, and EMCV-1 subdivided into seven lineages [67]. The group of EMCV-1 to 4 was defined by criteria extrapolating from the genus Enterovirus [113,114]; the same virus types share ≥ 75% nucleotide (> 85% amino acid) identity in 1D region and ≥ 90% amino acid identity in P1 region. In addition, different lineages of EMCV-1 share < 83% nucleotide sequence identity in 1D and < 85% in P1. In accordance with these criteria, ZM12/14 can be assigned to a new lineage H of EMCV-1. Phylogenetic trees of the P1 and P3 region also indicated that ZM12/14 can be classified in EMCV-1, which in consistent with pairwise sequence comparison result; however, the phylogenetic tree of the P2 region showed that ZM12/14 separates from the clade of EMCV-1 and even EMCV-2 and 3 without any recombination evidence (Fig. 4). These results suggest that EMCV in Zambia has a unique evolutional history.

Pathogenicity and tissue tropism of EMCV seemed to vary depending on virus strain and host species; however, detailed information is still unclear. The pathogenicity of EMCV to laboratory mice and rats has been reported to vary from asymptomatic to fatal accompanying encephalitis, myocarditis or diabetes mellitus [115]. Previous studies demonstrated that EMCV strains G424/90 and B279/95 isolated from pigs showing clinical signs caused mainly asymptomatic infection in Wistar rats and BALB/c mice

[83,84]. In contrast, strains NJ08 and BD2 were fatal for laboratory BALB/c mice [89,95,96]. Experimental infection of ZM12/14 to BALB/c mice showed no clinical signs, despite the high neutralizing antibody titer and viral RNA detection in some organs suggesting the establishment of systemic infection (Fig. 7). The pathogenicity of ZM12/14 in pigs and other animals will require further study.

In conclusion, the EMCV strain ZM12/14 isolated from *M. natalensis* in Zambia, had unique phylogenetic features. Given the high detection rate of the EMCV-genome and neutralizing antibody for EMCV in *M. natalensis*, this rodent species may be one of the reservoirs in African countries. Consequently, this study updates the knowledge of the current situation of EMCV in wild rodents in the African continent and highlights the potential risk of EMCV infection in domestic and wild animals and potentially humans in Zambia.

Table 2. Pairwise sequence identity (%) with ZR12/14 virus

Virus	P1		1D		P2		2C		P3		3D		ORF	
	nt	aa	nt	aa	nt	aa	nt	aa	nt	aa	nt	aa	nt	aa
EMCV-1	80.7–77.5	96.2–85.1	82.4–75.5	92.8–89.8	78.3–76.2	87.4–84.3	77.7–75.7	92.0–90.5	79.0–74.9	88.9–84.0	81.3–77.0	90.3–89.1	79.5–76.3	91.1–86.9
EMCV-2	67.8–66.7	75.7–75.6	60.4–59.7	64.3–63.8	72.3–71.6	79.2–77.6	75.6–74.5	89.0–87.4	73.6–72.4	81.7–80.6	75.9–75.8	86.7–86.4	71.2–70.5	79.1–78.3
EMCV-3	74.7	91.1–90.9	71.8–71.5	86.8–86.4	71.3	78.0	75.4–75.3	88.4	72.4	80.9	75.6	86.0	73.3	84.1–84.0
EMCV-4	-	-	65.3–64.8	71.5–71.1	-	-	-	-	-	-	-	-	-	-

nt: nucleotide, aa: amino acid

EMCV-1: NC_001479, AF356822, AF525466, AJ617356, AJ617357, AJ617358, AJ617359, AJ617360, AJ617361, AJ617362, AY296731, DQ288856, DQ464062, DQ464063, DQ517424, DQ835184, DQ835185, EU371993, EU780148, EU780149, EU979545, EU979548, FJ604852, FJ604853, FJ897755, HM641897, JN800421, JN800422, JN800423, DQ294633, JQ864080, KC110082, KC110083, KC110084, KC762214, KF293299, KF598860, KF598861, KF598862, KF598863, KF598864, KF709977, KF771002, KF836386, KF836387, KF836388, KF836389, KF836390, KJ524643, KM269482, KP892662, KU664327, KU955338, KX231802, L22089, L40427, M20167, M22457, M22458, M37588, M54935, M88547, MH191297, X00463, X67502, X74312, X87335, Y15445, Y15448

EMCV-2: JX257003, MN547968

EMCV-3: KC310737, KC310738

EMCV-4: KT944132, KT944133

Table 3. EMCV prevalence in wild rodents in Zambia

	No. of samples[a]				
Neutralization test	+	+	-	-	Total
RT-PCR	+	-	+	-	
Mpulungu					
Mastomys natalensis	5	3	0	19	27
Crocidura hirta	0	0	0	19	19
Crocidura luna	0	0	0	1	1
Rattus rattus	0	0	0	3	3
Aethomys chrysophilus	0	0	0	6	6
Cricetomys gambianus	0	0	0	3	3
Saccostomus sp.	0	0	0	3	3
Squirrel	0	0	0	2	2
Grammomys sp.	0	0	0	1	1
Steatomys sp.	0	0	0	1	1
Gerbilliscus leucogaster	0	0	0	1	1
Subtotal	5	3	0	59	67
Solwezi					
Mastomys natalensis	14	4	0	12	30
Crocidura luna	0	0	0	7	7
Rattus rattus	0	0	0	1	1
Arvicanthis niloticus	0	0	0	1	1
Saccostomys campestris	0	0	0	1	1
Mus minutoides	0	0	0	1	1
Subtotal	14	4	0	23	41
Mazabuka					
Mastomys natalensis	0	7	0	46	53
Crocidura hirta	0	0	0	4	4
Rattus rattus	0	0	0	1	1
Aethomys chrysophilus	0	0	0	5	5
Saccostomus campestris	0	0	0	2	2
Steatomys sp.	0	0	0	2	2
Graphiurus sp.	0	0	0	4	4
Subtotal	0	7	0	64	71
Total	19	14	0	146	179

[a]+; positive, -; negative

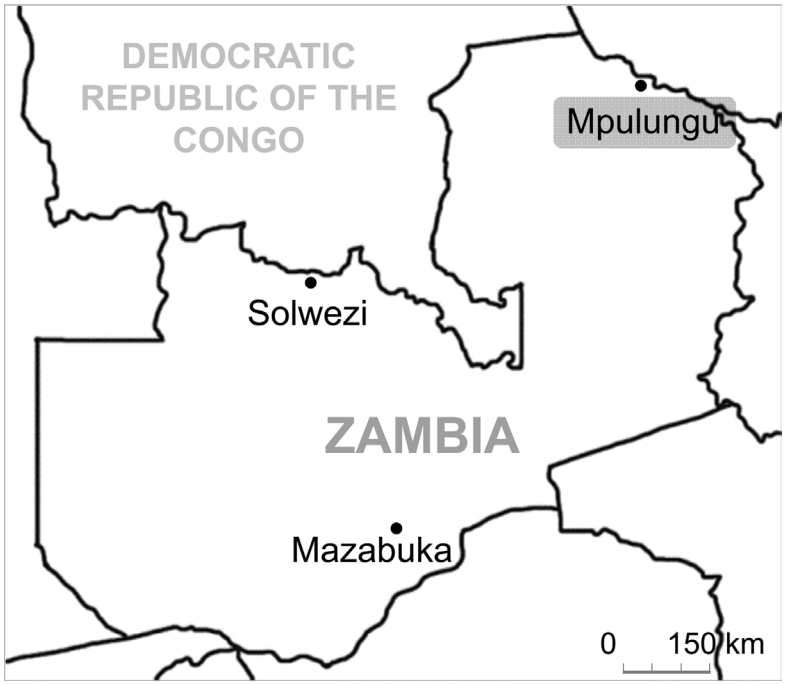

Fig. 3. Map of Zambia showing the locations of rodent sampling

Rodent collections were carried out in Mpulungu (Northern Province), Solwezi (North-Western Province) and Mazabuka (Southern Province). EMCV strain ZM12/14 was isolated from *M. natalensis* collected in Mpulungu area.

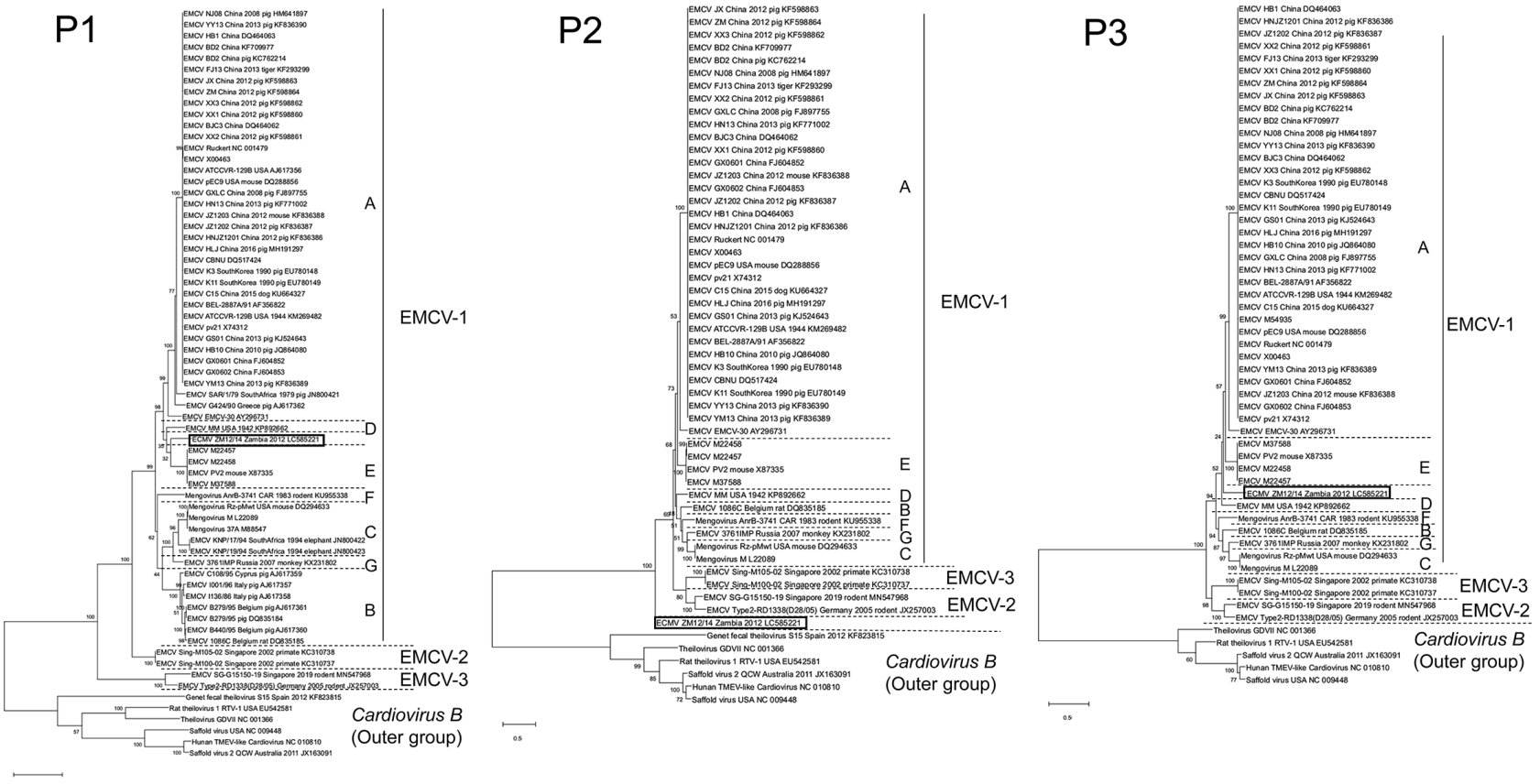

Fig. 4. Phylogenetic analysis of EMCV isolates based on the nucleotide sequence of P1, P2 and P3 regions

The species of Cardiovirus B were included as the outer group. Taxon of EMCV strain ZM12/14 was highlighted in the black square. In addition to serotype EMCV-1 and EMCV-2, EMCV-3 and lineages A–G proposed by Vyshemirskii *et al*. are shown as indicated. Phylogenetic trees were constructed by the ML method using models of GTR + G + I with bootstrap values of 1,000 replicates.

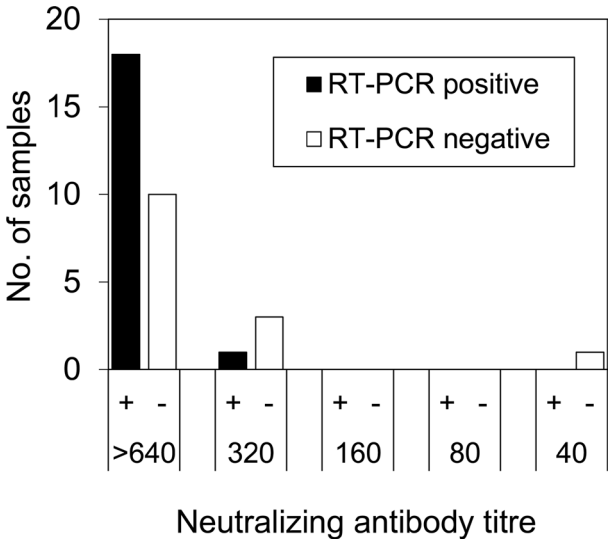

Fig. 5. Distribution of neutralizing antibody titers of *M. natalensis*

Black or white bars indicate RT-PCR-positive or -negative samples, respectively. The titer greater than 1:30 was considered as seropositive. The neutralizing test was performed twice.

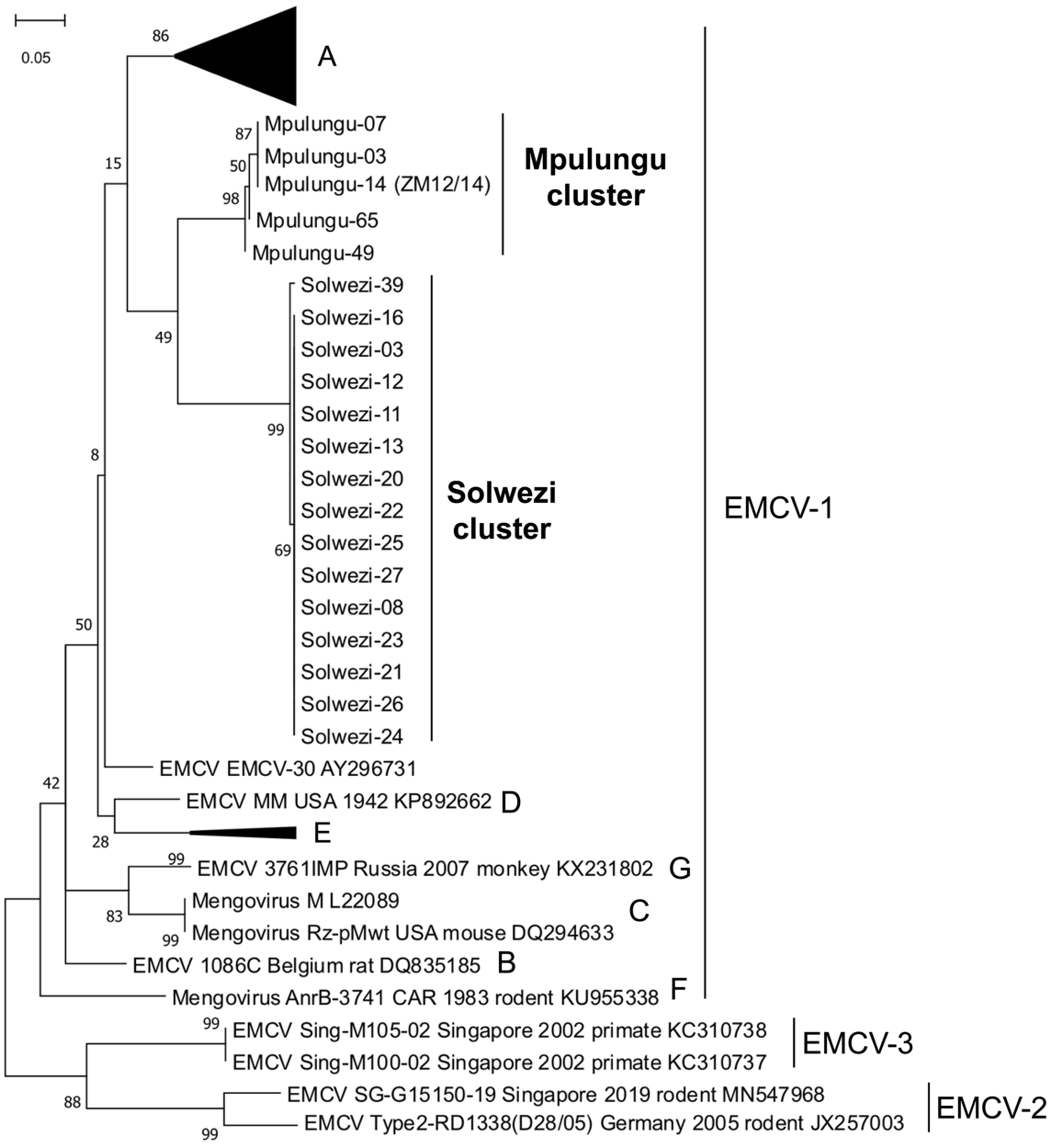

Fig. 6. Phylogenetic analysis of Zambian and reference EMCVs

Phylogenetic trees were constructed based on nucleotide sequences of partial 3D region (277 bp in length) by the ML method using models of K2 + G with bootstrap values of 1,000 replicates. In addition to serotype EMCV-1 and EMCV-2, EMCV-3 and lineages A–G proposed by Vyshemirskii *et al*. are shown.

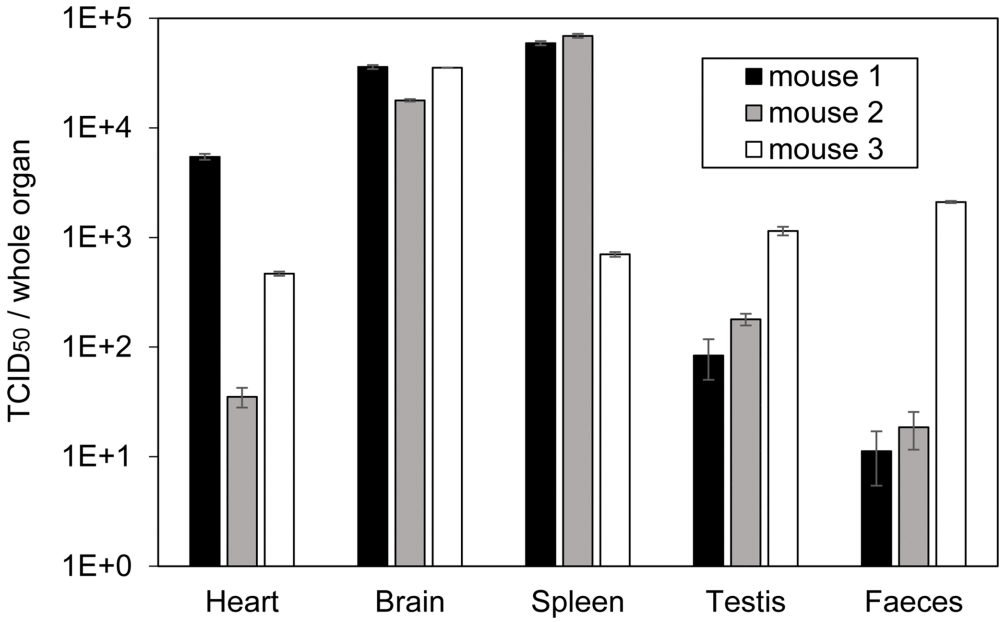

Fig. 7. Viral loads of ZM12/14 in the tissues and feces of challenged mice

The amount of viral RNA in the tissues and feces of BALB/c mice infected with ZM12/14 were determined by RT-PCR (n = 3). The Ct values of viral genome in each sample were converted to $TCID_{50}$ based on the standard curve. The values in the graphs were expressed as mean ± SD of three technical replicates.

Chapter III:
Isolation and characterization of distinct rotavirus A in bat and rodent hosts

Summary

RVA causes diarrheal disease in humans and various animals. Recent studies have identified bat and rodent RVAs with evidence of zoonotic transmission and genome reassortment. However, the virological properties of bat and rodent RVAs with currently identified genotypes remain to be better clarified. Here, virus isolation-based screening for RVA were performed in animal specimens using MA104 cells transduced with TMPRSS2 and TMPRSS11D, which facilitates proliferation of various RVAs, and isolated RVAs (representative strains: 16-06 and MpR12) from Egyptian fruit bat and Natal multimammate mouse collected in Zambia. Whole-genome sequencing and phylogenetic analysis revealed that genotypes of bat RVA 16-06 were identical to that of RVA BATp39 strain from the Kenyan fruit bat, but which has not as yet been characterized. Moreover, all segments of rodent RVA MpR12 were highly divergent and assigned to novel genotypes, but it was phylogenetically closer to bat RVAs than other rodent RVAs, indicating a unique evolutionary history. The virological properties of the isolated RVAs were further investigated. In brief, it was found that 16-06 entered into cells by binding to sialic acids (SAs) on cell surface, while MpR12 entered through a SA-independent manner. Experimental inoculation of suckling mice with 16-06 and MpR12 revealed that these RVAs are causative agents of diarrhea. Moreover, 16-06 and MpR12 demonstrated an ability to infect and replicate in a 3D-reconstructed primary human intestinal epithelium with comparable efficiency to the human RVA. Taken together, these results detail the unique genetic and virological features of bat and rodent RVAs and demonstrate need for further investigation on their zoonotic potential.

Introduction

RVA is the leading cause of diarrheal disease in young animals. In humans, RVA is responsible for > 120,000 deaths/year in infants < 5 years of age and children, mainly in developing countries [116]. Despite the fact that there is no specific treatment for RVA infection, two oral live attenuated vaccines (Rotarix and RotaTeq) have been recommended by the World Health Organization and are available in 114 countries [117]. While these vaccines have reduced the number of hospitalizations and deaths due to RVA infection, atypical RVAs with high genetic diversity and genetic reassortment have been occasionally described and origin of atypical RVAs should be monitored [118,119].

RVA belongs to the family *Sedoreoviridae*, genus *Rotavirus*, which contains 9 species designated *Rotavirus A–Rotavirus J*. The RVA genome consists of 11 dsRNA segments, encoding 6 structural viral proteins (VPs) and 5 or 6 nonstructural proteins (NSPs) in each segment. RVA has a non-enveloped and triple-layered virion, with the outer capsid layer consisting of the spike protein VP4 and the glycoprotein VP7. VP4 and VP7 are traditionally used for genotype-based classification defining the P-genotype and G-genotypes, respectively. Recently, a more comprehensive classification system based on the genotypes of all 11 segments has been proposed by the Rotavirus Classification Working Group (RCWG), defining the genotype constellation (GC) as follows: Gx-P[x]-Ix-Rx-Cx-Mx-Ax-Nx-Tx-Ex-Hx, representing each genotype of VP7-VP4-VP6-VP1-VP2-VP3-NSP1-NSP2-NSP3-NSP4-NSP5, respectively [120,121]. This classification and accumulation of the whole-genome sequence of RVA has facilitated our understanding of both the potential genetic diversity and genome reassortment events in RVA.

While livestock such as pigs and cattle are reported to be a source of zoonotic transmission of RVA to humans, there are limited reports involving wild animals [122–124]. Rodents and bats are the largest and the second-largest order of mammals, comprising about 40% and 20% of all classified mammal species in the world, respectively [125]. In proportion to the number of species, they harbor a range of viruses, including zoonotic pathogens: coronavirus, henipavirus, lyssavirus, and filovirus in bats and hantavirus and arenavirus in rodents [5–11]. As for bat RVAs, more than 30 strains have been identified

worldwide in seven bat families [126–136]. Even though some bat RVA genotypes are solely unique to bats, some genotypes are shared with human and other mammalian RVAs, indicating interspecies transmission and the zoonotic potential of bat-borne RVAs through genome reassortment events [126,129–132,134,136]. There has been considerably less research on rodent RVAs compared to bats. Some strains of mouse RVA were isolated before 1990 and have been used in experimental infections in laboratory mice [137]. According to recent studies in Germany, China, and the USA, more than 15 RVA strains have been detected in wild rodents and shrews [138–141]. Of note, Li *et al.* reported that rodent RVA and human RVA shared the same genotypes in some segments, indicative of local interspecies transmission [138]. Most of these studies were based on genome detection and sequence analysis of RVA. For example, RVAs with bat-specific genotypes have not been isolated, despite the discovery of diverse bat RVAs. Further investigations including virus isolation and investigation of the virological properties of bat and rodent RVAs such as the cellular and host tropisms, transmissibility, and pathogenicity are required to better characterize and confirm the zoonotic potential of animal RVAs.

RT-PCR with consensus primers has been widely used for RVA screening, but viral metagenomics have identified RVAs with diverse genomic sequences, which were not recognized by the screening primer sets [128]. Recent study reported that MA104-T2T11D cells exogenously transduced with human TMPRSS2 and TMPRSS11D, which belong to host TTSPs, promote RVA infection in a trypsin-independent manner [27]. The application of MA104-T2T11D cells for virus isolation offers high-throughput RVA screening in large numbers of field samples. In this study, RVAs with novel GCs were isolated from Zambian wild bats and rodents using MA104-T2T11D cells. Subsequently I investigated the affinity of the identified RVAs for cell surface glycans, pathogenicity in suckling mice, and growth properties in an *ex vivo* model of human small intestinal epithelial cells.

Materials and Methods

Sample collection

A total of 325 fruit bat, 48 rodent, and 24 shrew archived samples collected in Lusaka, Shimabala, and Mpulungu in Zambia from 2012 to 2018 (Fig. 8A and Table 4) were used in the present study. Bats were captured with harp traps, and rodents and shrews were captured with Sherman traps and cage traps. Captured animals were euthanized with diethyl ether, then contents of large intestines were collected and kept at −80°C. Bats were morphologically classified, and rodents and shrews were classified by nucleotide sequence analysis of the mitochondrial cytochrome *b* gene, as described previously [90]. The biological samples were collected under the approval by The Zambia Wildlife Authority, now the Department of National Parks and Wildlife, Ministry of Tourism and Arts, Zambia.

Cells and viruses

Rhesus monkey kidney MA104 cells were maintained in Eagle's minimum essential medium (MEM; Nissui, Tokyo, Japan) supplemented with 10% FBS, 10% tryptose phosphate broth (TPB), and PS. MA104-T2T11D cells were generated using the lentiviral vector system as described previously [27]. Simian RVA SA11 (VR-1565; ATCC, Manassas, VA), human RVA Wa (VR-2018; ATCC) and human RVA DS-1 (VR-2550; ATCC), and bovine RVA Azuk-1 strains were propagated in MA104 cells in serum-free MEM containing 10% TPB, PS, and trypsin (0.5 μg/ml) under rotary conditions. The virus titers were determined by a focus assay as described previously [27].

Virus isolation workflow

Fecal suspensions or intestinal homogenates of bats, rodents, and shrews were centrifuged at 3,000 × *g* for 5 min, and supernatants were filtrated through Vivaclear Mini Centrifugal 0.8 μm filters (Sartorius, Goettingen, Germany). Flow-through was inoculated to MA104-T2T11D cells with 2 ml isolation medium [MEM supplemented with 10% FBS, 10% TPB, PS, 25 μg/ml gentamycin, 1% antibiotic-antimycotic solution (Wako) and 15 mM HEPES] in 15 ml tissue culture tubes (TPP, Trasadingen,

Switzerland). Cells with the inoculum were rotated at 0.3 rpm/min for 7 days. After a single freeze-thaw cycle, part of cell suspension (P1 culture) was blindly passaged in fresh MA104-T2T11D cells. A part of passaged culture (P2 culture) was then pooled and ultracentrifuged at 110,880 × *g* for 2 h with a 20% sucrose cushion, and then pellets were subjected to nucleic acid extraction and next-generation sequencing (NGS) analysis as described below. The remaining P2 culture was used for RT-PCR screening for RVAs identified in NGS analysis. For RT-PCR, total RNA of P2 culture supernatants was extracted using High pure viral nucleic acid kit (Roche, Basel, Switzerland) and subjected to RT-PCR analysis using PrimeScript One Step RT-PCR Kit Ver.2 (TaKaRa Bio). The primer and probe sequences are listed in Table 5. The identified culture supernatants were further passaged in MA104-T2T11D to prepare working virus stocks for subsequent experiments.

Nested RT-PCR screening in bat and rodent feces

Total RNA was extracted from fecal suspensions or intestinal homogenates of bats, rodents, and shrews using High Pure Viral Nucleic Acid Kit. First RT-PCR was performed using SuperScript IV One-Step RT-PCR System (Thermo Fisher Scientific, Waltham, MA) with the following thermal cycling conditions: 50°C for 10 min, 98°C for 2 min, 40 cycles of 98°C for 10 sec, 55°C for 10 sec and 72°C 30 sec, followed by 72°C for 5 min. The first PCR products were subjected to second PCR using Tks Gflex DNA polymerase (TaKaRa Bio) with the following thermal cycling conditions: 98°C for 2 min, 40 cycles of 98°C for 10 sec, 55°C for 15 sec and 68°C 30 sec, followed by 68°C for 5 min. The primer sequences are listed in Table 5.

Transmission electron microscopy

For negative-stain electron microscopy, RVA virions in the culture were pelleted by ultracentrifugation for 2 h at 110,880 × *g* with a 20% sucrose cushion and resuspended in PBS. The concentrated RVAs were fixed with 4% paraformaldehyde, deposited on a nickel grid coated with polyvinyl formal (Nissin EM, Tokyo, Japan) and stained with 2% phosphotungstic acid (pH 5.8). Samples were observed under a transmission electron microscope (H-7650; Hitachi High-Technologies, Tokyo, Japan).

Indirect immunofluorescence assay (IFA)

MA104-T2T11D cells infected with RVA were fixed with 3.7% buffered-formaldehyde and permeabilized with ice-cold methanol. Subsequently, cells were incubated for 1 h with anti-RVA polyclonal antibody (AB1129; Merck) as primary antibody at a 1:500 dilution in PBS with 25% Block Ace (KAC). After washing three-times with PBS, secondary staining was performed with Alexa Fluor 488-conjugated anti-goat IgG antibody (A-11055, Invitrogen: Thermo Fisher Scientific, 1:1,000) and 10 μg/ml Hoechst 33342 (Invitrogen) for 1h. Fluorescence images were captured using a fluorescence microscope IX73 (Olympus, Tokyo, Japan).

Whole-genome sequencing

Viral RNA was extracted from working stocks of 16-06, 16-27, 18-12, and MpR12 using a High pure viral nucleic acid kit, reverse-transcribed into double-strand cDNA by PrimeScript Double Strand cDNA Synthesis Kit (Takara Bio), and then subjected to sequence library construction using Nextera XT DNA Library Preparation Kit (Illumina). The 300 bp paired-end sequencing was performed on an Illumina MiSeq sequencer (Illumina). Sequence reads were trimmed and assembled into contigs by *de novo* assembly using CLC Genomics Workbench 21 (Qiagen). The obtained contigs were analyzed by the BLASTn program (National Center for Biotechnology Information, Bethesda, MD). The 5′- and 3′- terminal sequences of each genome segment were determined using SMARTer RACE 5′/3′ Kit (TaKaRa Bio) with segment-specific primers listed in Table 5. The GCs of isolated strains were assigned based on whole-genome sequences in the Rotavirus A Genotype Determination tool in ViPR (https://www.viprbrc.org/brc/home.spg?decorator=vipr) provided by RCWG [142].

Phylogenetic analysis

The genome sequences of isolated RVAs were aligned with reference RVA sequences from GenBank using the MUSCLE algorithm with default parameters in CLC Genomics Workbench 21. ML trees were constructed using models of GTR + G + I for full-length ORFs of VP1, VP2, VP3, VP4, VP7, NSP1, and NSP2 and GTR + G

for VP6, NSP3, NSP4, and NSP5, as the best fit models, with bootstrap values of 1,000 replicates in the MEGA 10 software [93]. The phylogenetic trees were visualized and annotated in Interactive Tree Of Life version 6.5.2 [143].

Neuraminidase (NA) assays

NA assays were carried out as described previously with slight modifications [144]. Briefly, confluent monolayer MA104-T2T11D cells were pretreated with 200 mU/ml NA from *Vibrio cholerae* (Sigma-Aldrich) in MEM with 25 mM HEPES and 9 mM $CaCl_2$ (pH 6.0) at 37°C for 1 h. Either mock or NA-treated cells were infected with each RVA strain at a MOI of 0.1 (strain SA11 and 16-06) or 1 (strain DS-1 and MpR12) at 37°C for 1 h. After removing the inoculum, cells were cultured for 16 h in the overlay medium (MEM supplemented with 2% FBS and 0.5% methylcellulose). RVA-infected cells and cell nuclei were stained by anti-RVA antibody and Hoechst 33342 as described above, respectively, and counted using a IN Cell Analyzer 2500 (GE Healthcare, Waukesha, WI).

Sialic acid (SA) inhibition assays

SA inhibition assays were carried out as described previously with slight modifications [144]. Briefly, viruses were preincubated with various concentrations of N-acetylneuraminic acid (NeuAc: Wako) or N-glycolylneuraminic acid (NeuGc: Cayman Chemical, Ann Arbor, MI) in 2% FBS MEM with 25 mM HEPES (pH 7.6) for 2 h. The mixture was then added to confluent monolayer of MA104-T2T11D cells at an MOI of 0.1 (strain SA11 and 16-06) or 1 (strain DS-1 and MpR12) at 37°C for 1 h. After removing the inoculum, cells were cultured for 16 h in the overlay medium (MEM supplemented with 2% FBS and 0.5% methylcellulose). RVA-infected cells and cell nuclei were counted as described above.

Experimental infection in suckling mice

All animal experiments were performed following the Regulations on Animal Experimentation in Hokkaido University, and the protocol was approved by the Institutional Animal Care and Use Committee of Hokkaido University (approval no. 20-

0026). Litters of three-day-old BALB/c mice were inoculated orally with 1.0×10^5 focus forming units (FFU) of RVA strain SA11, 16-06, or MpR12 by gavage (n = 7 in each group). Control mice were treated with PBS as a mock-infected group (n = 7). For transmissibility test, one of littermates of three-day-old BALB/c mice were orally inoculated with 1.0×10^5 FFU of RVA strains 16-06, MpR12, and SA11 by gavage (n = 7 in each group). Then infected mice and uninfected littermates were caged together and subjected to subsequent analysis. The conditions of feces were monitored by palpation of the abdomen every day from 0 to 7 dpi. The state of the stool was classified into four categories based on color, texture, and amount of feces according to the criteria used in a previous study: 0, normal feces; 1, exceptional loose feces; 2, loose yellow feces; 3, liquid feces [145]. Stools with a score of ≧1 were considered to be diarrheal stools. Feces, small intestine, and large intestine were collected and suspended in PBS following RNA extraction using TRIzol LS (Thermo Fisher Scientific) and the Direct-zol RNA miniprep kit (Zymo Research). Extracted RNAs were subjected to qRT-PCR analysis using Thunderbird probe one-step qRT-PCR kit (TOYOBO). The primer and probe sequences are listed in Table 5 [146]. Serum for focus reduction neutralization test (FRNT) were collected from suckling mice (n = 3 in each group) at 15 dpi.

Focus reduction neutralization test (FRNT)

After inactivation at 56°C for 30 min, mouse sera were 2-fold serially diluted and thereafter incubated 1:1 with each virus (200 FFU/well) at 37°C for 1 h. The mixtures of sera and virus were the inoculated to MA104-T2T11D cells and cultured for 18 h. The foci were immunostained as described above and counted for neutralizing activity expressed as the dilution factor at which the number of viral focuses was reduced by 50% compared to the no serum control ($FRNT_{50}$).

RVA-infection in a human small intestinal epithelial model

Human EpiIntestinal Small Intestine Tissue Models (SMI-100; MatTek Life Science, Ashland, MA) were maintained with SMI-100 maintenance medium (MatTek) according to the manufacturer's instruction. Subsequently, the apical surface of SMI-100 were infected with 1.0×10^5 FFU of RVA in 100 μl of SMI-100 maintenance

medium. After 6 h incubation, the apical areas of SMI-100 were washed three times with PBS and fed with 100 µl of FBS-free MEM supplemented with 250 µg/ml trypsin in the apical areas. Progeny RVA in the culture supernatants in the apical areas were collected at each time point and titrated by a focus assay. At 72 hpi, RVA-infected SMI-100 was fixed with 3.7% buffered-formaldehyde and subjected to histopathology and immunohistochemistry.

Histopathology and immunohistochemistry

Mouse tissue samples were immersed in 3.7% buffered-formaldehyde and fixed. Then, the fixed tissue specimens were embedded in paraffin. Tissue sections (3 µm) were cut and mounted onto glass slides for either standard hematoxylin and eosin (H&E) staining. Histopathological images were acquired with a slide scanner (SLIDEVIEW VS200, Olympus, Tokyo, Japan). Fixed SMI-100 was embedded in the Tissue-Tek O.C.T. compound (Sakura Finetek Japan, Tokyo, Japan) and frozen at −80°C. Frozen tissue blocks were sectioned at 6 µm in thickness and mounted on CREST coat slides (Matsunami, Osaka, Japan). For histopathological analysis, slides were stained with H&E. For immunohistochemistry, slides were permeabilized with ice-cold ethanol, washed with PBS, and then stained with anti-RVA polyclonal antibody (AB1129; Merck) as primary antibody in PBS with 25% Block Ace. After three washes with PBS, secondary staining was performed with Alexa Fluor 488-conjugated anti-goat IgG antibody (A-11055, 1:1,000), 10 µg/ml Hoechst 33342, and Wheat Germ Agglutinin, Alexa Fluor 594 Conjugate (W11262; Invitrogen, 1:100). Fluorescence images were captured using a fluorescence microscope IX73.

Statistical analysis

Data were represented as the mean ± SD. Area under the curve (AUC) was calculated using Prism 9 (GraphPad Software, San Diego, CA). Statistical analysis was performed by the Student's *t*-test for growth kinetics assay, multiple *t*-tests with the Holm-Sidak method for the NA assay and the neutralizing antibody titers of suckling mice, one-way ANOVA with Dunnett's test for SA inhibition test, and one-way ANOVA with Turkey's test for AUC analysis using Prism 9 (GraphPad Software).

Results

Virus isolation-based RVA screening in wild animals

To identify RVA from numerous samples, virus isolation-based RVA screening were initially employed. Feces or intestinal homogenates from 325 bats, 48 rodents, and 24 shrews in Zambia (Lusaka, Shimabala, and Mpulungu) were individually inoculated into MA104-T2T11D cells and cultured under rotary conditions (Fig. 8A and 8B). After a single blind-passage, the supernatants were pooled and examined for RVA using NGS (Fig. 8B). Based on the RVA sequences identified from the NGS data, I designed specific primers and screened each culture supernatant to identify the RVA. As a result, three strains of bat RVA named as 16-06, 16-27, and 18-12 were isolated from Egyptian fruit bats (*Rousettus aegyptiacus*) which were captured in Shimabala and Lusaka. Additionally, one rodent RVA strain named as MpR12 was isolated from Natal multimammate mouse (*M. natalensis*) which was captured in Mpulungu (Table 4 and Fig. 8A). After virus isolation, the prevalence of the isolated RVA strains were investigated by RT-PCR with general screening primers and specifically designed primers for the isolated strains [147]. The RVA genome was detected exclusively from virus isolation-positive samples (Table 4).

Since the three bat-derived RVA strains showed high nucleotide sequence identities (93.5–100% in each ORF; Table 6), 16-06 was chosen as a representative strain for subsequent analyses. Expression of antigens of 16-06 and MpR12 was validated by IFA with an anti-RVA polyclonal antibody (Fig. 8C). Negative-stain electron microscopy identified 80–90 nm virus particles with wheel-like structures in the culture supernatants of the RVA-inoculated cells, which is the typical morphology of the RVA virion (Fig. 8D). To characterize growth property of the isolated strains, progeny virus titers in the supernatants were determined. Both 16-06 and MpR12 could be propagated in MA104-T2T11D cells, and the growth properties under rotary culture conditions were higher than those under static culture conditions (Fig. 9A). Notably, MpR12 showed limited growth in static culture, which is consistent with the growth characteristics of other RVA strains [148]. To determine trypsin dependency of the isolated strains, virus titers were examined at 48 hpi in MA104 in the presence or absence of

trypsin (Fig. 9B). Both 16-06 and MpR12 showed enhanced viral proliferation in a trypsin dose-dependent manner in MA104 cells (Fig. 9B). The virus titers of RVAs in MA104-T2T11D cells at 48 hpi were significantly higher than those in MA104 cells in the absence of trypsin (Fig. 9B). 16-06, MpR12, and Wa induced foci consisting of multiple cells in MA104-T2T11D cells but not in MA104 cells as described previously (Fig. 9C) [27]. The focus sizes formed by Wa and 16-06 were larger than those by MpR12 (Fig. 9C). These results indicate that the isolated 16-06 and MpR12 strains have different growth properties in MA104-T2T11D cells. In summary, infectious RVAs were successfully isolated from three Egyptian fruit bats and one Natal multimammate mouse from Zambia.

Whole-genome sequencing and phylogenetic analysis of isolated RVAs

The complete ORF sequences of all isolated RVAs (16-06, 16-27, 18-12, and MpR12) were obtained by *de novo* assembly of NGS sequence reads. In addition, the 5′- and 3′-UTRs of 16-06 and MpR12 were sequenced by rapid amplification of the cDNA end (RACE) method to determine the complete genome sequence. Both 16-06 and MpR12 had the typical genome size and structure of RVA with the terminal sequences of the 5′- and 3′-UTRs broadly conserved. (Table 7) [149]. Similar to other RVAs, 16-06 and MpR12 also encode nsp5 and nsp6 in the segment 11. The genome sequences of 16-06 and MpR12 were assessed with the Rotavirus A Genotype Determination tool to determine the GCs (Table 8) [142]. The GC of 16-06 was G36-P[51]-I16-R22-C20-M20-A31-N22-T22-E27-H22; consisting of recently approved new genotypes and completely identical to that of RVA/Bat-wt/KEN/BATp39/2015/G36P[51] (BATp39), which is deposited as a bat RVA from *R. aegyptiacus* in GenBank but has not yet been published (Fig. 10A). In contrast, all segments of MpR12 showed high nucleotide sequence diversities with known RVAs, falling below the cut-off values for genotype assignment [120]. Through consultation with RCWG, MpR12 was assigned to a new GC, G41-P[57]-I31-R27-C23-M23-A38-N27-T27-E31-H27 consisting of new genotypes (Fig. 10A). Finally, based on the nomenclature guideline of RCWG, the four isolated strains were formally named as RVA/Bat-tc/ZMB/16-06/2016/G36P[51] (GenBank accession nos. LC704642–LC704652), RVA/Bat-tc/ZMB/16-27/2016/G36P[51]

(GenBank accession nos. LC704653–LC704663), RVA/Bat-tc/ZMB/18-12/2018/G36P[51] (GenBank accession nos. LC704664–LC704674), and RVA/MultimammateMouse-tc/ZMB/MpR12/2012/G41P[57] (GenBank accession nos. LC638698–LC638708) [121]

To estimate potential reassortment events, GCs of the isolated strains were compared to those of genetically and geographically related strains. RVA/Bat-wt/ZMB/ZFB14-126/2014/GxP[x] (ZFB14-126) was detected in *R. aegyptiacus* in Zambia, and it was shown this has the same E27 genotype as 16-06 with 87.7% nucleotide identity (Fig. 10A). ZFB14-126 has the I22 and T17 genotypes detected in *Eidolon helvum*-derived RVA from Zambia and Cameroon [133]. In addition, RVA/Human-tc/KEN/B10/1987/G3P[2] (B10) originally detected in a human from Kenya has the same I16 genotype as 16-06 with 87.4% nucleotide identity (Fig. 10A). B10 shows SA11-like GC in segments other than VP1, VP6, and NSP4. These data suggest that ZFB14-126 and B10 may have a reassortment history involving the ancestor of 16-06 and other strains, while complete genotype constellation of ZFB14-126 remains to be determined.

Next, phylogenetic analysis were performed based on the isolated RVA strains with other bat-derived, rodent-derived, and type strains of each genotype. In VP7, 16-06 and other members of genotype G36 formed a single cluster with other bat RVAs assigned to genotype G25 (Fig. 10B). Similar tree topologies were observed in VP4, VP1, VP6, NSP1, NSP2, and NSP4 (Fig. 10C and 11). In contrast, 16-06 and other members of genotypes C20, M20, T22, and H22 segregated away from bat-specific genotypes and were phylogenetically closer to other mammalian RVAs in the VP2, VP3, NSP3, and NSP5 trees, respectively (Fig. 11). The observed phylogenetic incongruence could be due to: (i) evidence of interspecies transmission and reassortment in the ancestor of 16-06 or (ii) potential lack of sequence data from undiscovered RVAs to fill gaps to the full phylogenetic tree. On the other hand, MpR12 formed distinct lineages to known RVAs and may have arisen from a closer common ancestor with bat RVA, but not any known rodent RVAs in all segments except NSP1 (Fig. 10B, 10C, and 11), highlighting the unique evolutionary history of MpR12.

Glycan binding specificity of isolated RVAs

RVA initiates infection *via* interaction between the VP8* domain of VP4 and cell-surface glycans including SAs or histo-blood group antigens [150]. Liu *et al*. grouped RVAs into five genogroups (P[I] to P[V]) based on the amino acid sequence of VP8*, and showed that the glycan-binding property restricts the host specificity of RVAs [151,152]. To investigate the glycan-binding of the isolated RVAs, phylogenetic trees were constructed based on the amino acid sequence of the VP8* region (Fig. 12A). In the tree, almost all P-genotypes were assigned into P[I] to P[V] genogroups. RVAs 16-06, 16-27, 18-12, and MpR12 were classified into the cluster of P[I] genogroup with other known bat and rodent RVAs. The isolated RVAs diverged from the ancestor of the SA-dependent RVA group, consisting of P[1], P[2], P[3], and P[7] genotypes (Fig. 12A). Accordingly, the conserved amino acid residues responsible for the interaction with glycans were investigated based on the amino acid sequence alignment of VP8* (Fig. 12B). The residues interacting with SAs existed in VP8* of 16-06, 16-27, and 18-12 but not in that of MpR12, suggesting a different SA-affinity of VP8* between the bat-borne and rodent-borne RVAs employed in this study. Amino acid sequence alignment of VP8 from MpR12 and other rodent RVAs showed that conserved residues for the interaction with SA were not conserved in MpR12 (Fig. 12C).

To obtain direct evidence for SA-dependency of the isolated RVAs, I investigated whether the enzymatic removal of SAs might decrease the infectivity of the RVAs. NA removes the terminal SAs from cell-surface glycans by cleaving the glycosidic bond of neuraminic acids and decreases SA-dependent infection of RVAs [144,153]. The SA-dependent SA11 strain in P[I] genogroup were included in this assay as a positive control [152]. Both Wa and DS-1 were clustered in non-SA dependent P[II] genogroup, but Wa binds to internal SA in the sugar chain and is sensitive to NA treatment [154]. Thus, DS-1 strain was selected as a negative control. Cell treatment with NA reduced the infectivity of 16-06 and SA11, but not that of MpR12 and DS-1 (Fig. 13A and 13B). This observation was consistent with the presence of amino acid sequences in VP8* (Fig. 12A and 12B). Next, the neutralizing activity of SAs against RVAs using NeuAc and NeuGc was examined. The monosaccharides NeuAc and NeuGc were individually preincubated with 16-06, MpR12, SA11, and DS-1 prior to

infection. The infectivity of 16-06 and SA11 was reduced in a dose-dependent manner by NeuAc and NeuGc (Fig. 13C and 13D). Taken together, these data highlighted the different binding specificity to SAs between 16-06 and MpR12.

Pathogenicity of isolated RVAs in suckling mice

To assess the infectivity and pathogenicity of the isolated bat and rodent RVAs, three-day-old suckling mice were employed as an experimental model. The mice were inoculated orally with RVA strains 16-06, MpR12, or SA11 (n = 7 in each group). SA11 was used as a control RVA that causes diarrhea in suckling mice [155,156]. The mock group was inoculated with PBS as a control. None of suckling mice in each group died from 0 dpi to 7 dpi. None of the mock-treated mice developed diarrhea during the observation period, while mice inoculated with RVA strains 16-06, MpR12, and SA11 developed diarrhea from 1 to 5 dpi (Fig. 14A). SA11, 16-06, and MpR12 caused diarrhea in suckling mice with 100% morbidity (Fig. 14A). The disease severity score of diarrheas reached peak levels at 2–3 dpi in 16-06- and MpR12-infected mice, but the scores were lower than that of SA11-infected mice (Fig. 14B). Viral RNA copy number in feces and intestines were quantified using specific qRT-PCR assay for each strain with comparable detection sensitivity and amplification efficiency (Fig. 15). Viral RNA shedding was peaked at 1 dpi and continuously detected with a gradual decrease in the feces of 16-06-, MpR12-, and SA11-infected mice up to 7 dpi (Fig. 14C). We could not obtain feces from individual suckling mice after 7 dpi because they recovered from diarrhea. To estimate cumulative diarrheal severity and viral RNA shedding of infected mice, AUC was calculated based on the diarrheal score and viral RNA copy number in feces from each mouse. Mice inoculated with Wa and 16-06 displayed comparable cumulative diarrheal severity and viral RNA shedding, whereas MpR12 showed attenuated virulence in mice (Fig. 14D). Consistent with viral RNA in feces, the amount of viral RNA in small intestines of infected mice was peaked at 1 dpi and gradually decreased until 5 dpi, while the decrease of viral RNA signals was not clearly observed in large intestines (Fig. 14E). Histopathological analysis revealed focal histopathological changes which is vacuolization in the enterocytes lining most of the surface of the villi with increased inflammatory cell infiltrates into the lamina propria in

the small intestine of SA11-, 16-06-, or MpR12-infected mice (Fig. 14F) [145,157]. Particularly in the small intestine of SA11-infected mice, degeneration of surface epithelium was noted. In contrast, these histopathological changes were not observed in the those of animals in control group (Fig. 14F). To confirm the infection with RVAs in suckling mice, neutralizing antibody titers in mouse sera were examined at 15 dpi by FRNT. All mice developed neutralizing antibodies against the inoculum strains (Fig. 14G). In addition, transmissibility of the isolated strains from infected suckling mouse to uninfected littermates was examined. Compared with oral administration, cohabitation infection caused mild diarrhea and RNA shedding in suckling mice (Fig. 16). These data indicated that oral administration of 16-06 and MpR12 caused diarrheal disease and viral shedding in suckling mice, and MpR12 has attenuated growth and pathogenicity compared with 16-06 and SA11 in mice.

Infection and growth of isolated RVAs in a human small intestinal epithelial model

I next examined the infectivity of 16-06 and MpR12 in the *ex vivo* model of human small intestinal epithelium, SMI-100. SMI-100 is 3D-reconstructed from human primary intestinal epithelial cells and exhibits a tissue structure similar to small intestinal tissues [158]. The human RVA Wa strain, 16-06, and MpR12 were inoculated on the apical area of SMI-100 to mimic the infection from the luminal side of the intestine. The Wa strain was selected as a positive control because it has been employed in other studies of *ex vivo* infection models of RVA [159,160]. The titers of 16-06 and MpR12 in culture supernatants increased in a time-dependent manner and reached over 10^7 FFU/ml at 72 hpi (Fig. 17A). The growth curve of 16-06 was higher than that of Wa, whereas MpR12 exhibited a growth efficiency comparable to Wa. AUC of the viral titers in the culture supernatants of each SMI-100 culture insert shows that 16-06 produced progeny virus with significantly higher titer than MpR12 and Wa (Fig. 17B). Histopathological analysis showed acidophilic dead cells containing fragmented nuclei on the apical surface of SMI-100 infected with 16-06, MpR12, and Wa (Fig. 17C). Immunohistochemistry identified RVA antigen signals in the enterocytes located at the villus tips and detached cells from the apical surface at 3 dpi with 16-06, MpR12, and

Wa (Fig. 17D). These data demonstrated the ability of 16-06 and MpR12 to infect and replicate in the human intestinal epithelium.

Discussion

Recent advances in virus genome detection methods and RVA genotype classification have revealed the great diversity of animal RVAs and led to the identification of multiple new genotypes. However, most RVAs belonging to the new genotypes were identified from genomic RNA, and not from isolated infectious viruses or subjected to subsequent virological characterization [126,129–132,134,136,138]. There are two difficulties in the detection and isolation of RVA from wild animals. The first is that the large sequence diversity of the RVA genome hampers RT-PCR with broadly reactive consensus primers. A viral metagenomic approach is one of the practical strategies to identify diverse RVA strains with low sequence similarities to known RVA strains, but this method is not suitable for screening animal RVAs with large number of specimens considering the low prevalence rate of RVA in wild animals (< 10%) [136,138]. The second is the protease-dependent infectivity of RVA. RVA-inoculated cells are usually maintained in a serum-free medium supplemented with trypsin to cleave and activate viral spike protein VP4, which is essential for RVA entry [149]. However, some inocula, such as feces, show toxicity to cells under serum-free conditions. To overcome this limitation, I employed virus isolation-based RVA screening using MA104-T2T11D cells and successfully isolated three strains of bat RVA and one strain of rodent RVA (Fig. 8). The RVA isolation rate of *R. aegyptiacus* was 0 to 9.1% and that of *M. natalensis* was 3.6% (Table 4), which is consistent with the RVA genome positive rate in wild animals reported in previous studies [136,138]. Therefore, virus isolation-based RVA screening offers an alternative approach to conventional RT-PCR for large-scale and sensitive RVA detection from specimens of animals and humans, especially atypical RVAs with previously unrecognized genotypes.

Bat RVA 16-06 isolated in this study has the same GC (G36-P[51]-I16-R22-C20-M20-A31-N22-T22-E27-H22) as bat RVA strain BATp39 (Table 8). According to GenBank, the genome sequence of BATp39 was detected from *R. aegyptiacus* in Kenya in 2015; however, detailed information on the BATp39 strain is lacking at present. The identification of bat RVAs with the same GC from *R. aegyptiacus* in Kenya and Zambia indicates that this GC could be widespread in East Africa. The GC analysis also revealed evidence of genome reassortment between ancestors of bat-derived RVAs and

the atypical human RVA strain B10 (Fig. 10A). Notably, glycan-binding analysis suggests that 16-06 as well as SA11 recognize both human and animal-type SA, NeuAc and NeuGc (Fig. 12) [161]. It has been reported that the property of glycan-binding is involved in the host specificity of RVA [151,152]. Simsek *et al*. have identified SA11-related RVA in Gabonese bats, suggesting a multi-species host range of SA11-related RVAs [136]. The similarities in sugar chain utilization of 16-06 and SA11 raise the question whether 16-06 and relative RVAs are bat-specific or cross-species transmissible viruses.

To date, RVAs have been detected in wild rodents (*Mus* sp., *Rattus* sp., *Niviventer* sp., and *Apodemus* sp. in the family Muridae) in Germany, China, and the USA [138–141]. Due to the limited number of rodent RVAs identified, little is known about the genetic diversity and evolution of rodent viruses. MpR12 is the first rodent RVA detected from Natal multimammate mouse (*M. natalensis*). While *Mastomys* sp. is phylogenetically close to *Mus* sp. and *Niviventer* sp. [162], the phylogenetic analysis revealed that MpR12 was more related to bat RVA rather than other rodent RVAs (Fig. 10B, 10C and Fig. 11). In addition, all segments of MpR12 were distinct from any other RVAs and were assigned to novel genotypes. The origin and evolution of MpR12 remains to be elucidated.

The potential infectivity of some bat and rodent RVAs to humans has been speculated based on the detection of reassortment between these RVAs and human RVAs, but the zoonotic potential of bat and rodent RVAs needs to be further investigated [126,129–132,134,136,138]. Recently, human intestinal enteroids have been used as a cellularly diverse and physiologically relevant models for human RVA infection [159]. Here, a 3D-reconstructed human small intestinal epithelium, SMI-100, was used as an alternative *ex vivo* model to assess the infectivity of the isolated RVA strains to the human gut. SMI-100 was susceptible to infection by 16-06 and MpR12 and permitted growth at levels similar to human RVA (Fig. 17). Few cell lines, such as monkey kidney derived-MA104 and CV-1, have the capacity to propagate RVA infection. To the best of our knowledge, this is the first study to use SMI-100 for RVA infection, and this appears to be a relevant and reliable tool to study multiple aspects of RVA infection in the human gut.

A limitation of this study is the lack of direct evidence for the zoonotic potential of the isolated RVA strains. Some animal RVA can actively propagated even in human organoids but does not cause disease in human, because the host range of RVA is affected by a wide range of factors, including age and sex of the host, accessibility of susceptible cells, immune response [144]. RVA surveillance of human in Zambia have not detected RVA with genotypes reported in this study, as human RVAs with typical genotypes are the main targets of the surveillance [163–166]. To clarify the zoonotic transmission of RVA between humans and wild animals, further surveillance should be conducted on human clinical samples in Zambia.

In conclusion, novel bat and rodent RVA strains were isolated by virus isolation-based RVA screening. Furthermore, whole-genome analysis, glycan utilization analysis, experimental inoculation in suckling mice, and infectivity in a human small intestinal epithelial model enabled characterization of the unique virological properties of the isolated RVAs and have highlighted their zoonotic potential.

Table 4. Sample information and the results of virus isolation

	Species	Place	Year	Virus isolation positive/total	RT-PCR screening positive/total	Isolated strain
Bat	*Rousettus aegyptiacus*	Lusaka	2014	0/10	0/10	
			2015	0/178	0/178	
		Shimabala	2016	1/11 (9.1%)	1/11 (9.1%)	16-06
		Lusaka	2016	1/20 (5.0%)	1/20 (5.0%)	16-27
			2017	0/61	0/61	
			2018	1/45 (2.2%)	1/45 (2.2%)	18-12
Rodent	*Mastomys natalensis*	Mpulungu	2012	1/28 (3.6%)	1/28 (3.6%)	MpR12
	Other rodent species [a]			0/20	0/20	
Shrew	*Crocidura hirta*			0/23	0/23	
	Crocidura luna			0/1	0/1	

[a] Other rodents species contain *Aethomys chrysophilus*, *Rattus rattus*, *Cricetomys gambianus*, *Saccostomus* sp., *Steatomys* sp., *Grammomys* sp., *Gerbilliscus leucogaster*, and squirrels.

Table 5. Primers and probes used in this study

Assay	Target strain	Name	Type[a]	Sequence (5'-3')	Reference
RT-PCR	16-06, 16-27, 18-12	VP1 p39-like-F2	F	TAGTCACATGGGCAAACTCTGCAA	this study
		VP1 p39-like-R2	R	AACCCAACATGAAAGGACCACGA	
	MpR12	RotaA-MpR-F	F	CGCTGCTCTTGACCAACTTA	this study
		RotaA-MpR-R	R	CCTAGTTACGTCTCCGTAGGATAG	
qRT-PCR	SA11	SA11_F	F	TAACGCACCAGCCAATATACA	this study
		SA11_R	R	CGCGTCTGGTAGAAGAGTTATC	
		SA11_P	P	FAM-AGCATATTGTGCCACTCCGAAGAGT-BHQ	
	16-06	16-06_F	F	AGAAATTCAGGTTGCAGGATTTG	this study
		16-06_R	R	TATTAACGCTCCGGCCAACACACA	
		16-06_P	P	FAM-GCAGTCGTTAGAACTCGTCTTAG-BHQ	
	MpR12	MpR12_F	F	CAAAGTAGGAGGCAACGTACA	this study
		MpR12_R	R	TTGAACAGATCGCAACCGCAACAC	
		MpR12_P	P	FAM-GTAAGCCACATGGTACCCATTA-BHQ	
nested RT-PCR	16-06, 16-27, 18-12, MpR12	ZMB-RVA-VP7-170F	F	AATYTACCRATAACAGGYTCAATGG	this study
		ZMB-RVA-VP7-861R	R	TTGCCACCATTTYTTCCAGTTC	
		ZMB-RVA-VP7-254F	F	ATCCAACRGAAGCTAARACYGA	
		ZMB-RVA-VP7-778R	R	CGGCACCWCCYACTTGWATTAC	
RT-PCR	General	VP6screen-F	F	GACGGVGCRACTACATGGT	Gómara *et al.*
		VP6screen-R	R	GTCCAATTCATNCCTGGTG	
RACE	16-06	16-06_VP1_5'RACE	GSP	GATTACGCCAAGCTTCTGTTATATCCGCAACCAGCGCTTG	this study
		16-06_VP2_5'RACE	GSP	GATTACGCCAAGCTTCGTCTGTTTTTTCGCTTGCTCCG	
		16-06_VP3_5'RACE	GSP	GATTACGCCAAGCTTGTCCTTGCGTCATAATACCATTACAGCC	
		16-06_VP4_5'RACE	GSP	GATTACGCCAAGCTTGCTCCACCGATGTGACGTTTGG	
		16-06_NSP1_5'RACE	GSP	GATTACGCCAAGCTTCAGTCTGCTGTATGTAAACATTCTGCGC	
		16-06_VP6_5'RACE	GSP	GATTACGCCAAGCTTCAATTCCGTTGCGCTGAGACTCTC	
		16-06_NSP3_5'RACE	GSP	GATTACGCCAAGCTTCTTTCCGGGCACCCTTTTGACA	
		16-06_NSP2_5'RACE	GSP	GATTACGCCAAGCTTGCTTCGCAAACTAATGAAGCCACC	
		16-06_VP7_5'RACE	GSP	GATTACGCCAAGCTTGAGCCAGTTGGCCAACCTTTTGTC	
		16-06_NSP4_5'RACE	GSP	GATTACGCCAAGCTTCCTGTCCATTTGCTGTTCCATCAC	
		16-06_NSP5_5'RACE	GSP	GATTACGCCAAGCTTCGACTTGATCACATCCAACGCTG	
		16-06_VP1_3'RACE	GSP	GATTACGCCAAGCTTCACTTGGAGTGCCTAAGATCGACGC	

	16-06_VP2_3'RACE	GSP	GATTACGCCAAGCTTGTTGGAGCTTTGCCCTTCAATACG		
	16-06_VP3_3'RACE	GSP	GATTACGCCAAGCTTCAGACAACATGGTACCTGATGTGGTTG		
	16-06_VP4_3'RACE	GSP	GATTACGCCAAGCTTCAAGCACCACAGGTGTGTACCGA		
	16-06_NSP1_3'RACE	GSP	GATTACGCCAAGCTTGAACGCGTCTGTTAGCCAAGAACATC		
	16-06_VP6_3'RACE	GSP	GATTACGCCAAGCTTTCCTTCCAGCTTATGCGTCCACC		
	16-06_NSP3_3'RACE	GSP	GATTACGCCAAGCTTGCTCGGAAAGTAAATGAGACCGTGC		
	16-06_NSP2_3'RACE	GSP	GATTACGCCAAGCTTGCTGCAATCACGCATGGTAAAGG		
	16-06_VP7_3'RACE	GSP	GATTACGCCAAGCTTGCGACATTTGAAGAAGTAGCAACCG		
	16-06_NSP4_3'RACE	GSP	GATTACGCCAAGCTTGTTCCAACAGCAAAAATGGCGTTC		
	16-06_NSP5_3'RACE	GSP	GATTACGCCAAGCTTATGCAGATGCTGGTGTATCTATGGACTC		
MpR12	MpR12_VP1_5'RACE	GSP	GATTACGCCAAGCTTGGATTCAGTGAACAGATCTCGAGTCAGC	this study	
	MpR12_VP2_5'RACE	GSP	GATTACGCCAAGCTTTTGGTAGCTGCTTTGGTTCGAATATTC		
	MpR12_VP3_5'RACE	GSP	GATTACGCCAAGCTTGTAGACAAGTCTCCATCCAGGAAGCATG		
	MpR12_VP4_5'RACE	GSP	GATTACGCCAAGCTTTGCGGATAAATTCGGTTCCAGTAGTACTG		
	MpR12_NSP1_5'RACE	GSP	GATTACGCCAAGCTTCTGACAAGGTAATTGGCAAGAGTAGCTG		
	MpR12_VP6_5'RACE	GSP	GATTACGCCAAGCTTTTACGTAACGCATCGGACTGAGGC		
	MpR12_NSP3_5'RACE	GSP	GATTACGCCAAGCTTCCCGCATCTTCTGATCAATTCCC		
	MpR12_NSP2_5'RACE	GSP	GATTACGCCAAGCTTGATTGTTACGTGAACGCAGCACAAG		
	MpR12_VP7_5'RACE	GSP	GATTACGCCAAGCTTGAGAAAGTGTATCTGTCCACGTTGCGTC		
	MpR12_NSP4_5'RACE	GSP	GATTACGCCAAGCTTTTCTGTCTGTTTCTCTCTCAAATTCCCC		
	MpR12_NSP5_5'RACE	GSP	GATTACGCCAAGCTTGGAGTTCTCTCCAGAACGTGAATCCG		
	MpR12_VP1_3'RACE	GSP	GATTACGCCAAGCTTCTTTGGGTGTCCCACAAATAGATGCTG		
	MpR12_VP2_3'RACE	GSP	GATTACGCCAAGCTTGGCGCATTGCCATTTATTACCG		
	MpR12_VP3_3'RACE	GSP	GATTACGCCAAGCTTCCACATTTGACATTGGGAGTGTTGTAC		
	MpR12_VP4_3'RACE	GSP	GATTACGCCAAGCTTCCGGATATCGTTACTGAGGCTTCGG		
	MpR12_NSP1_3'RACE	GSP	GATTACGCCAAGCTTGATCCGCAATTAGTTCAGGGTGTG		
	MpR12_VP6_3'RACE	GSP	GATTACGCCAAGCTTCATGCAGTCGTTGGCGTCACTC		
	MpR12_NSP3_3'RACE	GSP	GATTACGCCAAGCTTGGATTGCTGCTGCATGCTCATC		
	MpR12_NSP2_3'RACE	GSP	GATTACGCCAAGCTTCAACTGATGCCAATCACCGATCC		
	MpR12_VP7_3'RACE	GSP	GATTACGCCAAGCTTCACATTCGAAGAGGTTGCTACTGCTG		
	MpR12_NSP4_3'RACE	GSP	GATTACGCCAAGCTTCGGATCACGCACCACTAGCTATACTTG		
	MpR12_NSP5_3'RACE	GSP	GATTACGCCAAGCTTCGTTTCGATGGATGCATCAACG		

[a]F; forward primer, R; reverse primer, P; probe, GSP; gene specific primer

Table 6. Nucleotide sequence similarity (%) of Bat RVA isolated in this study

		16-27	18-12
16-06	VP1	99.94	97.52
	VP2	99.96	96.71
	VP3	99.84	95.56
	VP4	99.83	94.72
	VP6	99.92	96.82
	VP7	99.59	93.48
	NSP1	99.76	96.92
	NSP2	99.79	97.27
	NSP3	99.89	95.93
	NSP4	99.81	97.54
	NSP5	100	97.99

Table 7. Molecular characteristics of genome segments of isolated RVA

Strain	Segment	Accession no.	Coding protein	Length (bp)			Terminal sequence	
				3′-UTR	ORF	5′-UTR	3′-UTR	5′-UTR
16-06	1	LC704642	VP1	18	3267	17	GGCUAUU	UGUGACC
	2	LC704643	VP2	16	2727	28	GGCUAUU	UAUGACC
	3	LC704644	VP3	49	2502	38	GGCUAUA	UGUGACC
	4	LC704645	VP4	11	2331	21	GGCUAUU	UGUGACC
	5	LC704646	NSP1	33	1686	88	GGCUUUU	UGUGACC
	6	LC704647	VP6	23	1194	139	GGCUUUU	UGUGACC
	7	LC704648	NSP3	34	933	102	GGCAUUU	UGUGACC
	8	LC704649	NSP2	46	954	59	GGCUUUU	UGUGACC
	9	LC704650	VP7	48	981	46	GGCUUUA	UGUGACC
	10	LC704651	NSP4	41	528	182	GGCUUUU	UGUGACC
	11	LC704652	NSP5 NSP6	21	597 279	49	GGCUUUU	UGUGACC
MpR12	1	LC638698	VP1	18	3264	17	GGCUAUU	UAUGACC
	2	LC638699	VP2	17	2676	29	GGCUAUA	UGUGACC
	3	LC638700	VP3	49	2517	34	GGCUAUU	UGUGACC
	4	LC638701	VP4	9	2328	21	GGCUAUA	UGUGACC
	5	LC638702	NSP1	10	1497	79	GGCUUUU	UGUGACC
	6	LC638703	VP6	23	1194	138	GGCUUUU	UGUGACC
	7	LC638704	NSP3	34	936	95	GGCAUUU	UGUGACC
	8	LC638705	NSP2	46	954	62	GGCUUUU	UAUGACC
	9	LC638706	VP7	47	981	28	GGCUUUA	UGUGACC
	10	LC638707	NSP4	40	558	187	GGCUUUU	UGUGACC
	11	LC638708	NSP5 NSP6	21	624 291	59	GGCUUUU	UGUGACC

Table 8. Genotypes of all segments of isolated strain 16-06 and MpR12 with reference strains exhibiting the closest nucleotide identities

Strain	Gene	Genotype [b]	Strain exhibiting highest identity [a]			Cut-off value (%) [c]
			Strain name	Accession no.	Nucleotide identity (%)	
16-06	VP1	R22	RVA/Bat-wt/KEN/BATp39/2015/G36P[51]_R22	MH285837	97.80	83
	VP2	C20	RVA/Bat-wt/KEN/BATp39/2015/G36P[51]_C20	MH285838	93.77	84
	VP3	M20	RVA/Bat-wt/KEN/BATp39/2015/G36P[51]_M20	MH285839	93.98	81
	VP4	P[51]	RVA/Bat-wt/KEN/BATp39/2015/G36P[51]_P[51]	MH285840	94.89	80
	VP6	I16	RVA/Bat-wt/KEN/BATp39/2015/G36P[51]	MH285841	97.24	85
	VP7	G36	RVA/Bat-wt/KEN/BATp39/2015/G36P[51]_G36	MH285842	93.88	80
	NSP1	A31	RVA/Bat-wt/KEN/BATp39/2015/G36P[51]_A31	MH285843	97.63	79
	NSP2	N22	RVA/Bat-wt/KEN/BATp39/2015/G36P[51]_N22	MH285844	97.90	85
	NSP3	T22	RVA/Bat-wt/KEN/BATp39/2015/G36P[51]_T22	MH285845	92.14	85
	NSP4	E27	RVA/Bat-wt/KEN/BATp39/2015/G36P[51]	MH285846	97.92	85
	NSP5	H22	RVA/Bat-wt/KEN/BATp39/2015/G36P[51]_H22	MH285847	98.16	91
MpR12	VP1	**R27**	RVA/Human-wt/RWA/669/2013/G1P[8]_R1	MN632939	72.73	83
	VP2	**C23**	RVA/Dog-xx/USA/A79-10/1979/G3P[3]_C2	EU708935	76.49	84
	VP3	**M23**	RVA/Human-wt/ZAF/2371WC/2008/G9P[8]_M1	JN013992	64.66	81
	VP4	**P[57]**	RVA/Human-wt/UGA/MUL-12-117/2012/G3P[6]	KX655476	68.73	80
	VP6	**I31**	RVA/Bat-wt/GHA/K212/2009/G30P[47]	MN567266	77.64	85
	VP7	**G41**	RVA/Cow-tc/USA/Cody I-801/xxxx/G8P[x]	U14999	73.12	80
	NSP1	**A38**	RVA/Human-wt/JPN/HK14-5/2014/G1P[8]_A1	LC105017	58.90	79

NSP2	**N27**	RVA/Horse-tc/JPN/MK9/2019/G13P[18]_N9	LC528248	68.02	85
NSP3	**T27**	RVA/Human-wt/ARG/Arg4605/2006/G4P[6]_T7	KC412037	66.63	85
NSP4	**E31**	RVA/Bat-wt/CHN/YSSK5/2015/G3P[3]_E3	KX814962	61.29	85
NSP5	**H27**	RVA/Human-wt/SUR/2014735512/2013/G20P[28]	KX257411	71.20	91

[a] Closest strains were identified using BLASTn on megablast setting.

[b] Novel genotypes identified by RCWG in this study were indicated in bold.

[c] Matthijnssens *et al*. Arch. Virol. 2011

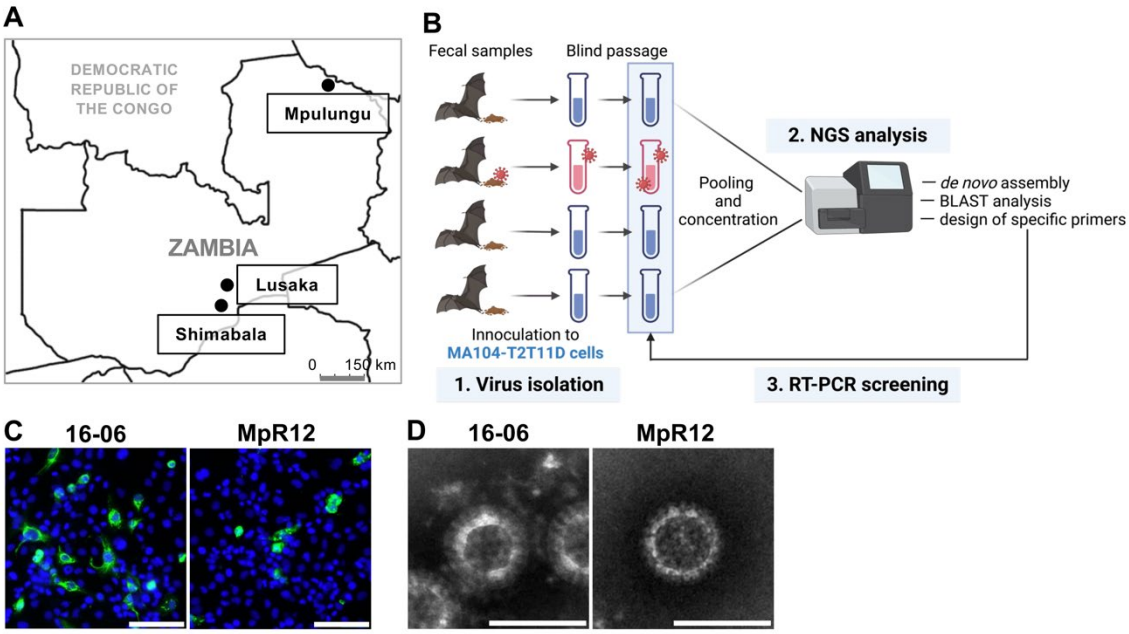

Fig. 8. Isolation of RVA from wild animals in Zambia

(A) Map of sampling sites in Zambia. Egyptian fruit bats were captured in Lusaka and Shimabala, and rodents and shrews were captured in Mpulungu. (B) Schematic workflow of virus isolation-based RVA screening. MA104-T2T11D cells were inoculated with fecal suspensions and cultured in roller tubes. After a single blind passage, the culture supernatants were pooled, concentrated, and analyzed by NGS. If RVA genomes were detected, passaged culture supernatants were screened for RVA by RT-PCR with specific primers for RVA sequences identified in the NGS analysis. This Figure was created with BioRender.com. (C) MA104-T2T11D cells infected with 16-06 and MpR12 were stained for RVA (green) and nuclei (blue). Scale bars, 50 μm. (D) Negative stain electron micrographs of 16-06 and MpR12 virions. Scale bars, 100 nm.

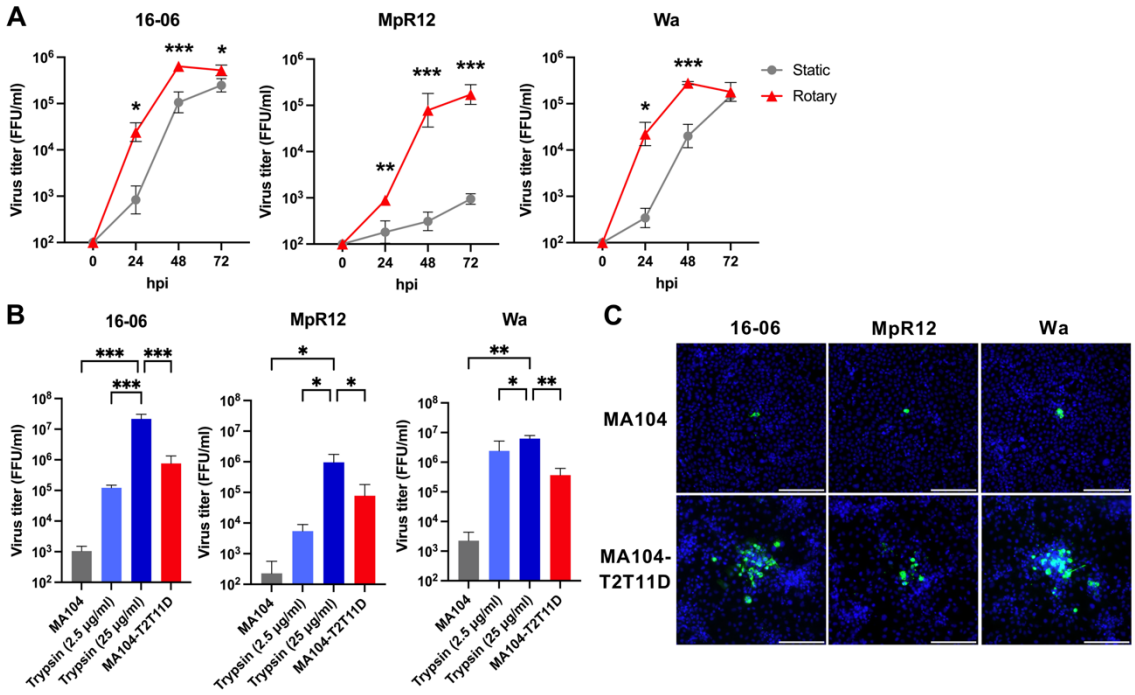

Fig. 9. Growth kinetics of 16-06, MpR12, and Wa in different culture conditions

Monolayered cells were inoculated with 16-06 (MOI = 0.005), MpR12 (MOI = 0.1) and Wa (MOI = 0.1). Progeny virus in the supernatants was harvested at the indicated time points (hours post infection; hpi) and titrated by a focus assay. (A) Infected MA104-T2T11D cells were cultured in static and rotary culture conditions. (B) The viruses were infected and cultured in MA104, MA104 with trypsin (25 μg/ml or 2.5 μg/ml), or MA104-T2T11D cells. Virus titers at 48 hpi of each virus were indicated as means ± SD of triplicate data from a representative experiment. Statistical analysis was performed by the Student's *t*-tests (A) or one-way ANOVA with Turkey's tests (B); ***, $p < 0.001$, **, $p < 0.01$, *, $p < 0.05$. (C) Representative focus induced by 16-06, MpR12 and Wa in MA104 cells and MA104-T2T11D cells. Infected cells were overlayed with 0.5% agar and cultured for 72 hpi. Fixed cells were stained for RVA (green) and nuclei (blue). Scale bars, 200 μm.

A

Strains	VP7	VP4	VP6	VP1	VP2	VP3	NSP1	NSP2	NSP3	NSP4	NSP5
RVA/MultimammateMouse-tc/ZMB/MpR12/2012/G41P[57]	G41	P[57]	I31	R27	C23	M23	A38	N27	T27	E31	H27
RVA/Bat-tc/ZMB/16-06/2016/G36P[51]	G36	P[51]	I16	R22	C20	M20	A31	N22	T22	E27	H22
RVA/Bat-wt/KEN/BATp39/2015/G36P[51]	G36	P[51]	I16	R22	C20	M20	A31	N22	T22	E27	H22
RVA/Bat-wt/ZMB/ZFB14-126/2014/GxP[x]	Gx	P[x]	I22	Rx	Cx	Mx	Ax	N21	T17	**E27**	Hx
RVA/Bat-wt/ZMB/ZFB14-52/2014/G31P[x]	G31	P[x]	I22	Rx	Cx	Mx	Ax	Nx	T17	Ex	Hx
RVA/Bat-wt/ZMB/ZFB14-135/2014/G31P[x]	G31	P[x]	I22	R15	Cx	Mx	Ax	Nx	T17	Ex	Hx
RVA/Bat-wt/CMR/Batli08/2014/G31P[42]	G31	P[42]	I22	R15	C15	M14	A25	N15	T17	E22	H17
RVA/Human-tc/KEN/B10/1987/G3P[2]	G3	P[2]	**I16**	R8	C5	M5	A5	N5	T5	E13	H5
RVA/Simian-tc/ZAF/SA11-H96/1958/G3P[2]	G3	P[2]	I2	R2	C5	M5	A5	N5	T5	E2	H5
RVA/Human-xx/CHN/ZTR-5/xxxx/G3P[2]	G3	P[2]	I2	R2	C5	M5	A5	N2	T5	E2	H5
RVA/Bat-wt/ZMB/LUS12-14/2012/G3P[3]	G3	P[3]	I3	R2	C2	M3	A9	N2	T3	E2	H3

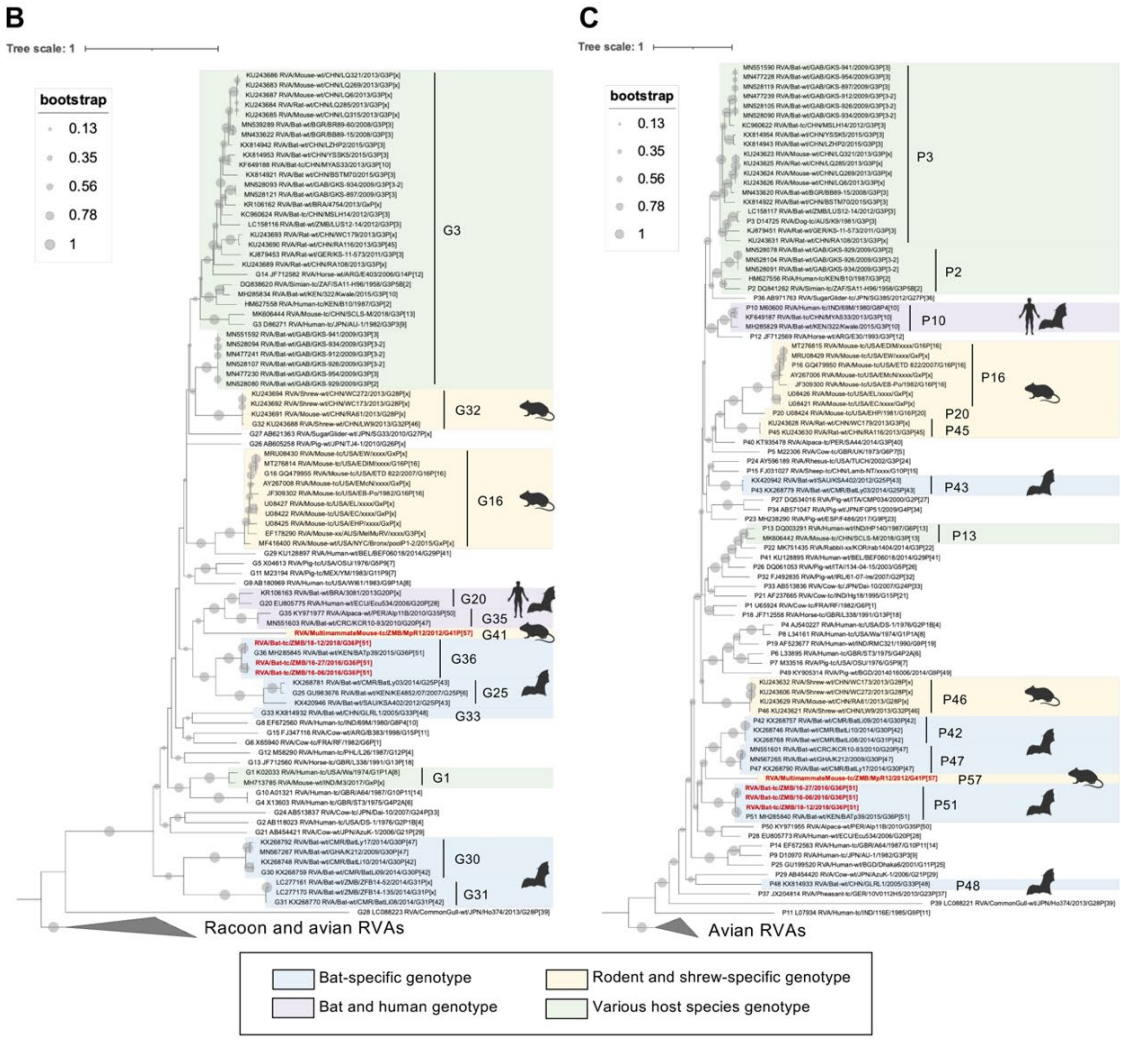

Fig. 10. Whole-genome characterization of the isolated RVAs

(A) Comparison of the genome constellation between the isolated RVAs and related RVA strains. Identical genotypes are displayed as the same color, and genotypes of undetermined segments are indicated by "x". (B and C) ML tree of VP7 (B) and VP4 (C) genes based on the sequence of the isolated RVAs, bat-derived RVAs, rodent-derived RVAs, and type strains of each genotype. Phylogenetic trees were constructed by the ML method using models of GTR + G + I with bootstrap

values of 1,000 replicates. Avian and raccoon RVAs were regarded as the outer group. The isolated RVAs are indicated in red. Bat-specific genotypes and rodent- and shrew-specific genotypes are highlighted in blue and yellow, respectively. The genotypes including bat-derived and non-typical human RVAs are colored in purple. The genotypes consisting of RVAs from multiple animal species are highlighted in green.

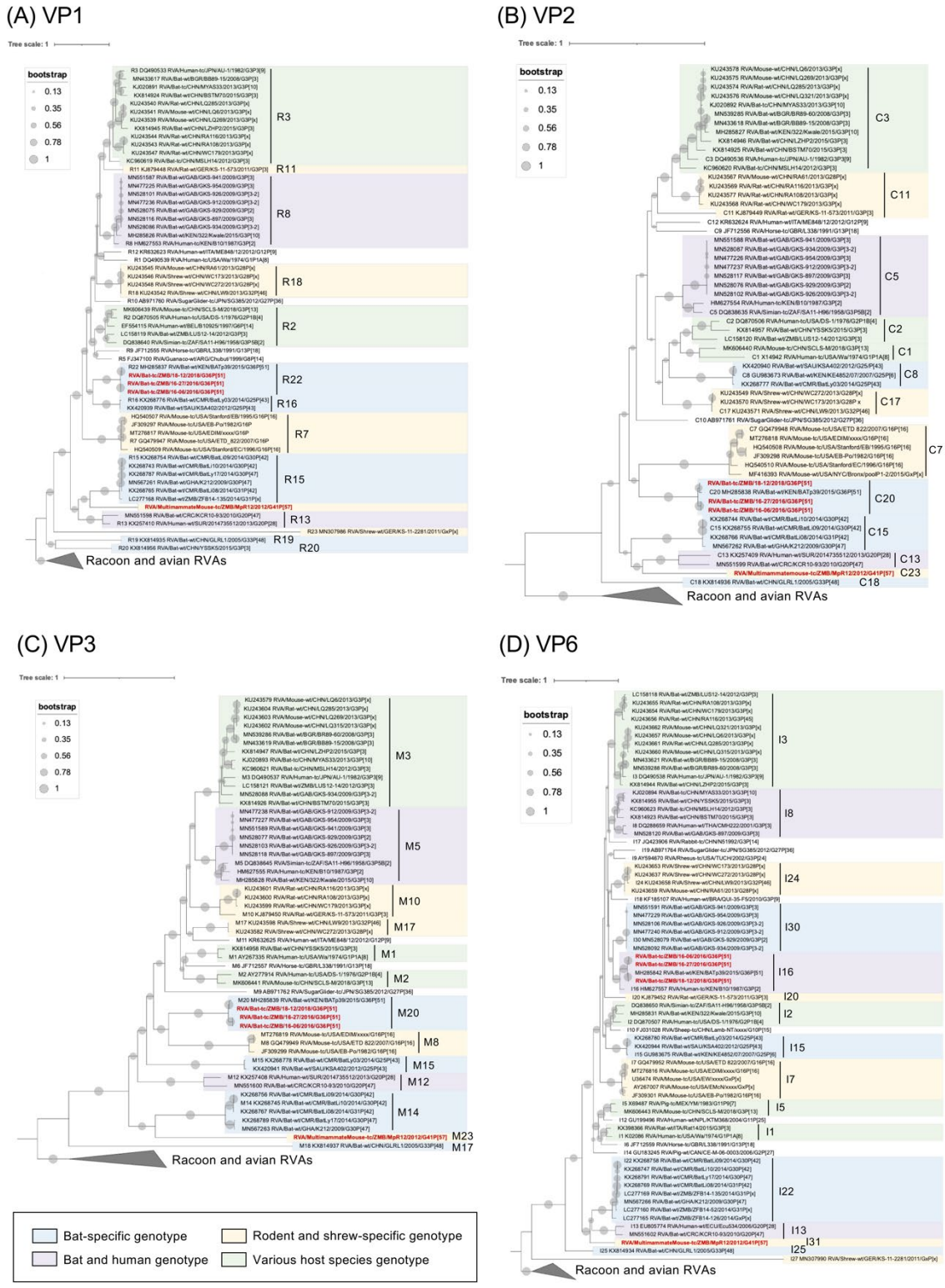
(A) VP1
(B) VP2
(C) VP3
(D) VP6
Tree scale: 1
bootstrap
0.13
0.35
0.56
0.78
1
Racoon and avian RVAs
Bat-specific genotype
Bat and human genotype
Rodent and shrew-specific genotype
Various host species genotype

(E) NSP1

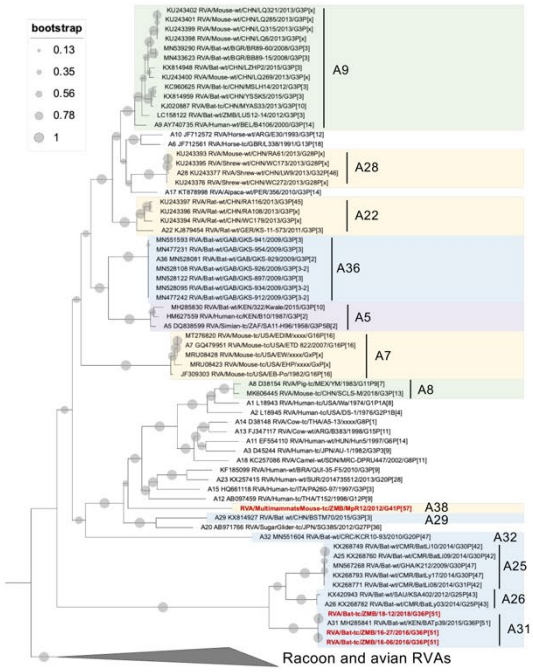

(F) NSP2

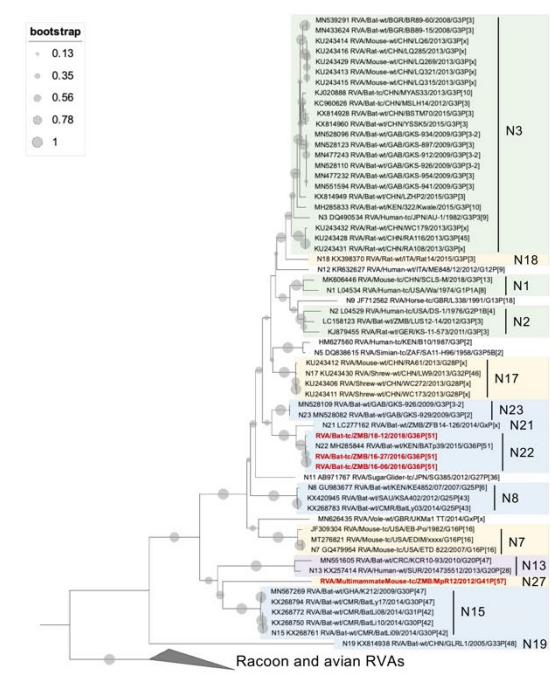

(G) NSP3

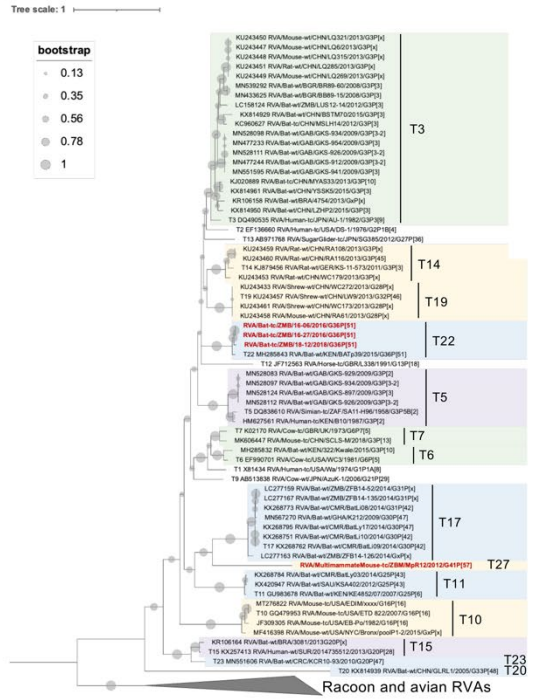

(H) NSP4

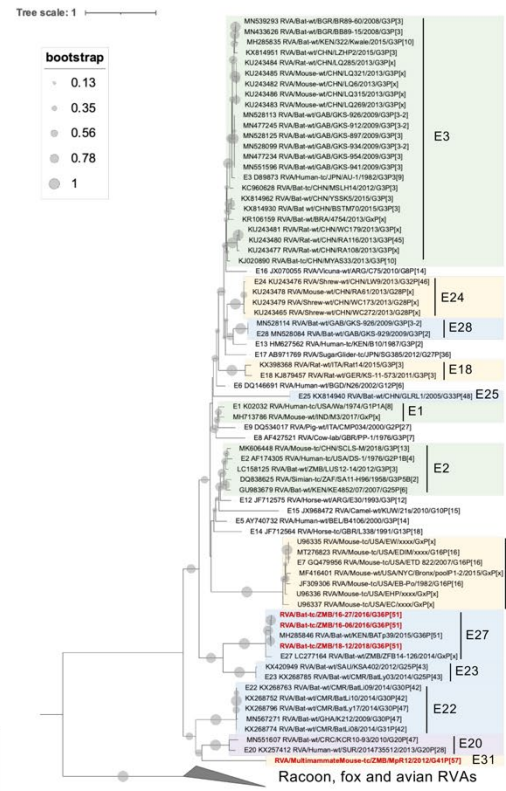

Bat-specific genotype
Rodent and shrew-specific genotype
Bat and human genotype
Various host species genotype

Fig. 11. ML trees of VP1 (A), VP2 (B), VP3 (C), VP6 (D), NSP1 (E), NSP2 (F), NSP3 (G), NSP4 (H), and NSP5 (I) genes

Phylogenetic trees were constructed based on the sequence of the isolated RVAs, bat-derived RVAs, rodent-derived RVAs, and type strains of each genotype by the ML method using models of GTR + G + I for VP1, VP2, VP3, NSP1, and NSP2 and GTR + G for VP6, NSP3, NSP4, and NSP5 with bootstrap values of 1,000 replicates. Avian, raccoon, and fox RVAs were included as the outer group. The isolated RVAs are indicated in red color. Bat-specific genotypes and rodent and shrew-specific genotypes are highlighted in blue and yellow, respectively. The genotypes include bat-derived and non-typical human RVAs are colored in purple. The genotypes consisting of RVAs from multiple animal species are highlighted in green.

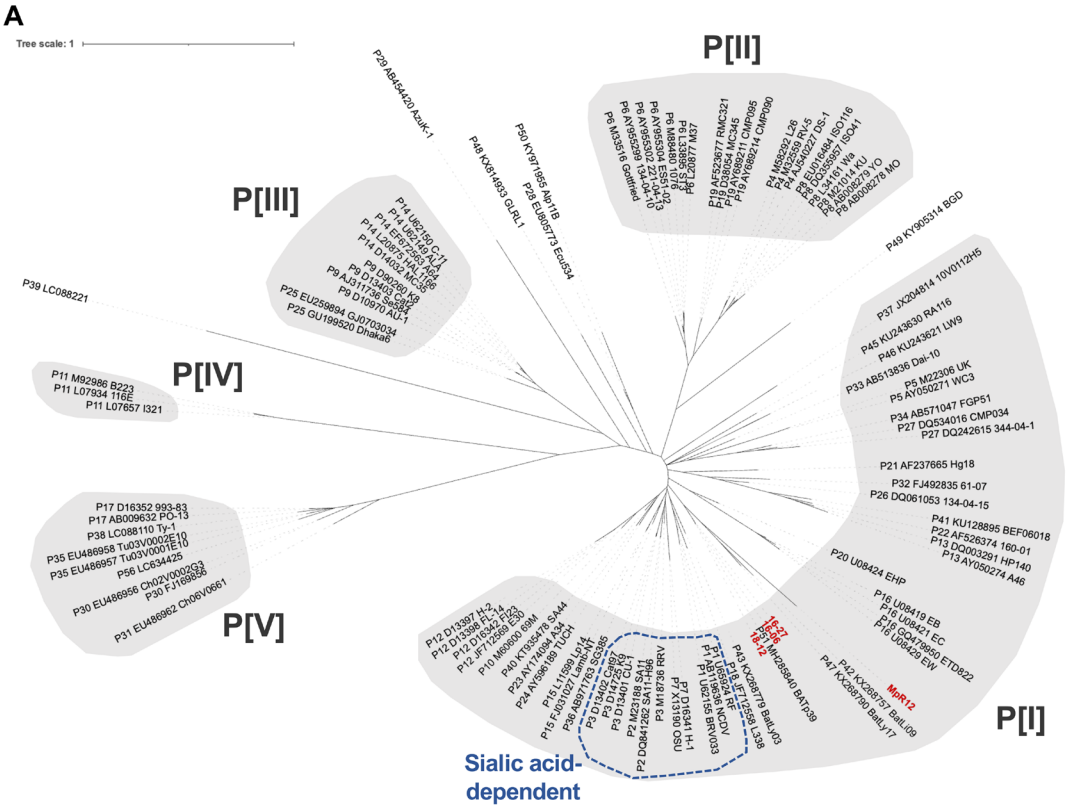

Fig. 12. Estimation of glycan-binding ability of the isolated RVAs

(A) ML tree of VP8* genes of the isolated and representative RVA strains. using models of GTR + G + I with bootstrap values of 500 replicates. The isolated RVAs are indicated in red color. Strains consisting genogroups of P[I] to P[V] were tinted in gray respectively. SA-dependent strains were surrounded by a red dotted line. (B) Partial amino acid sequence alignment of VP8* of the isolated and representative RVA strains. Residues interacting with SAs are highlighted in blue. Residues interacting with mucin cores and LNFPI glycans are highlighted in green, and type A histo-blood group antigens are highlighted in pink. (C) Partial amino acid sequence alignment of VP8* of MpR12 and other rodent RVA strains. Residues interacting with SAs are highlighted in blue.

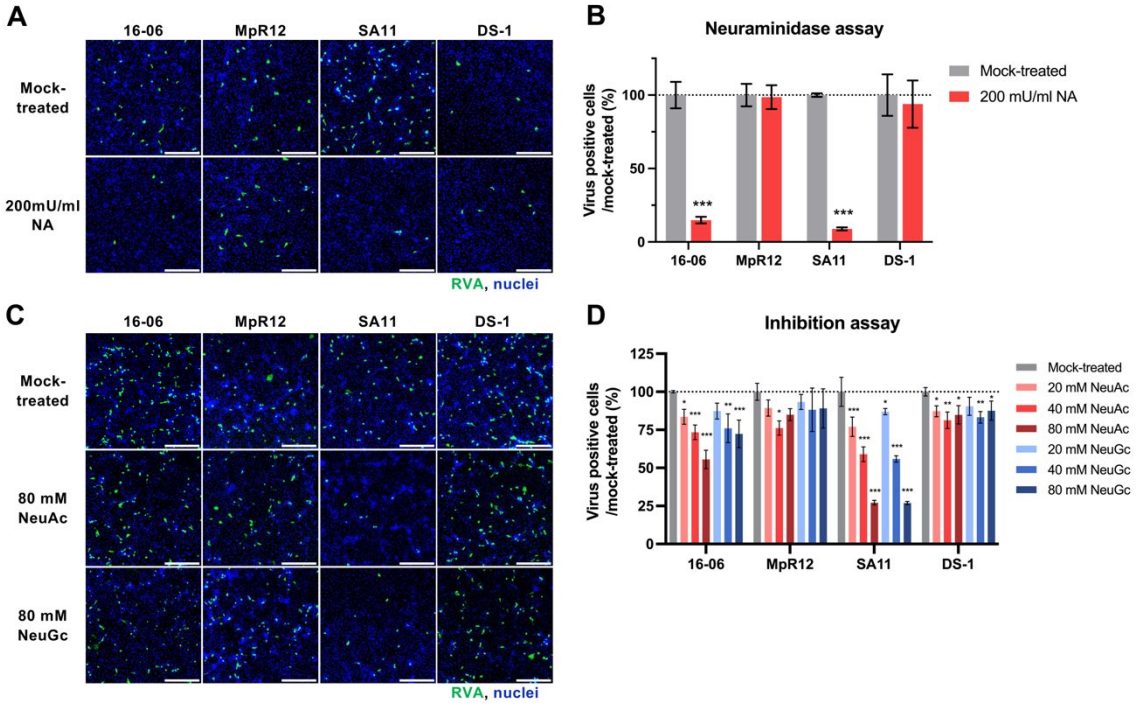

Fig. 13. Involvement of sialic acid on the infectivity of the isolated RVAs

(A and B) MA104-T2T11D cells were pretreated with NA at 200 mU/ml or reaction buffer (mock-treated) and infected with 16-06 and MpR12. The SA11 and DS-1 strains were used as positive and negative controls, respectively. (C and D) MA104-T2T11D cells were infected with RVA pretreated with NeuAc, NeuGc, or reaction buffer only (mock-treated). (A and C) Cells were stained with anti-RVA antibody (green) and Hoechst 33342 for nuclei (blue). Scale bars, 200 μm. The figures shown are representative images. (B and D) The number of infected cells with RVA is expressed as a percentage of the mock-treated control. Means ± SD of triplicate data from a representative experiment are shown in the graph. Statistical analysis was performed by multiple *t*-tests with the Holm-Sidak method for the NA assay and one-way ANOVA with Dunnett's test for SA inhibition test; ***, $p < 0.001$, **, $p < 0.01$, *, $p < 0.05$.

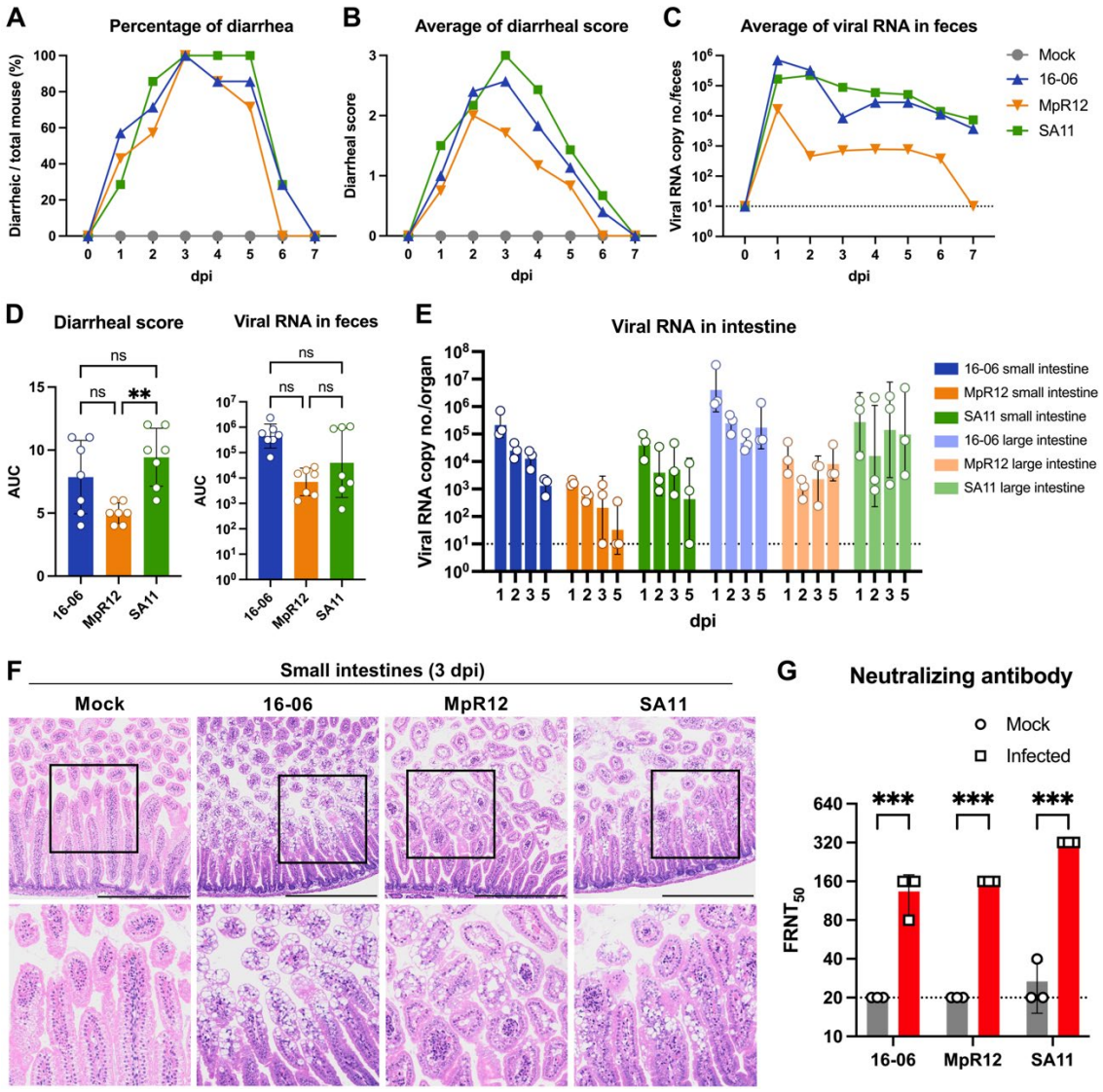

Fig. 14. Pathogenicity of the isolated RVAs in suckling mice

Three-day-old BALB/c mice were orally inoculated with 1.0×10^5 FFU of RVA strains 16-06, MpR12, SA11, or PBS (mock) by gavage (n = 7 in each group). (A) Incidence rate of diarrhea in each group was monitored from 0 to 7 dpi. (B) Fecal consistency in each group was scored according to the criteria described in the Methods. (C) Average of viral RNA copy numbers from the feces from 0 to 7 dpi were calculated based on the results of qRT-PCR. Dashed line indicates detection limit of qRT-PCR. (D) Viral RNA copy number of small and large intestines of infected mice at 1, 2, 3, and 5 dpi were determined using qRT-PCR. (E) AUCs were calculated based on the diarrheal score and viral RNA copy number in feces of each mouse. (F) Infected sucking mice were sacrificed at 3 dpi for histopathological examinations. Representative images of the small intestine of 16-06-, MpR12-, or SA11-infected mice and the control mice are shown. In these infected mice at

3 dpi, histopathological changes were characterized by vacuolization of the enterocytes in the villus tips. Hematoxylin and eosin staining. Scale bars, 500 μm. Areas in black squares are magnified in lower panels. (G) Neutralizing titers of mouse sera at 15 dpi were expressed as the dilution at which the number of viral focuses was reduced by 50% compared to the no serum control ($FRNT_{50}$). Dashed line indicates detection limit of focus reduction neutralization test. Means ± SD of each group from a representative experiment are shown in the graph. Each dot represents one value from each mouse. Statistical analysis was performed by one-way ANOVA with Turkey's test for AUC analysis and multiple t-tests with the Holm-Sidak method for the neutralizing antibody titers; ***, $p < 0.001$, **, $p < 0.01$, *, $p < 0.05$.

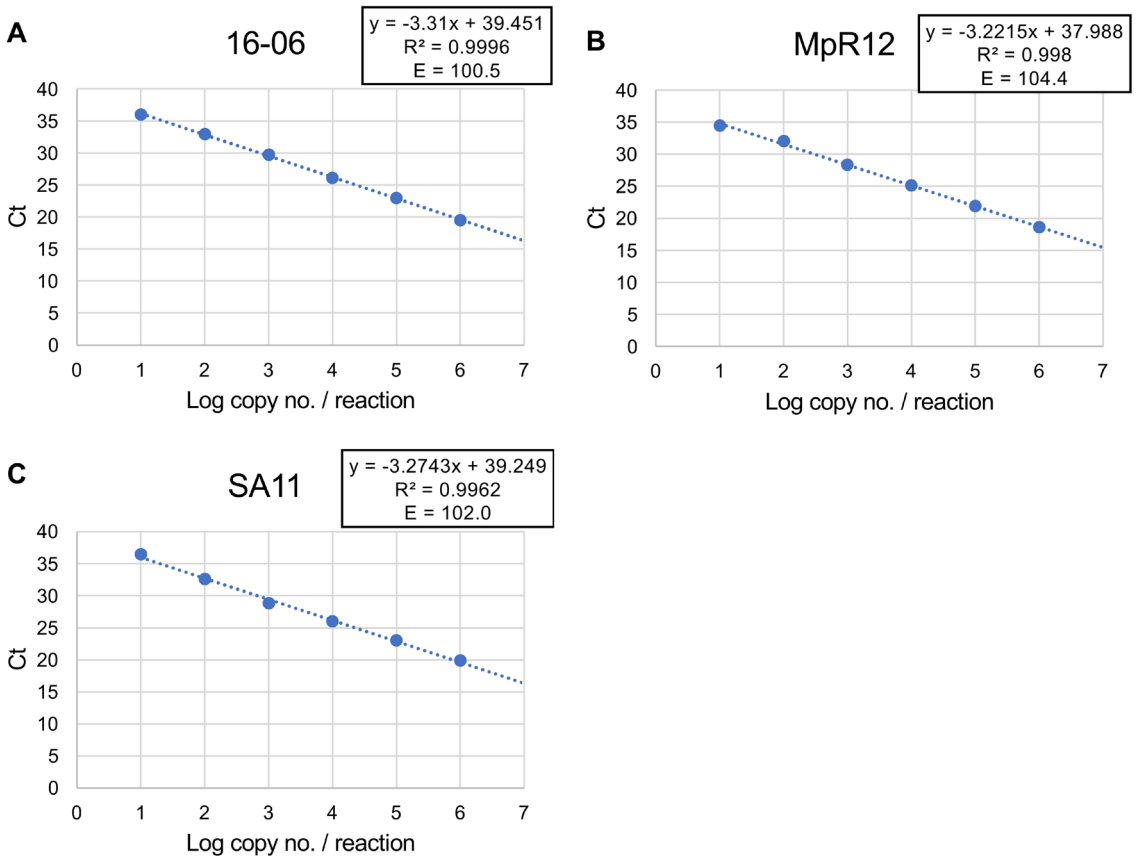

Fig. 15. Standard curves of qRT-PCR targeting 16-06 (A), MpR12 (B), and SA11 (C)

Ct values were plotted against the log copy number of control plasmids. The regression curve (y), correlation coefficient (R2), and PCR efficiency (E) were indicated, respectively.

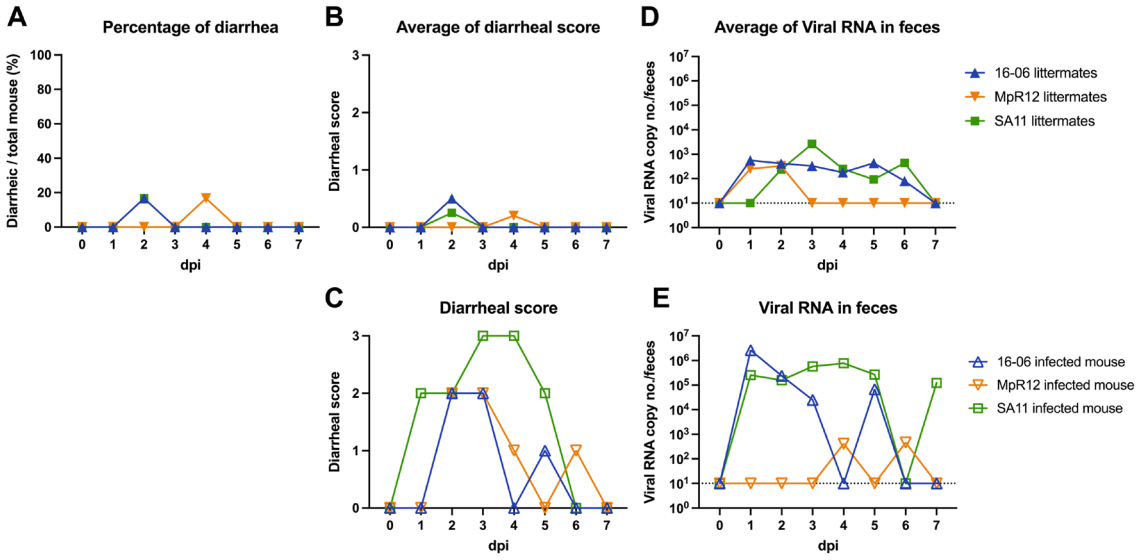

Fig. 16. Transmissibility of the isolated RVAs to uninfected litter suckling mice

One of littermates of three-day-old BALB/c mice were orally inoculated with 1.0×10^5 FFU of RVA strains 16-06, MpR12, SA11 by gavage (n = 7 in each group). (A) Incidence rate of diarrhea of uninfected littermates in each group was monitored from 0 to 7 dpi. (B and C) Fecal consistency of uninfected littermates (B) and infected mouse (C) in each group was scored according to the criteria described in the Methods. (D and E) Average of viral RNA copy numbers from the feces of uninfected littermates (D) and infected mouse (E) from 0 to 7 dpi were calculated based on the results of qRT-PCR. Dashed line indicates detection limit of qRT-PCR.

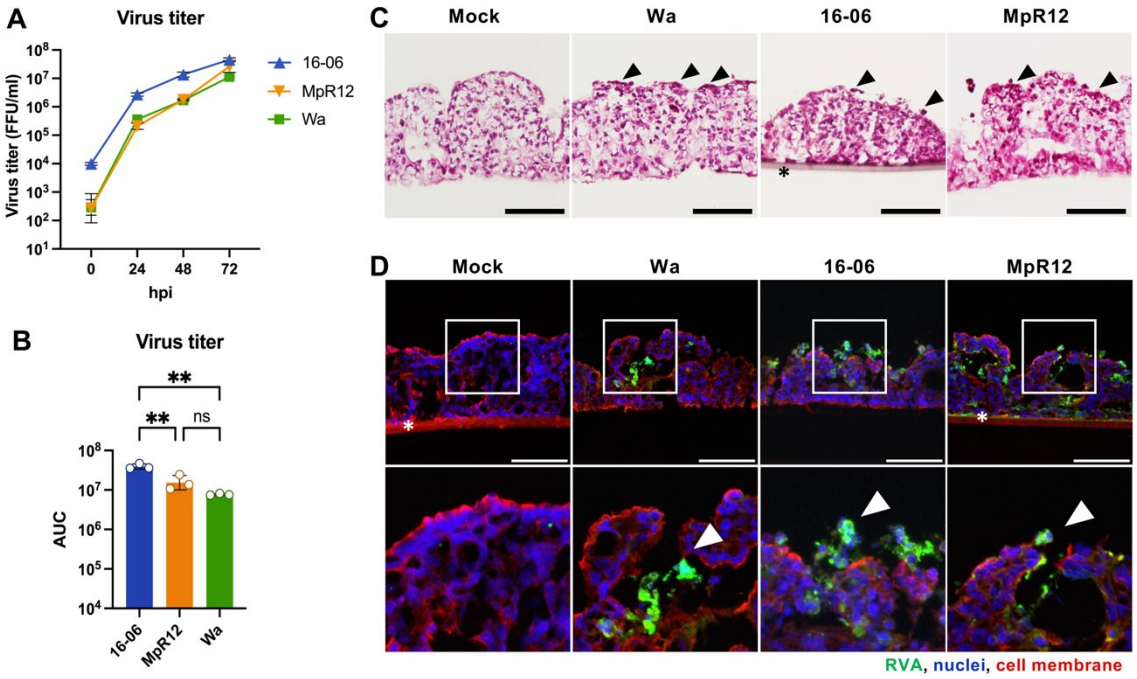

Fig. 17. Infectivity of the isolated RVAs in a human small intestinal epithelial *ex vivo* model, SMI-100

(A) Growth kinetics of 16-06, MpR12, or Wa in SMI-100. SMI-100 was inoculated with 1.0×10^5 FFU of 16-06, MpR12, or Wa. Supernatants were collected at the indicated time points (hours post infection; hpi), and virus titers were measured by a focus assay. Means ± SD of triplicate data from a representative experiment are shown in the graph. (B) AUCs based on the viral titers in the culture supernatants of each SMI-100 well infected with 16-06, MpR12, or Wa. Means ± SD of triplicate data from a representative experiment are shown in the graph. Each dot represents one AUC value from each SMI-100 well. Statistical analysis was performed by one-way ANOVA with Turkey's test; ***, $p < 0.001$, **, $p < 0.01$, *, $p < 0.05$. (C) Histopathological images of vertical sections of SMI-100 at 3 dpi with H&E staining. The black arrowheads indicate the acidophilic dead cells with fragmented nuclei. Scale bars, 100 μm. (D) Vertical sections of SMI-100 at 3 dpi were stained for RVA (green), nuclei (blue), and cell membrane (red). Scale bars, 100 μm. Areas in white squares are magnified in lower panels. The white arrowheads indicate the exfoliated infected cells. Asterisks show mesh membranes that support the epithelium. The figures shown are representative images.

Conclusion

In this century, various emerging and re-emerging infectious diseases have raised and threatened global public health. Many emerging and re-emerging viral infections are zoonotic diseases that spilled over from wild animals. Therefore, researchers have focused on the search for wild animal-derived viruses using genomic analysis techniques. However, most of these studies were based on genome detection and sequence analysis of the novel viruses. Further investigations including virus isolation and investigation of the virological properties are required to better understand zoonotic potential or outbreak risk of these viruses. Here, virus isolation from wild animal samples and the virological and epidemiological characterizations of the isolated viruses were performed.

In this study, host TTSP-expressing cells were used to efficiently isolate protease-dependent viruses. In chapter I, it is demonstrated that TMPRSS11D, and TMPRSS13 facilitate SARS-CoV-2 infection. Based on the findings in chapter I and other previous studies, TMPRSS2 and TMPRSS11D co-expressing cells were selected for virus isolation. As a result, four isolates of protease-dependent RVA were successfully isolated. The use of TTSP-expressing cells eliminates the washout step of serum for trypsin treatment and allows us to handle a large number of specimens for virus isolation.

In the general approach for virus screening, genomic screening of target viruses is prior to virus isolation from genome-positive samples. However, the approach cannot detect unexpected viruses or viruses with low genome similarity to known viruses. Here, virus isolation was performed from a large number of wild animal samples without virus genome screening. As a result, EMCV, which had not been reported in Zambia, and RVAs with atypical GC were isolated, demonstrating the validity of this method. Further investigations using this method are expected to detect a large number of novel viruses.

In chapter II and III, I demonstrated the virological and epidemiological characterization of EMCV and RVA isolated from bats and rodents in Zambia. For the isolated EMCV, high EMCV prevalence in *M. natalensis* indicated that this rodent

species would be one of the reservoirs in African countries and highlights the potential risk of EMCV infection in domestic and wild animals and potentially humans in Zambia. For the isolated bat and rodent RVAs, whole-genome analysis, glycan utilization analysis, experimental inoculation in suckling mice, and infectivity in a human small intestinal epithelial model enabled characterization of the unique virological properties of the isolated RVAs and have highlighted their zoonotic potential.

This is a proof-of-concept study for the high-throughput virus isolation method using TTSP-expressing cells. Subsequent virological and epidemiological characterizations lead to further understanding of EMCV and RVA and reveal the need for investigation to assess zoonotic potential or outbreak risk of these viruses.

Acknowledgements

I would like to deeply appreciate my supervisors Professor Hirofumi Sawa, Dr. Michihito Sasaki, and Dr. Yasuko Orba (Division of Molecular Pathobiology, International Institute for Zoonosis Control, Hokkaido University) for all their support and guidance during my studies. I truly enjoyed “science” under their mentorship.

I would like to appreciate Professor Yoshihiro Sakoda (Laboratory of Microbiology, Faculty of Veterinary Medicine, Hokkaido University) and Professor Kentaro Yoshii (National Research Center for the Control and Prevention of Infectious Diseases (CCPID), Nagasaki University). The intellectual discussion, critical review, and suggestions greatly improved this study.

I also would like to appreciate all of collaborators; Dr. Kentaro Uemura, Dr, Shinsuke Toba, Dr. Takao Sanaki, Professor Akihiko Sato (Drug Discovery and Disease Research Laboratory, Shionogi & Co., Ltd), Dr. Masahiro Kajihara, Dr. Akina Mori-Kajihara, Dr. Yoshiki Eto, Professor Ayato Takada (Division of Global Epidemiology, International Institute for Zoonosis Control, Hokkaido University), Dr. Seiya Ozono, Dr. Yuko Sato, Dr. Tadaki Suzuki (Department of Pathology, National Institute of Infectious Diseases), Professor Naoto Ito (Joint Graduate School of Veterinary Sciences, Gifu University), Professor Hiroaki Kariwa (Laboratory of Public Health, Faculty of Veterinary Medicine, Hokkaido University), Dr. Yongjin Qiu, Dr. Hayato Harima (Division of International Research Promotion, International Institute for Zoonosis Control, Hokkaido University), Dr. Katendi Changula, Professor Bernard M. Hang’ombe (Department of Para-clinical Studies, School of Veterinary and Medicine, University of Zambia), Dr.Daniel Mwizabi (Department of National Parks and Wildlife, the Ministry of Tourism and Arts, Zambia), Professor William W. Hall (National Virus Reference Laboratory, School of Medicine, University College Dublin).

Finally, I am grateful to all members of the Division of Molecular Pathobiology. Especially, I would like to acknowledge Yukari Itakura and Koshiro Tabata for mutual support and encouragement.

My graduate school days and these Ph.D. works were financially supported by the World-leading Innovative and Smart Education (WISE) Program from the Ministry of Education, Culture, Sports, Science, and Technology (2019–2020, Adopted person: Mai Kishimoto) and the Research fellowship for Young Scientists from the Japan Society for the Promotion of Science fellows (2021–2023, Project number: 21J21075). I greatly appreciate their supports for my works.

References

1. Coker, R. *et al.* Towards a conceptual framework to support one-health research for policy on emerging zoonoses. *Lancet Infect. Dis.* **11**, 326–331 (2011).
2. Woolhouse, M. E. J. & Gowtage-Sequeria, S. Host Range and Emerging and Reemerging Pathogens. *Emerg. Infect. Dis. J.* **11**, 1842–1847 (2005).
3. Wolfe, N. D., Dunavan, C. P. & Diamond, J. Origins of major human infectious diseases. *Nature* **447**, 279–283 (2007).
4. Cutler, S. J., Fooks, A. R. & Poel, W. H. M. van der. Public Health Threat of New, Reemerging, and Neglected Zoonoses in the Industrialized World. *Emerg. Infect. Dis. J.* **16**, 1–7 (2010).
5. Badrane, H. & Tordo, N. Host switching in lyssavirus history from the Chiroptera to the carnivora orders. *J. Virol.* **75**, 8096–8104 (2001).
6. Chua, K. B. *et al.* Isolation of Nipah virus from malaysian island flying-foxes. *Microbes Infect.* **4**, 145–151 (2002).
7. Halpin, K., Young, P. L., Field, H. E. & Mackenzie, J. S. Y. Isolation of Hendra virus from pteropid bats: a natural reservoir of Hendra virus. *J. Gen. Virol.* **81**, 1927–1932 (2000).
8. Towner, J. S. *et al.* Isolation of genetically diverse Marburg viruses from egyptian fruit bats. *PLOS Pathog.* **5**, e1000536 (2009).
9. Li, W. *et al.* Bats are natural reservoirs of SARS-like coronaviruses. *Science* **310**, 676–679 (2005).
10. Plyusnin, A., Vapalahti, O. & Vaheri, A. Hantaviruses: genome structure, expression and evolution. *J. Gen. Virol.* **77**, 2677–2687 (1996).
11. Charrel, R. N. & de Lamballerie, X. Zoonotic aspects of arenavirus infections. *Vet. Microbiol.* **140**, 213–220 (2010).
12. Roux, S. *et al.* Minimum Information about an Uncultivated Virus Genome (MIUViG). *Nat. Biotechnol.* **37**, 29–37 (2019).
13. Sasaki, M. *et al.* Isolation and Characterization of a Novel Alphaherpesvirus in Fruit Bats. *J. Virol.* **88**, 9819–9829 (2014).

14. Intaruck, K. *et al.* Isolation and characterization of an orthoreovirus from Indonesian fruit bats. *Virology* **575**, 10–19 (2022).
15. Laporte, M. & Naesens, L. Airway proteases: an emerging drug target for influenza and other respiratory virus infections. *Curr. Opin. Virol.* **24**, 16–24 (2017).
16. Arias, C. F. & López, S. Rotavirus cell entry: not so simple after all. *Curr. Opin. Virol.* **48**, 42–48 (2021).
17. Roth, A. N. *et al.* Ins and Outs of Reovirus: Vesicular Trafficking in Viral Entry and Egress. *Trends Microbiol.* **29**, 363–375 (2021).
18. Shirogane, Y. *et al.* Efficient Multiplication of Human Metapneumovirus in Vero Cells Expressing the Transmembrane Serine Protease TMPRSS2. *J. Virol.* **82**, 8942–8946 (2008).
19. Böttcher-Friebertshäuser, E. *et al.* Cleavage of Influenza Virus Hemagglutinin by Airway Proteases TMPRSS2 and HAT Differs in Subcellular Localization and Susceptibility to Protease Inhibitors. *J. Virol.* **84**, 5605–5614 (2010).
20. Matsuyama, S. *et al.* Efficient Activation of the Severe Acute Respiratory Syndrome Coronavirus Spike Protein by the Transmembrane Protease TMPRSS2. *J. Virol.* **84**, 12658–12664 (2010).
21. Matsuyama, S. *et al.* Enhanced isolation of SARS-CoV-2 by TMPRSS2-expressing cells. *Proc. Natl. Acad. Sci.* **117**, 7001–7003 (2020).
22. Nygaard, R. M., Golden, J. W. & Schiff, L. A. Impact of Host Proteases on Reovirus Infection in the Respiratory Tract. *J. Virol.* **86**, 1238–1243 (2012).
23. Abe, M. *et al.* TMPRSS2 Is an Activating Protease for Respiratory Parainfluenza Viruses. *J. Virol.* **87**, 11930–11935 (2013).
24. Bertram, S. *et al.* TMPRSS2 and TMPRSS4 Facilitate Trypsin-Independent Spread of Influenza Virus in Caco-2 Cells. *J. Virol.* **84**, 10016–10025 (2010).
25. Zmora, P. *et al.* DESC1 and MSPL Activate Influenza A Viruses and Emerging Coronaviruses for Host Cell Entry. *J. Virol.* **88**, 12087–12097 (2014).
26. Zmora, P. *et al.* TMPRSS11A activates the influenza A virus hemagglutinin and the MERS coronavirus spike protein and is insensitive against blockade by HAI-1. *J. Biol. Chem.* **293**, 13863–13873 (2018).

27. Sasaki, M. *et al.* Host serine proteases TMPRSS2 and TMPRSS11D mediate proteolytic activation and trypsin-independent infection in group A rotaviruses. *J. Virol.* **95**, e00398-21 (2021).
28. Wu, F. *et al.* A new coronavirus associated with human respiratory disease in China. *Nature* **579**, 265–269 (2020).
29. Zhou, P. *et al.* A pneumonia outbreak associated with a new coronavirus of probable bat origin. *Nature* **579**, 270–273 (2020).
30. Harrison, A. G., Lin, T. & Wang, P. Mechanisms of SARS-CoV-2 Transmission and Pathogenesis. *Trends Immunol.* **42**, 1100–1115 (2020).
31. Xiao, F. *et al.* Evidence for Gastrointestinal Infection of SARS-CoV-2. *Gastroenterology* **158**, 1831–1833 (2020).
32. Cholankeril, G. *et al.* High Prevalence of Concurrent Gastrointestinal Manifestations in Patients With Severe Acute Respiratory Syndrome Coronavirus 2: Early Experience From California. *Gastroenterology* **159**, 775–777 (2020).
33. Leung, W. K. *et al.* Enteric involvement of severe acute respiratory syndrome-associated coronavirus infection. *Gastroenterology* **125**, 1011–1017 (2003).
34. Huang, J. *et al.* Potential of SARS-CoV-2 to Cause CNS Infection: Biologic Fundamental and Clinical Experience. *Front. Neurol.* **11**, 659 (2020).
35. Saleki, K., Banazadeh, M., Saghazadeh, A. & Rezaei, N. The involvement of the central nervous system in patients with COVID-19. *Rev. Neurosci.* **31**, 453–456 (2020).
36. Hoffmann, M. *et al.* SARS-CoV-2 Cell Entry Depends on ACE2 and TMPRSS2 and Is Blocked by a Clinically Proven Protease Inhibitor. *Cell* **181**, 271–280 (2020).
37. Boopathi, S., Poma, A. B. & Kolandaivel, P. Novel 2019 coronavirus structure, mechanism of action, antiviral drug promises and rule out against its treatment. *J. Biomol. Struct. Dyn.* **39**, 3409–3418 (2020).
38. Cai, Y. *et al.* Distinct conformational states of SARS-CoV-2 spike protein. *Science* **369**, 1586–1592 (2020).

39. Tang, T., Bidon, M., Jaimes, J. A., Whittaker, G. R. & Daniel, S. Coronavirus membrane fusion mechanism offers a potential target for antiviral development. *Antiviral Res.* **178**, 104792 (2020).
40. Hoffmann, M., Kleine-Weber, H. & Pöhlmann, S. A Multibasic Cleavage Site in the Spike Protein of SARS-CoV-2 Is Essential for Infection of Human Lung Cells. *Mol. Cell* **78**, 779–784 (2020).
41. Moreira, R. A., Guzman, H. V., Boopathi, S., Baker, J. L. & Poma, A. B. Characterization of Structural and Energetic Differences between Conformations of the SARS-CoV-2 Spike Protein. *Materials* **13**, 5362 (2020).
42. Moreira, R. A., Chwastyk, M., Baker, J. L., Guzman, H. V. & Poma, A. B. Quantitative determination of mechanical stability in the novel coronavirus spike protein. *Nanoscale* **12**, 16409–16413 (2020).
43. Casalino, L. *et al.* Beyond Shielding: The Roles of Glycans in the SARS-CoV-2 Spike Protein. *ACS Cent. Sci.* **6**, 1722–1734 (2020).
44. Simmons, G., Zmora, P., Gierer, S., Heurich, A. & Pöhlmann, S. Proteolytic activation of the SARS-coronavirus spike protein: Cutting enzymes at the cutting edge of antiviral research. *Antiviral Res.* **100**, 605–614 (2013).
45. Ou, T. *et al.* Hydroxychloroquine-mediated inhibition of SARS-CoV-2 entry is attenuated by TMPRSS2. *PLOS Pathog.* **17**, e1009212 (2021).
46. Antalis, T. M., Bugge, T. H. & Wu, Q. Membrane-Anchored Serine Proteases in Health and Disease. *Prog. Mol. Biol. Transl. Sci.* **99**, 1–50 (2011).
47. Bertram, S., Glowacka, I., Steffen, I., Kühl, A. & Pöhlmann, S. Novel insights into proteolytic cleavage of influenza virus hemagglutinin: Proteolytic activation of influenza virus. *Rev. Med. Virol.* **20**, 298–310 (2010).
48. Laporte, M. *et al.* Hemagglutinin Cleavability, Acid Stability, and Temperature Dependence Optimize Influenza B Virus for Replication in Human Airways. *J. Virol.* **94**, e01430-19 (2019).
49. Shi, W. *et al.* TMPRSS2 and MSPL Facilitate Trypsin-Independent Porcine Epidemic Diarrhea Virus Replication in Vero Cells. *Viruses* **9**, 114 (2017).

50. Bertram, S. *et al.* Cleavage and Activation of the Severe Acute Respiratory Syndrome Coronavirus Spike Protein by Human Airway Trypsin-Like Protease. *J. Virol.* **85**, 13363–13372 (2011).
51. Xia, S. *et al.* The role of furin cleavage site in SARS-CoV-2 spike protein-mediated membrane fusion in the presence or absence of trypsin. *Signal Transduct. Target. Ther.* **5**, 92 (2020).
52. Ou, X. *et al.* Characterization of spike glycoprotein of SARS-CoV-2 on virus entry and its immune cross-reactivity with SARS-CoV. *Nat. Commun.* **11**, 1620 (2020).
53. Zang, R. *et al.* TMPRSS2 and TMPRSS4 promote SARS-CoV-2 infection of human small intestinal enterocytes. *Sci. Immunol.* **5**, eabc3582 (2020).
54. Sasaki, M. *et al.* SARS-CoV-2 variants with mutations at the S1/S2 cleavage site are generated in vitro during propagation in TMPRSS2-deficient cells. *PLOS Pathog.* **17**, e1009233 (2021).
55. Thai, H. T. C. *et al.* Development and Evaluation of a Novel Loop-Mediated Isothermal Amplification Method for Rapid Detection of Severe Acute Respiratory Syndrome Coronavirus. *J. Clin. Microbiol.* **42**, 1956–1961 (2004).
56. Emery, S. L. *et al.* Real-Time Reverse Transcription–Polymerase Chain Reaction Assay for SARS-associated Coronavirus. *Emerg. Infect. Dis.* **10**, 311–316 (2004).
57. Corman, V. M. *et al.* Detection of 2019 novel coronavirus (2019-nCoV) by real-time RT-PCR. *Eurosurveillance* **25**, 23–30 (2020).
58. Overbergh, L. *et al.* Validation of real-time RT-PCR assays for mRNA quantification in baboons. *Cytokine* **31**, 454–458 (2005).
59. Hörnich, B. F. *et al.* SARS-CoV-2 and SARS-CoV Spike-Mediated Cell-Cell Fusion Differ in Their Requirements for Receptor Expression and Proteolytic Activation. *J. Virol.* **95**, e00002-21 (2021).
60. Belouzard, S., Millet, J. K., Licitra, B. N. & Whittaker, G. R. Mechanisms of Coronavirus Cell Entry Mediated by the Viral Spike Protein. *Viruses* **4**, 1011–1033 (2012).

61. Fuentes-Prior, P. Priming of SARS-CoV-2 S protein by several membrane-bound serine proteinases could explain enhanced viral infectivity and systemic COVID-19 infection. *J. Biol. Chem.* **296**, 100135 (2020).
62. Kido, H. & Okumura, Y. MSPL/TMPRSS13. *Front Biosci* **13**, 754–8 (2008).
63. Carocci, M. & Bakkali-Kassimi, L. The encephalomyocarditis virus. *Virulence* **3**, 351–367 (2012).
64. Cardeti, G. *et al.* Encephalomyocarditis virus infection in Macaca sylvanus and Hystrix cristata from an Italian rescue centre for wild and exotic animals. *Virol. J.* **13**, 193 (2016).
65. Reddacliff, L., Kirkland, P., Hartley, W., & Reece, R. Encephalomyocarditis Virus Infections in an Australian Zoo. *J. Zoo Wildl. Med.* **28**, 153–157 (1997).
66. Susan K. Wells, Andrew E. Gutter, Kenneth F. Soike and Gary B. Baskin. Encephalomyocarditis Virus: Epizootic in a Zoological Collection. *J. Zoo Wildl. Med.* **20**, 291–296 (1989).
67. Vyshemirskii, O. I. *et al.* Isolation and genetic characterization of encephalomyocarditis virus 1 from a deceased captive hamadryas baboon. *Virus Res.* **244**, 164–172 (2018).
68. Yeo, D. S.-Y. *et al.* A highly divergent Encephalomyocarditis virus isolated from nonhuman primates in Singapore. *Virol. J.* **10**, 248 (2013).
69. Canelli, E. *et al.* Encephalomyocarditis virus infection in an Italian zoo. *Virol. J.* **7**, 64 (2010).
70. van Sandwyk, J. H. d. T., Bennett, N. C., Swanepoel, R. & Bastos, A. D. S. Retrospective genetic characterisation of Encephalomyocarditis viruses from African elephant and swine recovers two distinct lineages in South Africa. *Vet. Microbiol.* **162**, 23–31 (2013).
71. Lamglait, B., Joris, A., Romey, A., Bakkali-Kassimi, L. & Lemberger, K. Fatal encephalomyocarditis virus infection in an African savanna elephant (Loxodonta africana) in a french zoo. *J. Zoo Wildl. Med.* **46**, 393–396 (2015).
72. Grobler, D. G., Raath, J. P., Braack, L. E. O., Keet, D. F. & Gerdes, G. H. An outbreak of encephalomyocarditis virus infection in free-ranging African

elephants in the Kruger National Park. *Onderstepoort J. Vet. Res.* **62**, 97–108 (1995).

73. Jones, P. *et al.* Encephalomyocarditis virus mortality in semi-wild bonobos (Pan panicus): Encephalomyocarditis in semi-wild bonobos. *J. Med. Primatol.* **40**, 157–163 (2011).
74. Luo, Y.-K. *et al.* Isolation and Characterization of Encephalomyocarditis Virus from Dogs in China. *Sci. Rep.* **7**, 438 (2017).
75. Maurice, H., Nielen, M., Vyt, Ph., Frankena, K. & Koenen, F. Factors related to the incidence of clinical encephalomyocarditis virus (EMCV) infection on Belgian pig farms. *Prev. Vet. Med.* **78**, 24–34 (2007).
76. Koenen F, Vanderhallen H, Castryck F, Miry C. Epidemiologic, pathogenic and molecular analysis of recent encephalomyocarditis outbreaks in Belgium. *Zentralblatt Vet. Reihe B J. Vet. Med. Ser. B* **46**, 217–231 (1999).
77. Zhang, G. Q., Ge, X. N., Guo, X. & Yang, H. C. Genomic analysis of two porcine encephalomyocarditis virus strains isolated in China. *Arch. Virol.* **152**, 1209–1213 (2007).
78. Feng, R. *et al.* National serosurvey of encephalomyocarditis virus in healthy people and pigs in China. *Arch. Virol.* **160**, 2957–2964 (2015).
79. Deutz, A. *et al.* [Seroepidemiological studies of zoonotic infections in hunters in southeastern Austria—prevalences, risk factors, and preventive methods]. *Berl. Munch. Tierarztl. Wochenschr.* **116**, 306–311 (2003).
80. Oberste, M. S. *et al.* Human Febrile Illness Caused by Encephalomyocarditis Virus Infection, Peru. *Emerg. Infect. Dis.* **15**, 640–646 (2009).
81. Czechowicz, J. *et al.* Prevalence and Risk Factors for Encephalomyocarditis Virus Infection in Peru. *Vector-Borne Zoonotic Dis.* **11**, 367–374 (2011).
82. Spyrou, V. *et al.* Transmission and pathogenicity of encephalomyocarditis virus (EMCV) among rats. *Vet. Res.* **35**, 113–122 (2004).
83. Psalla, D. *et al.* Pathogenesis of Experimental Encephalomyocarditis: a Histopathological, Immunohistochemical and Virological Study in Rats. *J. Comp. Pathol.* **134**, 30–39 (2006).

84. Psalla, D. *et al.* Pathogenesis of Experimental Encephalomyocarditis: A Histopathological, Immunohistochemical and Virological Study in Mice. *J. Comp. Pathol.* **135**, 142–145 (2006).
85. Haydon, D. T., Cleaveland, S., Taylor, L. H. & Laurenson, M. K. Identifying Reservoirs of Infection: A Conceptual and Practical Challenge. *Emerg. Infect. Dis.* **8**, 1468–1473 (2002).
86. Zell, R. Picornaviridae—the ever-growing virus family. *Arch. Virol.* **163**, 299–317 (2018).
87. Philipps, A. *et al.* Isolation and molecular characterization of a second serotype of the encephalomyocarditis virus. *Vet. Microbiol.* **161**, 49–57 (2012).
88. Helwig, F. C. & Schmidt, C. H. A filter-passing agent producing interstitial myocarditis in anthropoid apes and small animals. *Science* **102**, 31–33 (1945).
89. Feng, R. *et al.* Isolation, molecular and phylogenetic analysis of encephalomyocarditis virus strain GS01 in China. *Infect. Genet. Evol.* **30**, 19–26 (2015).
90. Ishii, A. *et al.* Molecular surveillance and phylogenetic analysis of Old World arenaviruses in Zambia. *J. Gen. Virol.* **93**, 2247–2251 (2012).
91. Sasaki, M. *et al.* Molecular epidemiology of paramyxoviruses in Zambian wild rodents and shrews. *J. Gen. Virol.* **95**, 325–330 (2014).
92. An, D.-J. *et al.* Encephalomyocarditis in Korea: Serological survey in pigs and phylogenetic analysis of two historical isolates. *Vet. Microbiol.* **137**, 37–44 (2009).
93. Kumar, S., Stecher, G., Li, M., Knyaz, C. & Tamura, K. MEGA X: Molecular Evolutionary Genetics Analysis across Computing Platforms. *Mol. Biol. Evol.* **35**, 1547–1549 (2018).
94. Martin, D. P., Murrell, B., Golden, M., Khoosal, A. & Muhire, B. RDP4: Detection and analysis of recombination patterns in virus genomes. *Virus Evol.* **1**, vev003 (2015).
95. Yuan, W. *et al.* Porcine encephalomyocarditis virus strain BD2 isolated from northern China is highly virulent for BALB/c mice. *Acta Virol.* **59**, 300–304 (2015).

96. Bai, J. *et al.* Pathogenicity and molecular analysis of an encephalomyocarditis virus isolate from mideastern China. *Can. J. Vet. Res.* **76**, 157–160 (2012).
97. Billinis, C. Encephalomyocarditis Virus Infection in Wildlife Species in Greece. *J. Wildl. Dis.* **45**, 522–526 (2009).
98. Gainer, J. H. Encephalomyocarditis virus infections in Florida, 1960-1966. *J. Am. Vet. Med. Assoc.* **151**, 421–425 (1967).
99. Hill, B. D., Ketterer, P. J., Rodwell, B. J., Eaves, F. W. & Webster, W. R. Encephalomyocarditis virus infection and pig disease in Queensland. *Aust. Vet. J.* **62**, 433–434 (1985).
100. Hubbard, G. B. *et al.* An encephalomyocarditis virus epizootic in a baboon colony. *Lab. Anim. Sci.* **42**, 233–239 (1992).
101. Roca-Garcia, M. & Sanmartin-Barberi, C. The Isolation of Encephalomyocarditis Virus from Aotus Monkeys 1. *Am. J. Trop. Med. Hyg.* **6**, 840–852 (1957).
102. Ghosh, S. N. & Rajagopalan, P. K. Encephalomyocarditis virus activity in Mus booduga (Gray) in Barur Village (1961-1962), Sagar KFD area, Mysore State, India. *Indian J. Med. Res.* **61**, 989–991 (1973).
103. Vizoso, A. D., Vizoso, M. R. & Hay, R. Isolation of a Virus resembling Encephalomyocarditis from a Red Squirrel. *Nature* **201**, 849–850 (1964).
104. Amaddeo, D., Cardeti, G. & Autorino, G. L. Isolation of Encephalomyocarditis Virus from Dormice (Myoxus glis) in Italy. *J. Wildl. Dis.* **31**, 238–242 (1995).
105. Pope, J. A virus of the encephalomyocarditis group from a water-rat, Hydromys chrysogaster, in north queensland. *Aust. J. Exp. Biol. Med. Sci.* **37**, 117–124 (1959).
106. Gainer, J. H. & Bigler, W. I. Encephalomyocarditis (EMC) Virus Recovered From Two Cotton Rats and a Raccoon. *Bull. Wildl. Dis. Assoc.* **3**, 47–49 (1967).
107. Causey, O.R., Shope, R.E. and Laemmert, H. Report of an epizootic of encephalomyocarditis virus in Para, Brazil. *Rev Serv Esp* **12**, 47–50 (1962).
108. Orba, Y. *et al.* Orthopoxvirus infection among wildlife in Zambia. *J. Gen. Virol.* **96**, 390–394 (2015).

109. Sasaki, M. *et al.* Metagenomic analysis of the shrew enteric virome reveals novel viruses related to human stool-associated viruses. *J. Gen. Virol.* **96**, 440–452 (2015).
110. Maurice, H. *et al.* The occurrence of encephalomyocarditis virus (EMCV) in European pigs from 1990 to 2001. *Epidemiol. Infect.* **133**, 547–557 (2005).
111. Seaman, J. T., Boulton, J. G. & Carrigan, M. J. Encephalomyocarditis virus disease of pigs associated with a plague of rodents. *Aust. Vet. J.* **63**, 292–294 (1986).
112. Liu, H. *et al.* Complete genome sequences and phylogenetic analysis of encephalomyocarditis virus strains isolated from pigs and rats origin. *Infect. Genet. Evol.* **55**, 277–280 (2017).
113. Oberste, M. S. *et al.* Enteroviruses 76, 89, 90 and 91 represent a novel group within the species Human enterovirus A. *J. Gen. Virol.* **86**, 445–451 (2005).
114. Oberste, M. S., Peñaranda, S., Maher, K. & Pallansch, M. A. Complete genome sequences of all members of the species Human enterovirus A. *J. Gen. Virol.* **85**, 1597–1607 (2004).
115. Doi, K. Experimental Encephalomyocarditis Virus Infection in Small Laboratory Rodents. *J. Comp. Pathol.* **144**, 25–40 (2011).
116. Clark, A. *et al.* Estimating global, regional and national rotavirus deaths in children aged <5 years: Current approaches, new analyses and proposed improvements. *PLOS ONE* **12**, e0183392 (2017).
117. Jonesteller, C. L., Burnett, E., Yen, C., Tate, J. E. & Parashar, U. D. Effectiveness of rotavirus vaccination: a systematic review of the first decade of global postlicensure data, 2006–2016. *Clin. Infect. Dis.* **65**, 840–850 (2017).
118. Sadiq, A., Bostan, N., Khan, J. & Aziz, A. Effect of rotavirus genetic diversity on vaccine impact. *Rev. Med. Virol.* **32**, e2259 (2022).
119. Malik Y. S. *et al.* Evolving rotaviruses, interspecies transmission and zoonoses. *Open Virol. J.* **14**, 1–6 (2020).
120. Matthijnssens, J. *et al.* Full genome-based classification of rotaviruses reveals a common origin between human Wa-like and porcine rotavirus strains and human DS-1-like and bovine rotavirus strains. *J. Virol.* **82**, 3204–3219 (2008).

121. Matthijnssens, J. *et al.* Uniformity of rotavirus strain nomenclature proposed by the Rotavirus Classification Working Group (RCWG). *Arch. Virol.* **156**, 1397–1413 (2011).
122. Kumar, N. *et al.* Molecular characterization of unusual bovine rotavirus A strains having high genetic relatedness with human rotavirus: evidence for zooanthroponotic transmission. *Zoonoses Public Health* **65**, 431–442 (2018).
123. Steyer, A., Poljšak-Prijatelj, M., Barlič-Maganja, D. & Marin, J. 2008. Human, porcine and bovine rotaviruses in Slovenia: evidence of interspecies transmission and genome reassortment. *J. Gen. Virol.* **89**, 1690–1698 (2008).
124. Papp, H. *et al.* Zoonotic transmission of reassortant porcine G4P[6] rotaviruses in Hungarian pediatric patients identified sporadically over a 15year period. *Infect. Genet. Evol.* **19**, 71–80 (2013).
125. Han, B. A., Kramer, A. M. & Drake, J. M. Global patterns of zoonotic disease in mammals. *Trends Parasitol.* **32**, 565–577 (2016).
126. Esona, M. D. *et al.* Reassortant group A rotavirus from straw-colored fruit bat (Eidolon helvum). *Emerg. Infect. Dis. J.* **16**, 1844–1852 (2010).
127. Waruhiu, C. *et al.* Molecular detection of viruses in Kenyan bats and discovery ofnovel astroviruses, caliciviruses and rotaviruses. *Virol. Sin.* **32**, 101–114 (2017).
128. Yinda, C. K. *et al.* Novel highly divergent reassortant bat rotaviruses in Cameroon, without evidence of zoonosis. *Sci. Rep.* **6**, 34209 (2016).
129. He, B. *et al.* Group A rotaviruses in chinese bats: genetic composition, serology, and evidence for bat-to-human transmission and reassortment. *J. Virol.* **91**, e02493-16 (2017).
130. Xia, L. *et al.* The complete genome sequence of a G3P[10] Chinese bat rotavirus suggests multiple bat rotavirus inter-host species transmission events. *Infect. Genet. Evol.* **28**, 1–4 (2014).
131. He, B. *et al.* Characterization of a novel G3P[3] rotavirus isolated from a lesser horseshoe bat: a distant relative of feline/canine rotaviruses. *J. Virol.* **87**, 12357–12366 (2013).

132. Asano, K. M. *et al.* Group A rotavirus in Brazilian bats: description of novel T15 and H15 genotypes. *Arch. Virol.* **161**, 3225–3230 (2016).
133. Sasaki, M. *et al.* Identification of group A rotaviruses from Zambian fruit bats provides evidence for long-distance dispersal events in Africa. *Infect. Genet. Evol.* **63**, 104–109 (2018).
134. Sasaki, M. *et al.* Multi-reassortant G3P[3] group A rotavirus in a horseshoe bat in Zambia. *J. Gen. Virol.* **97**, 2488–2493 (2016).
135. Mishra, N. *et al.* A viral metagenomic survey identifies known and novel mammalian viruses in bats from Saudi Arabia. *PLOS ONE* **14**, e0214227 (2019).
136. Simsek, C. *et al.* At least seven distinct rotavirus genotype constellations in bats with evidence of reassortment and zoonotic transmissions. *mBio* **12**, e02755-20 (2021).
137. Burns, J. W. *et al.* Analyses of homologous rotavirus infection in the mouse model. *Virology* **207**, 143–153 (1995).
138. Li, K. *et al.* Identification of novel and diverse rotaviruses in rodents and insectivores, and evidence of cross-species transmission into humans. *Virology* **494**, 168–177 (2016).
139. Johne, R. *et al.* Distantly related rotaviruses in common shrews, Germany, 2004–2014. *Emerg. Infect. Dis.* **25**, 2310–2314 (2019).
140. Sachsenröder, J. *et al.* Metagenomic identification of novel enteric viruses in urban wild rats and genome characterization of a group A rotavirus. *J. Gen. Virol.* **95**, 2734–2747 (2014).
141. Williams, S. H. *et al.* Viral diversity of house mice in New York City. *mBio* **9**, e01354-17 (2018).
142. Maes, P., Matthijnssens, J., Rahman, M. & Van Ranst, M. RotaC: A web-based tool for the complete genome classification of group A rotaviruses. *BMC Microbiol.* **9**, 238 (2009).
143. Letunic, I. & Bork, P. Interactive Tree Of Life (iTOL) v5: an online tool for phylogenetic tree display and annotation. *Nucleic Acids Res.* **49**, W293–W296 (2021).

144. Alfajaro, M. M. *et al.* Dual recognition of sialic acid and αGal epitopes by the VP8* domains of the bovine rotavirus G6P[5] WC3 and of its mono-reassortant G4P[5] RotaTeq vaccine strains. *J. Virol.* **93**, e00941-19 (2019).
145. Boshuizen, J. A. *et al.* Changes in small intestinal homeostasis, morphology,and gene expression during rotavirus infection of infant mice. *J. Virol.* **77**, 13005–13016 (2003).
146. Jothikumar, N., Kang, G. & Hill, V. R. Broadly reactive TaqMan® assay for real-time RT-PCR detection of rotavirus in clinical and environmental samples. *J. Virol. Methods* **155**, 126–131 (2009).
147. Iturriza Gómara, M., Wong, C., Blome, S., Desselberger, U. & Gray, J. Molecular Characterization of VP6 Genes of Human Rotavirus Isolates: Correlation of Genogroups with Subgroups and Evidence of Independent Segregation. *J. Virol.* **76**, 6596–6601 (2002).
148. Imagawa, H. *et al.* Isolation of foal rotavirus in MA-104 cells. *Bull. Equine Res. Inst.* **18**, 119–128 (1981).
149. Desselberger, U. Rotaviruses. *Virus Res.* **190**, 75–96 (2014).
150. Huang, P. *et al.* Spike protein VP8* of human rotavirus recognizes histo-blood group antigens in a type-specific manner. *J. Virol.* **86**, 4833–4843 (2012).
151. Liu, Y. *et al.* Rotavirus VP8*: phylogeny, host range, and interaction with histo-blood group antigens. *J. Virol.* **86**, 9899–9910 (2012).
152. Liu, Y. *et al.* Glycan specificity of P[19] rotavirus and comparison with those of related P genotypes. *J. Virol.* **90**, 9983–9996 (2016).
153. Kim, J.-Y. *et al.* Glycan-specificity of four neuraminidase-sensitive animal rotavirus strains. *Vet. Microbiol.* **207**, 159–163 (2017).
154. Haselhorst, T. *et al.* Sialic acid dependence in rotavirus host cell invasion. *Nat. Chem. Biol.* **5**, 91–93 (2009).
155. Fukuda, S. *et al.* Rotavirus incapable of NSP6 expression can cause diarrhea in suckling mice. *J. Gen. Virol.* **103**, 001745 (2022).
156. Mori, Y., Borgan, M. A., Ito, N., Sugiyama, M. & Minamoto, N. Diarrhea-Inducing Activity of Avian Rotavirus NSP4 Glycoproteins, Which Differ

Greatly from Mammalian Rotavirus NSP4 Glycoproteins in Deduced Amino Acid Sequence, in Suckling Mice. *J. Virol.* **76**, 5829–5834 (2002).

157. Lynch, M. *et al.* The Pathology of Rotavirus-Associated Deaths, Using New Molecular Diagnostics. *Clin. Infect. Dis.* **37**, 1327–1333 (2003).
158. Cui, Y., Claus, S., Schnell, D., Runge, F. & MacLean, C. In-depth characterization of epiIntestinal microtissue as a model for intestinal drug absorption and metabolism in human. *Pharmaceutics* **12**, 405 (2020).
159. Saxena, K. *et al.* Human intestinal enteroids: a new model to study human rotavirus infection, host restriction, and pathophysiology. *J. Virol.* **90**, 43–56 (2015).
160. Guo, Y., Candelero-Rueda, R. A., Saif, L. J. & Vlasova, A. N. Infection of porcine small intestinal enteroids with human and pig rotavirus A strains reveals contrasting roles for histo-blood group antigens and terminal sialic acids. *PLOS Pathog.* **17**, e1009237 (2021).
161. Varki, A. Loss of N-glycolylneuraminic acid in humans: Mechanisms, consequences, and implications for hominid evolution. *Am. J. Phys. Anthropol.* **116**, 54–69 (2001).
162. Steppan, S. J. & Schenk, J. J. Muroid rodent phylogenetics: 900-species tree reveals increasing diversification rates. *PLOS ONE* **12**, e0183070 (2017).
163. Simwaka, J. C. *et al.* Diversity of rotavirus strains circulating in children under five years of age who presented with acute gastroenteritis before and after rotavirus vaccine introduction, University Teaching Hospital, Lusaka, Zambia, 2008–2015. *Vaccine* **36**, 7243–7247 (2018).
164. Maringa, W. M. *et al.* Molecular Characterisation of a Rare Reassortant Porcine-Like G5P[6] Rotavirus Strain Detected in an Unvaccinated Child in Kasama, Zambia. *Pathogens* **9**, 663 (2020).
165. Maringa, W. M. *et al.* Whole Genome Analysis of Human Rotaviruses Reveals Single Gene Reassortant Rotavirus Strains in Zambia. *Viruses* **13**, 1872 (2021).
166. Rakau, K. G. *et al.* Genetic characterization of G12P[6] and G12P[8] rotavirus strains collected in six African countries between 2010 and 2014. *BMC Infect. Dis.* **21**, 107 (2021).

Summary in Japanese

研究の背景

国際社会ではこれまでに、COVID-19 をはじめとした様々な新興・再興感染症が出現し、公衆衛生上の脅威となっている。約 3/4 以上の新興・再興感染症は人獣共通感染症であり、中でもウイルス感染症の多くは野生動物からの伝播を経て出現したと考えられる。そのため、野生動物の保有するウイルスの調査はワンヘルスの観点から重要である。近年、メタゲノム解析技術の普及に伴い、多くの検体から様々な新規ウイルスゲノムが検出されている。しかし、ほとんどの報告はゲノム解析に留まっており、ウイルス分離およびウイルス学的な性状解析の試みは十分ではない。特に、プロテアーゼ依存性ウイルスは、培養細胞での増殖時に無血清培地下でトリプシンを作用させる必要があるため、検体の接種による細胞傷害が生じやすく、ウイルス分離が困難である。これまで、宿主 II 型膜貫通型セリンプロテアーゼ（TTSP）発現細胞において、トリプシン非存在下においてもプロテアーゼ依存性ウイルスの感染増殖が可能であることが明らかになっているが、プロテアーゼ発現細胞を野生動物からの網羅的なウイルス分離に用いた例は少ない。そこで本研究では、プロテアーゼ発現細胞を用いて野生動物由来検体からウイルス分離を実施し、分離したウイルスのウイルス学的および疫学的性状解析を実施することを目的とした。

第一章：新型コロナウイルス（SARS-CoV-2）スパイクタンパク質を活性化する TTSP の検討

まず、代表的なプロテアーゼ依存性ウイルスである SARS-CoV-2 の感染を促進する TTSP を検索した。SARS-CoV-2 は、TMPRSS2 などの TTSP を利用して、ウイルスのスパイクタンパク質を切断・活性化し細胞侵入効率を上昇させるが、SARS-CoV-2 の感染における TMPRSS2 以外の TTSP の役割については解明されていない。本章では、ヒト ACE2 発現 HEK293T 細胞および Vero E6 細胞を用いて 12 種類の TTSP をスクリーニングし、TMPRSS11D および TMPRSS13 が SARS-CoV-2 の感染増殖を促進することを明らかにした。また、SARS-CoV-1 と SARS-CoV-2 は、ウイルス侵入過程において同様の TTSP を利用することが明らかになった。本研究は、宿主の TTSP が SARS-CoV-2 の感染に影響を与えることを示し、細胞や組織の指向性、病原性に影響することを示唆している。

第二章：潜在的レゼルボアである齧歯類動物マストミスからの脳心筋炎ウイルス（EMCV）の分離および性状解析

EMCV は様々な哺乳類動物に感染し、脳炎、心筋炎、生殖障害、糖尿病などを引き起こす。特に、養豚場における繁殖障害や、動物園や野生動物保護区等での希少動物の突然死は経済・環境の観点から重要な問題である。動物との接触によってヒトへも稀に感染し、発熱性疾患を引き起す人獣共通感染症である。本章では、ザンビアで採取した齧歯類動物（マストミス、*Mastomys natalensis*）から EMCV ZM12/14 株を分離し、性状解析を実施した。系統解析の結果，ZM12/14 株は P1 および P3 領域で EMCV-1 と同じ系統に分類されたが、P2 領域では既知の EMCV 株と異なる系統に分類され、特徴的な進化系統を有することが示唆された。さらに、ザンビア各地で捕獲した各種齧歯類動物（n=179）の組織および血清を用いて、EMCV の RT-PCR スクリーニングと中和抗体測定を実施した。その結果、*M. natalensis* のみから EMCV ゲノム（19/179 = 10.6%）および中和抗体が検出され（33/179 = 18.4%）、RT-PCR 陽性、陰性検体どちらにおいても、高い中和抗体価（≧320）が確認された。他種の齧歯類動物ではゲノムおよび中和抗体は検出されなかった。また、ZM12/14 株を腹腔内接種した BALB/c マウスは無症候性の持続感染を引き起こした。感染マウスでは感染 2 週間後において、高い中和抗体価と脳および脾臓における高いウイルスゲノム量が認められ、上記の疫学調査と一致する結果が得られた。本研究では、ザンビアで初めて EMCV を検出し、*M. natalensis* が自然感染宿主としてレゼルボアの役割を担うことを示唆する結果を得た。

第三章：コウモリおよび齧歯類動物由来ロタウイルス A（RVA）の分離と性状解析

RVA は、ヒトや様々な動物に下痢性疾患を引き起こす。近年、ヒト RVA との遺伝子再集合を示唆するコウモリおよび齧歯類動物由来 RVA が複数報告されている。しかし、様々な非典型的遺伝子型が含まれるコウモリおよび齧歯類動物由来 RVA のウイルス学的性状はほとんど解明されていない。そこで、ヒト TMPRSS2/TMPRSS11D 共発現 MA104 細胞とザンビアで採取した野生動物検体を用いて RVA のウイルス分離先行型スクリーニングを実施し、コウモリ（*Rousettus aegyptiacus*）およびマストミス（*M. natalensis*）から RVA を単離した。全ゲノム配列解析の結果、コウモリ由来 RVA 16-06 株の遺伝子型は、ケニアの *R. aegyptiacus* から検出された BATp39 株と同一であったが、マストミス由来 RVA MpR12 株は、既知の遺伝子型と配列類似性が低く、全分節が新規の遺伝子型として

登録された。さらに、MpR12 株は、系統学的に他の齧歯類由来 RVA よりもコウモリ由来 RVA に近く、特徴的な進化系統を有することが示された。次に、分離株のウイルス学的性状を解析した。RVA が細胞侵入する際の接着因子である細胞表面糖鎖と RVA の結合性を調べた結果、16-06 株は細胞表面のシアル酸と結合して細胞内に侵入する一方、MpR12 株はシアル酸とは結合しないことが明らかになった。さらに、乳飲みマウスへの経口接種により分離株の病原性を評価した結果、16-06 株および MpR12 株はどちらも乳飲みマウスに感染し、下痢を引き起こすことが示された。また、3 次元再構築したヒト初代腸管上皮に対する RVA の感染性を調べた結果、16-06 株および MpR12 株は、ヒト由来 RVA Wa 株と同等の効率で感染増殖することが明らかになった。本研究から、特徴的な遺伝学的背景を有するコウモリおよび齧歯類由来 RVA のウイルス学的性状が明らかになり、それらの RVA が人獣共通感染症となる可能性についてさらなる調査が必要であることが示唆された。

まとめと今後の展望

本研究では、プロテアーゼ依存性ウイルスに着目して野生動物検体からのウイルス分離を実施し、分離された EMCV および RVA の性状解析を実施した。野生動物の保有するウイルスの調査では通常、標的とする病原体のゲノムスクリーニング実施後、陽性検体からウイルス分離を実施する。しかし、このような手法では標的外のウイルスや既知ウイルスと配列類似性の低いゲノムを有するウイルスを検出することは困難である。多数の野生動物検体からゲノムスクリーニングを介さずにウイルス分離を実施する本研究の手法により、今回分離した EMCV の様に採材地における分布が不明であったウイルスや、既知配列と低い配列類似性を持つコウモリおよび齧歯類動物由来 RVA が分離され、本手法の有効性が実証された。今後本手法を、野生動物を含む様々な検体からのウイルス探索に用いることにより、多数の新規ウイルスが分離されることが期待される。さらに本研究は、分離した EMCV および RVA のウイルス学的性状を解析した。EMCV の性状解析では、*M. natalensis* が EMCV のレゼルボアである可能性が示されたため、今後ザンビアの養豚場や野生動物保護区における EMCV の調査が必要である。RVA の性状解析では、非典型的な遺伝子型構造を持つコウモリおよび齧歯類動物由来 RVA のウイルス学的性状および宿主特異性に関する基礎的な知見を得た。今回検出した RVA が実際にヒトへの感染やヒト RVA との遺伝子再集合を起こすか調べるため、今後、多様な遺伝子型の RVA を標的としたザンビアのヒト検体の疫学調査が必要である。